NASA CONTRACTOR REPORT

NASA CR-15

NASA CR-1532

A STUDY OF PROTON-INDUCED EFFECTS ON REFLECTIVE SURFACES OF SPACE MIRRORS

by Roger B. Gillette and Bruce A. Kenyon

Prepared by
THE BOEING COMPANY
Seattle, Wash.
for Langley Research Center

NATIONAL AERONAUTICS AND SPACE ADMINISTRATION • WASHINGTON, D. C. • FEBRUARY 1970

A STUDY OF PROTON-INDUCED EFFECTS ON REFLECTIVE SURFACES OF SPACE MIRRORS

By Roger B. Gillette and Bruce A. Kenyon

Prepared under Contract No. NAS 1-7627 by
THE BOEING COMPANY
Seattle, Wash.

for Langley Research Center

NATIONAL AERONAUTICS AND SPACE ADMINISTRATION

For sale by the Clearinghouse for Federal Scientific and Technical Information
Springfield, Virginia 22151 – CFSTI price $3.00

TABLE OF CONTENTS

A STUDY OF PROTON-INDUCED EFFECTS ON REFLECTIVE SURFACES OF SPACE MIRRORS

By Roger B. Gillette and Bruce A. Kenyon
The Boeing Company, Seattle, Washington

1.0 SUMMARY

The results of a research program to study the effects of low energy protons on reflective surfaces for space optical systems, are presented in this report. The primary objective of the program was to determine the effects on telescope mirror reflective surfaces, of the proton radiation environment at synchronous Earth orbit. Secondary objectives of the study were to obtain information on surface finish characteristics and reflectance characteristics of three promising mirror substrates.

Mirror test specimens evaluated in the study included polished substrates of fused silica, Cer-Vit*, and Kanigen**-nickel-plated beryllium; coated with aluminum and overcoated with MgF_2. Also included were specimens of polished fused silica coated with aluminum and LiF. The experimental program studied the dependence of specular reflectance and scattering properties on: (1) proton integrated flux; (2) proton flux; (3) post-irradiation exposure to air; and (4) coating and substrate type. The effects of integrated fluxes up to 10^{16} protons-cm^{-2} sec^{-1} of 10 keV energy were evaluated.

Results of experiments showed that the primary mechanism of damage was proton-induced deposition of a contaminant film onto the mirror surfaces. Cleaning experiments and theoretical predictions of reflectance changes on MgF_2/Al-coated mirrors, showed that the contaminant film accounted for essentially all of the observed damage. Similarly cleaning experiments on LiF/Al-coated mirrors indicated that the majority of the observed damage was a contaminant film effect. In relating experimental results to the synchronous-orbit space environment, it was concluded that negligible degradation will occur over a two-year period if no contaminant film deposition occurs.

An oxidation cleaning technique was developed which could be used for removing the film and restoring the reflectance to nearly the pre-irradiation value. Results suggested that this cleaning technique could be utilized for salvaging space mirrors which may become contaminated in either Earth tests or space use.

---

* Cer-Vit is the trade name for a low coefficient of expansion material produced by Owens-Illinois Company.

** Kanigen is the General American Transportation Corporation trade name for a non-electrical technique of plating nickel-phosphorous.

Light scattering measurements at wavelengths of 253.7 nm and 500 nm revealed no significant radiation-induced changes in scattering from either type of surface. Surface finish studies also showed that the fused silica and Cer-Vit substrates were polished smoother than beryllium substrates, and the deposition of reflective coatings had a negligible effect on microroughness.

2.0 INTRODUCTION

The primary objective of this study was to determine the effects of the proton radiation environment at synchronous Earth orbit, on telescope mirror reflective surfaces. Secondary objectives of the study were to obtain information concerning the surface finish and reflectance characteristics of three promising mirror substrates. It is intended that the results will be of assistance in choosing the mirror substrate and coating combination which will provide the optimum combination of high reflectance and low degradation in the space environment. The radiation environment and mirror test specimens were selected for compatibility with plans (ref. 1) to place a large astronomical telescope mirror at synchronous altitude. However, the study results should be applicable to many other space optical systems (ref. 2).

Mirror test specimens evaluated in the study included polished substrates of fused silica, Cer-Vit, and Kanigen-nickel-plated beryllium; all were coated with aluminum and overcoated with MgF_2. Also included were specimens of polished fused silica coated with aluminum and overcoated with LiF. These vacuum deposited coatings were applied with techniques which produce maximum reflectance in the vacuum-ultraviolet wavelength region. Uncoated, polished specimens of each substrate type were also prepared for surface finish experiments.

The experimental program studied the dependence of specular reflectance and scattered light properties on: (1) proton integrated flux; (2) proton flux; (3) post-irradiation exposure to air; and (4) substrate and coating type. The effect of the vacuum deposited coatings on substrate micro-roughness was also evaluated. Proton integrated fluxes to 10^{16} protons-cm^{-2} and fluxes between 2×10^{9} and 10^{12} protons-cm^{-2} sec^{-1} were used. Flux dependence was evaluated to establish the validity of testing at exposure rates far higher than those encountered in space. Post-irradiation reflectance measurements (before and after exposure to air) were performed to determine whether specimens of this type need to be held in vacuum in the time period between irradiation and reflectance measurements. Reflectance measurements were performed over the wavelength range from 90 to 50,000 nm. The region from 90 to 250 nm was covered with an ultraviolet reflectometer which provided capability for performing both reflectance and scattered light measurements in the irradiation chamber. Reflectance at longer wavelengths was measured in more conventional, commercial reflectometers.

At the beginning of the study an analysis was made of the most recent charged-particle environment data at synchronous altitude. Solar electromagnetic radiation was not considered because planned configurations for telescope mirrors were shielded from the sun. The trapped proton environment suggested for this study is presented in Figure 1. Both the integral flux (f) and the differential flux (df/dE)* spectra of these trapped protons are shown. These spectra are based primarily upon the low energy results reported by Frank (refs. 3 and 4) and are consistent with the results of Katz, et al. (ref. 5). The average omnidirectional

* (E) represents proton energy

integral flux of protons is expected to be 3.5×10^8 protons-cm^{-2} sec^{-1} or 2.8×10^7 protons-cm^{-2} sec^{-1} ster^{-1}. A surface with 2π geometry will encounter 5.5×10^{15} protons cm^{-2} year^{-1} with roughly 70 percent having energies less than 30 keV.

The trapped electron environment at synchronous altitude, based upon the results presented by Frank (ref. 3) and Vette (ref. 6), yields a time averaged electron flux of about 1×10^{16} electrons-cm^{-2} year^{-1} with energies greater than 10 keV on a 2π surface. The high energy component is adequately represented by an exponential spectrum with an integral flux of 1.5×10^{15} electron-cm^{-2} year^{-1} having a mean energy of 215 keV (ref. 6).

The surface ionization dose for the combined proton and electron environment was estimated to be about 2×10^8 Joules-kg^{-1}-yr^{-1}, with about 5 percent being due to the electrons. Displacement damage in the overcoating would be predominantly proton induced. Based on these considerations, this study was directed towards determining the effects of low energy protons.

In selecting a proton energy for this program, consideration was given to the ionization dose and displacement damage expected from the above environment. The differential surface dose rate was found to peak between 15 and 40 keV, while the displacement yield was largely due to the protons below 10 keV. Thus, an energy of 10 keV was chosen for the tests. It was anticipated that this energy would best simulate the competition of displacement and ionization damage mechanisms occurring at synchronous altitude.

Results of radiation effects studies on specularly reflecting surfaces have been reported by numerous authors (refs. 7-13). In these references, primary emphasis was placed on specular surfaces to be used in solar concentrators and for spacecraft thermal control. Several flight experiments are presently in progress in which mirror specimens are being evaluated in space. These include the Air Force OV1-10 vehicle, and NASA OSO-3 and ATS-3 vehicles. Mirrors having high ultraviolet reflectance were not included in these or similar earlier experiments.

At the outset of this program only a limited amount of radiation effects studies had been done on vacuum-ultraviolet reflecting optical surfaces. In studies by Canfield, et al. (ref. 14), MgF_2-overcoated aluminum films were irradiated with 1-MeV electrons, 5-MeV protons, and ultraviolet radiation. It was reported that negligible changes in reflectance occurred at 121.6 nm as a result of exposures to the above types of radiation. It was apparent from available literature that inadequate data existed for predicting degradation of mirrors in a synchronous-orbit proton environment. Additional information was needed on: (1) the effects of low energy protons; (2) the effects of high integrated fluxes; (3) the effects of irradiating at a rate higher than that experienced in space; and (4) the effects of air exposure prior to performing post-irradiation reflectance measurements. It was of primary interest to relate the above effects to specular reflectance changes over the wavelength region in which space mirrors will be used.

Special acknowledgement is given to Dr. Georg Hass of the U. S. Army Electronics Command, Night Vision Laboratory, and Mr. William R. Hunter of the Naval Research Laboratory for preparation of certain test specimens, numerous helpful suggestions, and supplying optical properties data. Acknowledgement is also extended to Mr. Reynold Wilbert for experimental equipment design and preparation, Mr. Sheridan Cannaday for assistance in conducting radiation experiments, Dr. William Doherty for space environment and radiation effects analyses, Dr. Sarojini Das for performing interferometric measurements, Mr. William Woods for electronic design and for analysis and programming assistance in the theoretical reflectance calculations, Mr. Melvin Horman for reflectometer aberrations calculations, and Mr. Edward Hoffman of NASA/Langley Research Center for program technical guidance.

3.0 TEST SPECIMENS

The mirror test specimens chosen for study in this program were typical of those used in ultraviolet reflecting optical systems. The basic requirements for those mirrors are that they maintain high reflectance down to at least 120 nm wavelength, and that they be sufficiently polished to minimize scattered light.

Three different types of substrates were evaluated. These were: Corning fused silica #7940, Cer-Vit (Owens-Illinois premium grade mirror blank material C-101), and Kanigen-nickel-plated beryllium (Berylco grade HP-40). Two different coating systems were evaluated; MgF_2 overcoated aluminum, and LiF overcoated aluminum. The MgF_2 overcoating was applied to all three types of substrates, whereas, the LiF overcoating was applied only to a batch of fused silica substrates. LiF overcoated mirrors were included because of their ability to maintain high reflectance down to a wavelength of about 102 nm (MgF_2 begins to absorb at wavelengths shorter than about 130 nm).

The detailed specification used for procurement of mirror test specimens is given in Appendix A, and a brief description follows: The mirrors were nominally 5.08 x 5.08 cm square and 1.90 cm thick. The front surface was to be figured to $\lambda/10$ for the mercury green line (546.1 nm). Surface polish was to be adequate for minimizing scattered light in the vacuum-ultraviolet region with the exception of the Kanigen-nickel-plated beryllium, which was polished on a best-effort basis. In the case of the MgF_2 overcoated surfaces, reflectance was to be maximized at 121.6 nm in accordance with coating thicknesses and procedures given by Canfield, et al. (ref. 14). In the case of LiF overcoated surfaces, reflectance was to be maximized at 102.6 nm using procedures given by Cox, et al. (ref. 15). Mirror substrates were prepared and polished by Tinsley Laboratories. MgF_2/aluminum coatings were applied by Optical Coating Laboratory of Santa Rosa, California and LiF/aluminum coatings were applied by Dr. Georg Hass and associates at the U. S. Army Electronics Command, Night Vision Laboratory, Ft. Belvoir, Virginia.

Detailed information regarding chemical and physical properties of the specific batches of substrate materials is given in Appendix B. Data obtained from the vacuum coating laboratories on cleaning and coating procedures is also given in Appendix B.

Vacuum deposited film thickness measurements were performed on microscope slides which were coated along with the MgF_2 overcoated specimens. The slides were prepared with an uncoated strip to provide a step for interferometer measurements. The entire surface was then overcoated with about 15 nm of aluminum to obtain uniform optical properties. Results of these measurements indicated an average total film thickness of about 115 nm on the beryllium and Cer-Vit mirrors, and an average of about 128 nm on the fused silica mirrors. These values are in agreement with the film thicknesses specified in the procurement specification (60-120 nm of Al and 25 nm of MgF_2).

4.0 APPARATUS AND PROCEDURES

Included in this section are detailed descriptions of the proton radiation facility, the ultraviolet reflectometer, the scattered-light measurement apparatus, the visible and infrared reflectometers, and the interferometers utilized in this study. In accordance with the program requirement that reflectance be measurable without exposing specimens to air after irradiation, the first three above items were combined into a single in-situ facility. The following discussion includes a general description of the overall radiation test facility, and detailed descriptions of the ultraviolet reflectometer and scattered light measurement apparatus. Discussions on experimental and operational procedures, where applicable, are integrated with descriptions of the apparatus.

4.1 Proton Radiation Facility

A schematic of the overall radiation test facility is shown in Figure 2. The major items of the facility are the proton source (accelerator), the irradiation test chamber, and the ultraviolet monochromator. Protons entered the test chamber through a 5-cm diameter hole in the collimating mirror, and impinged on the test mirror at the opposite end of the chamber. To perform reflectance and scattered light measurements, light from the monochromator* entered the optical system through an aperture behind and to the side of the specimen.

An ORTEC** rf-excited ion source was used on the accelerator for generating protons from hydrogen gas. Electrostatic lenses were used for accelerating and focusing the proton beam. Separation of protons from mass 2 and 3 ions was achieved with an electromagnet.

The test specimen was mounted in a fixture which exposed a 3.81-cm (1.500-in) diameter area to the proton beam (Figure 3). The exposed area was defined by a thin, stainless steel aperture located 0.025-cm in front of the specimen. This arrangement provided a sharp definition between the irradiated and non-irradiated areas to aid interpretation of results in subsequent interferometric examination.

Proton flux was measured with an array of three Faraday cups which traversed through the beam just ahead of the test mirror. The Faraday cups, having apertures of 0.476-cm, scanned across the beam at the top, bottom, and center of the 3.81-cm diameter aperture. Flux readings taken at various positions within the irradiated area were averaged. Uniformity of the proton flux over the irradiated area was maintained within $\pm$ 5 percent for most tests. During long term exposures, readings were taken about every half hour and integrated flux values were calculated from these data.

---

* McPherson Instrument Corporation Model 225

** Oak Ridge Technical Enterprises Company

Proton energy was established by the accelerating voltage in the ion source; in this case 10 kV. Beam energy measurements were not performed because earlier experiments (ref. 13) had shown that measuring the accelerating voltage is adequate.

The procedure for irradiating specimens was as follows: A mirror specimen* was installed in the masking fixture, placed in the chamber and optically aligned. The chamber was evacuated and scattered light measurements were made in accordance with procedures discussed in a later section. The pre-irradiation ultraviolet reflectance measurement was then made. During the optical measurements the test chamber was open to the monochromator and isolated from the accelerator by a gate valve. Typical chamber pressures during reflectance measurements were in the order of 7×10^{-6} torr. Following completion of reflectance measurements, the test chamber cold trap was filled with nitrogen and the chamber was closed to the monochromator and opened to the accelerator beam tube. During tuning of the accelerator the Faraday cup array and attached shield protected the test mirror. When a satisfactory proton flux and uniformity were obtained, the Farday cup was moved to a park position and irradiation was begun. Typical chamber pressures during irradiation were $2\text{-}5 \times 10^{-7}$ torr when operating with a flux of 10^{11} protons-cm^{-2} sec^{-1}, and $7\text{-}9 \times 10^{-7}$ torr for a flux of 10^{12} protons-cm^{-2} sec^{-1}. It should be noted that residual gas analyses indicated hydrogen to be the predominant gas in the chamber. Since ion gauges are normally calibrated for air, these pressures are therefore subject to some error.

At selected levels of integrated flux, irradiation was interrupted by closing the beam-tube gate valve, and reflectance measurements were performed. Many of the low-flux exposures were completed over a period of several days. In these cases, the test was shut down at night after completing a reflectance measurement. Preliminary experiments had shown that negligible changes in reflectance occurred during such overnight shut-down periods.

As soon as possible following completion of irradiation, the reflectance and scattered-light distribution were measured. The chamber was then backfilled with ambient air. Some specimens were allowed to stand in air for periods of time after irradiation to determine whether any post-irradiation reflectance and scattered-light changes would occur. The chamber was re-evacuated for the optical measurements.

It was assumed at the outset of the program that contamination of test specimens might be a problem. Therefore, care was taken in selection of materials to be used in the radiation facility to minimize the use of organic compounds. An ideal facility would have been fabricated with non-organic, bakeable materials and all pumps would have been ion pumps. However, the cost of such a system seemed prohibitive.

---

* Prior to this step, pre-irradiation reflectance measurements in the near-ultraviolet, visible, and infrared wavelength regions had been completed.

No such monochromator was commercially available, and extensive modification of the existing proton accelerator would have been required. In consideration of such factors, compromises were made on the use of organic materials.

The system assembled for this study utilized stainless steel vacuum chambers and seals of both Viton-A O-rings and metal gaskets. Apiezon-L grease was used for lubrication of O-rings. The accelerator beam tube was evacuated with an ion pump, the test chamber with a Turbomolecular* pump, and the monochromator with a diffusion pump. The diffusion pump was operated with DC-704 silicone oil and was trapped with a liquid nitrogen chevron baffle. No cold trap was employed between the Turbomolecular pump and the test chamber, although a cold-finger type trap was used in the chamber.

4.2 In-Situ Optical Measurement Facility

The in-situ optical measurement facility consisted of an ultraviolet reflectometer and apparatus for measuring changes in scattered light from mirror specimens. The following section includes discussions of general design requirements, the ultraviolet reflectometer, and the scattered light apparatus, in respective order.

4.2.1 Design Requirements.- Proton-induced damage on telescope mirrors may result in either of two types of optical degradation: (1) an increase in the amount of scattered light; or (2) a change in reflectance produced by increased absorption or by shifted interference effects. An increase in scattered light will reduce telescope image contrast; a decrease in reflectance makes the detection of faint objects more difficult. Measurements of both scattering and reflectance properties are necessary to predict the type and amount of degradation expected of a space mirror.

It was assumed from the outset that reflectance measurements should be made in-situ, i.e., immediately after irradiation without exposure to air. Imposition of this design requirement was based on the numerous oxygen-induced recovery effects which have been noted in radiation effects studies of spacecraft thermal control coatings. The initial equipment design dictated that irradiated specimens be exposed to air before performing scattered light measurements, however, final equipment modifications allowed measurements to be made in-situ.

4.2.2 Ultraviolet Reflectometer.- A schematic showing the reflectometer and scattered-light measurement apparatus is given in Figure 4. The general arrangement was patterned after the Ebert-Fastie monochromator, with the specimen in the grating position. The beam from a 1-meter vacuum-ultraviolet monochromator (McPherson Model 225) expands until it strikes the spherical collimating mirror. At this point, the spherical

* Trade name for a vacuum pump manufactured by Welsh Scientific Company.

mirror redirects the light to the specimen. Light reflected from the specimen illuminates the opposite side of the collimating mirror and is then focused on the exit aperture. In the absolute reflectance measurement mode, an internal* photomultiplier (PM) tube can be positioned to intercept the light either before it reaches the specimen or after it is reflected from the specimen ("incident" and "reflected" positions, respectively). With careful management of the system aperture stop to account for the optical non-equivalence of the two positions, the ratio of outputs then yields the absolute reflectance of the specimen.

The reflectometer was designed to cover the wavelength range from 90 to 250 nm. To obtain sufficient power for operation of photomultiplier (PM) tubes in this range, a grating blazed at 150 nm was selected and mirrors were overcoated with LiF to get high reflectance down to about 100 nm. A Hinteregger-type light source for the monochromator was operated windowless with a d.c. hydrogen discharge.

Several small modifications were made to the monochromator for its use with the reflectometer. These included replacement of the exit slit assembly with a circular aperture 0.762 mm (0.0300 inch) in diameter, installation of an aperture stop about halfway between the grating and exit aperture, and installation of a movable filter between the entrance slit and the grating (Figure 4). The exit aperture, combined with an entrance slit setting of 0.762 mm, defined a passband of about 1.4 nm**. The aperture stop in the monochromator had two openings which divided the output into side by side beams (Figure 4). One opening limited the size of the collimated beam at the test specimen location to 3.528 cm diameter, and the other opening defined a beam intercepted totally by the diagonal mirror and reference PM tube. Light incident on the test mirror was completely contained within the 3.81-cm diameter radiation mask. The active aperture used on the internal PM tube was 3.56 cm, large enough to accept all of the incident and reflected beam. These aperturing techniques controlled stray light within the reflectometer, thus permitting quite sensitive measurements of scattering distributions.

The movable filter was installed in the monochromator to correct a problem that occurred after several months of operation. The problem involved fluorescence on the spherical collimating mirror which introduced an erroneously high output from the internal PM tube when it was nearest the mirror in the "incident" position. It was determined that the fluorescence (resulting in a reduced reflectance in a band at 195 nm) was caused by second-order (i.e., 98 nm) light from the grating. The problem was eliminated by insertion of a sapphire filter in the light beam when measuring at wavelengths longer than 170 nm. The defocusing effect of the filter on the monochromator is negligible for passbands of the width used in this program (less than one percent increase in passband). This filter also eliminated second-order radiation in light from the monochromator at wavelengths below 290 nm.

---

* "Internal" means that the tube was located inside of the vacuum chamber.

** Measured width at half power. Theoretical width at half power is 1.26 nm; full width is 2.52 nm.

For ultraviolet reflectometry, the angle of incidence on the specimen was 6,056 deg. at arc from normal. The monochromator exit aperture, as noted earlier, was 0.762 mm in diameter. Its subtense of 3.7 minutes of arc at the spherical mirror was the nominal decollimation of the incident beam. The exit aperture for the reflected beam subtended 6.2 minutes of arc. Adding 0.6 minute for astigmatism, the instrument profile for scattering was 10.5 arc minutes. The collimating mirror was an f/4.3 spherical reflector with a radius of 141.61 cm (55.75 in.). The effective speed of the test apparatus was f/18.6, as compared with f/17.7 for the largest circular area that can be illuminated by the monochromator. (The monochromator used a 56- by 106-mm, 1-meter focus grating with a constant 15° between incident and diffracted beams.)

Each detector assembly comprised a sodium salicylate fluorescent screen followed by a 13-stage photomultiplier. The internal PM tube was a type EMI 9514 S, and the reference and scattering PM tubes, type 9635 B. An electronic feedback control circuit was developed for operating the PM tubes during both reflectance and scattered light measurements. A schematic of the control circuit is shown in Figure 5. All three PM tubes including the reference PM, the internal PM and the scattering PM were supplied from a single high voltage source. Voltage variation of the supply was controlled by feedback from the reference PM to hold the PM current output at a constant value. In this way, temporal variations caused by a varying light source output were compensated. The operating point, about which this control was exercised, was set by proportioning the voltage output from the reference PM tube electrometer (electrometer A).

To make an absolute reflectance measurement the monochromator was set at a desired wavelength and the internal PM was moved to intercept light usually incident on the specimen. The feedback current control was used to vary the power supply voltage to produce a convenient full-scale reading on electrometer-B which indicated internal PM current (typically 1.00 μ A. The internal PM was then turned to receive the reflected light from the specimen, and its output current was read as a fraction of the full scale reading on electrometer-B. This fraction directly gives the specimen reflectance.

The use of photomultipliers with slightly different gain vs voltage characteristics resulted in a second order variation in the compensation applied to the internal PM. Temporal variations in the lamp output produced voltage variations which kept the reference PM tube output current constant. Slope differences between the characteristic curves for the reference and internal PM tubes caused minor variations in the current output from the internal PM tube. To guard against serious error from this cause, each measurement sequence included as its final step a repeat of the initial reading. A major shift in the full scale reading for incident light was interpreted as a light source variation beyond the scope of compensation, requiring a repeat measurement.

The general performance of the reflectometer was good. Reflectance values could be reproduced to within 0.005 reflectance units (for example, 0.800 ± 0.005 or 0.100 ± 0.005). The absolute accuracy of the reflectance data was not determined.

4.2.3 Scattered-Light Measurement Apparatus.- Scattered-light measurements were performed at wavelengths of 253.7 and 500 nm. Light sources for scattering measurements were attached to the monochromator at the position normally occupied by the Hinteregger lamp. This arrangement permitted scattering measurements to be made in-vacuum immediately after reflectance measurements. For visible-light scattering (500 nm), the monochromator was set at zero wavelength and the grating used as a mirror. An external, tungsten-filament lamp, supplied from a constant voltage source, illuminated the monochromator entrance slit through an interference filter. The filter has a 21 nm (half power) pass band centered at 500 nm. Changeover from reflectance to scattering mode was accomplished without exposing the specimen to air with the aid of a flap valve in the monochromator. This flap valve isolated the entrance slit body from the remainder of the equipment.

For scattering measurements at 253.7 nm, a low pressure mercury-vapor discharge tube was mounted inside the entrance slit body. This lamp is similar in characteristics to the commercial Pen-Ray lamp, but is specially designed to work in a vacuum environment. The monochromator was set at 253.7 nm to isolate that radiation. Although the monochromator was operated with a 2.6 nm pass band, the only radiation present in significant amount was the 253.7 nm line.

In the scattered-light measurement mode, the internal PM tube was placed in a park position so that the beam from the specimen could be collected on the opposite side of the collimating mirror and focused thereby on the exit aperture. Light that fell within the exit aperture could then pass through and illuminate the scattering PM tube. To measure the scattered-light distribution the specimen was rotated through a small angle ($\pm$ 2 deg. of arc). This rotation caused the image to move across the exit aperture, thus bringing into focus light scattered through twice the angle of mirror displacement.

For scattering measurements, the scattering-signal PM tube was connected to the feedback control circuit in the place of the reference PM tube (Figure 5). The reference PM and the internal PM were both disconnected. The system then functioned as a logarithmic photometer with the high voltage analog output indicating the quantity of light received by the scattering PM tube. A decrease in light input was indicated by the increase in voltage required to keep the PM current constant.

To calibrate the photometer, the specimen was rotated to the specular peak and the input resistance of the electrometer was decreased by decades. This increased the control current by decades* causing the system voltage to increase. Over the linear range of the PM tube the effect is equivalent to a reduction of the input light by decades while keeping the control current constant. To extend the calibration beyond this range, a neutral density filter was inserted in the light path and the process was repeated.

* The reflectometer provides an output voltage analog of the current input.

To record the scattering distribution, the high-voltage analog signal was fed to the y-axis of an x-y plotter. The x-axis was driven from a potentiometer circuit directly connected to the cam which produced specimen rotation.

Early in the program it was planned to perform a portion of the reflectance measurements with the scattered-light measurement setup. This arrangement has the basic capability of measuring relative reflectance (by comparing to readings taken on the internal PM) with strong discrimination against scattered light*. It was desired to obtain such data to ascertain whether reflectance changes measured with the internal PM were influenced by increased scattering. Although initial experiments included such anti-scattering reflectance measurements, the precision of the data was quite poor. The technique was abandoned when analysis indicated that scattering from irradiated mirrors created negligible error in reflectances measured with the internal PM.

4.3 Visible and Infrared Reflectometers

Reflectance measurements in the wavelength region from 220 to 2500 nm were made with a Cary Instruments Company Model 14 Spectrophotometer using a specular reflectance attachment (Model 1413). These measurements were made in air. The data obtained with this instrument was absolute specular reflectance and thus could be correlated with data taken with the vacuum-ultraviolet reflectometer. In special experiments conducted to measure this correlation, data from the two instruments overlapped in the wavelength region from 220 nm to about 400 nm. The agreement was within 2 percent.

The procedure for measuring reflectance with the Cary-14 reflectometer was as follows: All mirror specimens including a control specimen, were measured in one batch before irradiation. Following irradiation, each specimen was remeasured along with the control mirror. The control mirror was included in the reflectance measurements to obtain corrections for small systematic errors. This permitted a more accurate determination of reflectance changes after irradiation.

Infrared reflectance measurements from 1000 to 50,000 nm wavelength were made with a Beckman IR-12 Spectrophotometer using a specular reflectance attachment. Data from this instrument is relative, thus, a control specimen had to be run with the two batches of specimens (before and after irradiation).

---

* With the specimen set to image the reflectometer entrance aperture onto the exit aperture, the light reaching the scattering PM includes only a small amount of scattered light (i.e., that within a cone of 9 arc minutes about the angle of regular reflection).

4.4 Interferometers

Interferometric analyses were made to determine the overall flatness of the polished mirror surfaces, the thicknesses of vacuum deposited reflective films, the microfinish of the polished surfaces, and the differences between irradiated and non-irradiated areas. Three different types of interferometers were used. The first type, a Fizeau interferometer*, was used for measuring overall flatness on the polished surfaces. This instrument uses the double beam Fizeau fringes, formed with mercury 546.1 nm light, to measure variations in path difference between an NBS calibrated reference flat and the test surface. The second type, a Zeiss Interference Microscope, was used to examine the surface finish of the mirrors. This instrument is, in principle, a double-beam Michelson interferometer using either white light or monochromatic light (Thallium 535.0 nm). The third type, a Hilger-Watts thin film interferometer, was used for film thickness measurements and examination of the irradiated mirrors. This instrument utilizes fringes of equal chromatic order.

The general procedure used in interferometer measurements was to overcoat the test mirrors with a thin layer of aluminum to provide both uniform optical properties across the surface, and sharper fringes. A minimum of three similar measurements were taken and averaged for thickness measurements.

---

* Davidson Optronics Inc. Plano-Interferometer Model D-309

5.0 RESULTS AND DISCUSSION

The primary objective of the proton experiments was to obtain sufficient data for predicting degradation during an extended period in a synchronous orbit environment. Secondary objectives of the experiments were to determine whether different substrates and coating batches affect the amount or type of radiation damage, and whether any physical changes occur on the specimen surface during irradiation. To accomplish these objectives, radiation experiments were run to determine dependence of damage on proton flux and integrated flux. All experiments were run using ambient specimen temperature and 10 keV protons. Results showed that substantial degradation in reflectance occurred in selected wavelength bands during irradiation. Experiments and calculations strongly indicated that the degradation was caused by the deposition of a proton-induced contaminant film. In reviewing test results, the reader should be aware that numerous effects observed during irradiation may be related to the presence of a contaminant film.

Typical experimental results for MgF_2 and LiF overcoated mirrors are presented first, and then are jointly discussed in a subsequent section.

5.1 MgF_2/Aluminum Coated Mirrors

In this section of the report typical data is presented from studies on proton integrated-flux dependence, flux dependence, post-irradiation reflectance changes, and surface-finish evaluation.

5.1.1 Integrated-Flux Dependence.- The typical effects of protons on the spectral reflectance of MgF_2/Al-coated surfaces were production of: (1) a broad absorption band centered at about 210 nm; (2) a narrow absorption band centered at about 109 nm; and (3) a slight increase (1 to 2 percent) in reflectance in the region near 130 nm. Reflectance data from a MgF_2/Al-coated Cer-Vit mirror are shown in Figures 6 and 7, illustrating typical radiation effects at a flux of 1.4×10^{11} protons-cm^{-2} sec^{-1}. Figure 6 is a plot of the specular reflectance versus wavelength, and Figure 7 shows the percent change in specular reflectance ($\Delta R/R \times 100$). Integrated flux is the parameter in each plot. Negative values of $\Delta R/R$ represent a decrease in reflectance.

It can be noted in Figure 7 that irradiation with 2×10^{14} protons-cm^{-2} produced a slight increase in reflectance at wavelengths below 140 nm, and initiated growth of the longer wavelength absorption band. The long-wavelength absorption band peaks at about 190 nm (Figure 7) after the initial dose of radiation. Further exposure to radiation produces growth and broadening of the long-wavelength band and initiates the growth of a short-wavelength absorption band at about 109 nm. After an exposure of 10^{16} protons-cm^{-2}, the maximum change in reflectance of both bands is 30 to 35 percent. The peak of the long-wavelength absorption band shifts from about 190 to 210 nm with increasing radiation dose. It

is significant to note that the reflectance at 130 nm does not change after the initial 2 percent increase exhibited after exposure to 2×10^{14} protons-cm^{-2}. It is also significant to note that the reflectance in the wavelength region shorter than 105 nm remains higher than its pre-irradiation value even up to 10^{16} protons-cm^{-2}.

Reflectance measurements on the Cary-14 and IR-12 spectrophotometers indicated no significant degradation beyond about 600 nm wavelength.

A comparison of radiation damage produced on fused silica and Cer-Vit substrate mirrors can be made in Figure 8. In this figure the percent change in reflectance at 210 nm was plotted versus integrated proton flux for two identical mirrors of each type. Mirrors were irradiated at a flux of 1.4×10^{11} protons-cm^{-2} sec^{-1} to an integrated flux of 1×10^{16} protons-cm^{-2}. As can be seen from the small spread in data points, excellent agreement was obtained between the two Cer-Vit mirrors and between the two fused silica mirrors. This reproducibility between similar specimens is an indication that the radiation and environmental conditions were accurately controlled, and that specimens from the same batch produced similar results. The lack of agreement between data from the fused silica and Cer-Vit mirrors can probably be attributed to a slight difference in MgF_2 thicknesses. As discussed later in Section 5.3.5, the spectral character of the reflectance changes is strongly related to MgF_2 thickness. Subtle differences (probably related to MgF_2 thickness) can be noted in Figures 6 and 9 "before-irradiation" reflectance data for fused silica and Cer-Vit mirrors. Fused-silica substrate mirrors had a higher reflectance in the wavelength region from 130 to 250 nm and exhibited lower reflectance from 90 to 110 nm.

5.1.2 Flux Dependence.- The proton flux-dependence study was conducted to establish the validity of irradiating mirrors at fluxes 10^3 to 10^5 higher than the space rate. Fluxes studied in this work included 2×10^9, 1.4×10^{10}, 1.4×10^{11}, and 1.4×10^{12} protons-cm^{-2} sec^{-1}. It was hoped that the nearly thousand-fold spread in fluxes would provide sufficient information to conclude whether or not accelerated tests were valid.

Results showed that damage was essentially independent of flux up to 1.4×10^{11} protons-cm^{-2} sec^{-1}, however, a flux of 1.4×10^{12} protons-cm^{-2} sec^{-1} produced much less damage than lower fluxes (for equivalent integrated fluxes). Thus, damage became dependent on flux between 1.4×10^{11} and 1.4×10^{12} protons-cm^{-2} sec^{-1}. This conclusion is apparent in a summary plot of data (Figure 10) for MgF_2/Al-coated mirrors irradiated at different fluxes. The percent change in reflectance at 210 nm wavelength* is plotted versus integrated flux, with flux as a parameter. With the exception of three points derived from a beryllium mirror, all data shown are for Cer-Vit substrate mirrors.

---

* This wavelength was chosen because it is near the peak of a broad absorption band and changes consistently with radiation exposure.

To illustrate the observed rate effects (Figure 10), a $\Delta R/R$ value of -5 percent was obtained at an integrated flux of 10^{15} protons-cm^{-2} for a flux of 1.4×10^{12} protons-cm^{-2} sec^{-1}. For equivalent integrated fluxes, respective $\Delta R/R$ values of about -10.5 and -11 percent were obtained at fluxes of 1.4×10^{11} and 1.4×10^{10} protons-cm^{-2} sec^{-1}. Similar results can be noted for the specimen irradiated at 2×10^{9} protons-cm^{-2} sec^{-1}.

5.1.3 Post-Irradiation Reflectance Changes.- The primary purpose of this portion of the study was to determine whether reflectance changes would occur as a function of time after irradiation, in both vacuum and air environments. Numerous reflectance measurements were made throughout the program after various periods in vacuum and/or air. Some mirrors were stored in air starting immediately after irradiation, and some were kept under vacuum for various periods of time before beginning air exposure. The shortest air exposure was about 18 minutes (defined by the length of time the chamber pressure was above 10^{-3} torr), and the longest was 2600 hours.

Results of these experiments showed that substantial reflectance changes occurred after irradiation. Reflectance increased (recovered) with time in the wavelength region above about 140 nm, and decreased with time at shorter wavelengths. Reflectance changes are similar for storage in vacuum (5×10^{-7} torr) or at ambient air pressure, although the rate of change is greater in air. To illustrate the post-irradiation reflectance changes, the $\Delta R/R_a$ values at both the short and long wavelength absorption peaks are plotted versus time accumulated after irradiation in Figure 11. The $\Delta R/R_a$ values are referenced to the "after-irradiation" reflectance (R_a) rather than "before-irradiation" (R) values.

Data shown in the figure represents specimens exposed to 10^{16} protons-cm^{-2} at a flux of about 1.4×10^{11} protons-cm^{-2} sec^{-1}. Mirrors exposed to air immediately after irradiation exhibited a -10 to -15 percent change in reflectance (decrease in absolute reflectance) at the short wavelength peak in the first 18 minutes. The increase in reflectance at 210 nm was slightly more than 1 percent in the same time period. It was found that the reflectance at both short and long wavelengths continued to change even up to 2600 hours after irradiation. The respective $\Delta R/R_a$ values at 2600 hours are about -30 percent and +6.5 percent for the Cer-Vit substrate mirrors. Results for fused silica mirrors showed slightly larger changes with time.

To evaluate effects of standing in vacuum ($\sim 5 \times 10^{-7}$ torr), a fused silica mirror was measured immediately after irradiation and then again after 50 hours in vacuum. It was found that the reflectance at the short-wavelength absorption peak decreased about 12 percent, compared to 21 percent for specimens exposed to air for equivalent time. No change

in reflectance occurred at 210 nm after 50 hours in vacuum. The specimen was then exposed to air for time periods of 13 hours and 1012 hours. As noted in Figure 11, the rate of change in reflectance of this specimen was considerably higher than specimens which had been kept in air for the first 50 hours. Furthermore, the total change experienced after 1000 hours at both wavelengths was greater than the specimens which were placed in air immediately after irradiation.

5.1.4 Surface Finish Studies.- The objectives of the surface finish studies were to determine: (1) the comparative microroughness of the three types of substrates; (2) the effect of vacuum deposited coatings on microroughness; and (3) whether or not the protons had any physical effect on the irradiated surface.

A comparison of the microroughness of uncoated Kanigen-nickel/beryllium, fused silica, and Cer-Vit substrates can be made in the electron micrographs shown in Figure 12. These photomicrographs were prepared using a standard replication process and by shadowing the replica with germanium at an angle of 78 degrees from normal. On the polished nickel surface (Figure 12a), grooves and cold flow of material are visible. The approximate width of the largest groove is 260 nm.

It is interesting to compare the difference between the polished nickel surface and the fused silica and Cer-Vit surfaces. In contrast to the nickel surface, the Cer-Vit and fused silica surfaces do not show any evidence of scratches or flow (smearing) of material. This is presumed to be a result of the difference in mechanism of material removal between ductile and brittle materials. The Cer-Vit and fused silica surfaces both have a granular appearance, with the Cer-Vit appearing to be the roughest of the two. The lack of resolution and magnification prohibited measurement of the size distribution of surface irregularities.

Reflectance data from different types of coated mirror surfaces revealed a substantially lower reflectance for beryllium-substrate mirrors in the wavelength region below 600 nm. A comparison of reflectance data from beryllium and Cer-Vit substrates is given in Figure 13. It is presumed that the lower reflectance observed for the beryllium substrate was a result of scattering.

Electron micrograph replicas of surfaces which were coated with Al and MgF_2 were similar in appearance to Figures 12b and c. Thus, it was concluded that the coatings did not significantly change the surface roughness (at 30,000 X magnification).

To conclude whether proton irradiation affects the microroughness of mirror coatings, electron micrographs were made at higher resolution and magnification than those shown in Figure 12. Higher resolution was obtained by shadowing the replica of the surface at a more oblique angle

(80 degrees from normal). A magnification of 52,000 X was employed. An electron micrograph of a MgF_2-overcoated fused silica mirror, irradiated with 10^{16} protons-cm^{-2} at a flux of 1.4×10^{11} protons-cm^{-2} sec^{-1}, is shown in Figure 14a. The unirradiated area of the surface is shown in Figure 14b. It can be noted that the irradiated surface was covered with undulating patterns which are about 19 to 38 nm wide. No evidence of these patterns is present on the unirradiated portion of the surface. A detailed examination indicates considerable undulation but always in the same general direction. Similar surfaces were noted earlier in reference 7 (NASA CR-1024, Figures 18 and 19) where silicon oxide surfaces were irradiated with 16 keV protons. Two possible explanations of these patterns are: (1) preferential sputtering of the MgF_2 surface by the protons; or (2) growth of chains of contaminant film molecules on the surface.

Irradiated MgF_2/Al-coated surfaces were examined with an interferometer to determine whether there was any change in surface height in the irradiated area. Selected mirror specimens were overcoated with aluminum and then examined. It was found that a 4.5 nm increase in height occurred on a specimen which had been exposed to 10^{16} protons-cm^{-2} at a flux of 1.4×10^{11} protons-cm^{-2} sec^{-1}. Conversely, no measurable increase in height was observed on a surface which had received the same integrated flux but at a higher rate (1.3×10^{12} protons-cm^{-2} sec^{-1}). This effect correlates with the observation discussed earlier that less degradation was produced at higher fluxes.

5.1.5 Scattered-Light Data.- Scattered-light measurements performed on the mirrors before and after irradiation did not reveal any significant change in scattering at wavelengths of 253.7 nm or 500 nm. These results should be anticipated because of the small size of the irregularities formed 19 to 38 nm.

A set of typical scattered-light distributions for a fused silica substrate mirror at wavelengths of 500 and 253.7 nm, respectively, are shown in Figures 15 and 16. These plots represent the variation in relative power passing through the exit aperture as the image is scanned across the aperture. The flat top on the peak of the distribution is a result of the image being smaller than the aperture. For these particular records, the theoretical width of the spectral peak is about 10.5 arc minutes. The calibrations in the vertical dimension represent flux relative to the specular peak. The stray light at a scattering angle of minus seven minutes is probably a result of a slight asymmetry in the alignment of the stainless steel baffle tube which extends out from the exit aperture. At 253.7 nm the effect is less than at 500 nm because the reflectance of stainless steel is much lower at shorter wavelengths. Comparing this with the data for positive scattering angles to get a first estimate of the effect of this stray light, it can be seen that it has only a very small effect on the distribution recorded for positive angles. In each case (500 nm and 253.7 nm), the dark current was recorded so that appropriate corrections

could be made. Note that in Figure 15 (500 nm) the dark current was sufficiently low to have a negligible effect on the relative power signal. On the other hand, at 253.7 nm (Figure 16) the output must be corrected for dark current.

A comparison of scattered light distributions at the two wavelengths and for several specimens is shown in Figure 17*. The data for 253.7 nm has been corrected for dark current. The significant observations which can be made from this figure are: (1) there are no strong differences between substrates; the differences shown are not much larger than the experimental error; (2) data at 500 nm is much more reliable than that at 253.7 nm because of dark current corrections in the latter; and (3) despite the uncertainty associated with the 253.7 nm data, scattering at the shorter wavelength is definitely 6 to 9 times that of 500 nm light.

A calculation was performed to obtain an upper limit estimate of the effect of scattering on absolute reflectance measurements. The experimentally-observed scattering distributions were integrated over the solid angle which the internal PM subtends at the specimen when the former is receiving reflected light. These calculations imply that only 0.11 percent of the 500 nm light and 0.99 percent of the 253.7 nm light reaching the PM is scattered light. Thus, the upper limits for the effect of an assumed 10 percent irradiation induced change in scattered light on reflectance data, are about 0.01 percent at 500 nm and 0.1 percent at 253.7 nm. Changes in reflectance observed at these wavelengths are therefore not due to scattering.

It is important to realize that the scattering data shown in Figures 15, 16 and 17 are affected by scattering from both the spherical mirror and the test specimen mirror. Thus, a somewhat more realistic estimate of the scattering distribution of the test specimen would account for the scattering distribution from the reflectometer spherical mirror. Unfortunately, there is no simple way to measure scattering from the spherical mirror alone while it is mounted in the reflectometer. However, if it is assumed that the spherical mirror is of the same initial quality and reflectance as the specimen, it can be shown that about 2/3 of the scattered light in the measured distribution comes from the spherical mirror and only 1/3 from the specimen. Applying this reasoning to the measurement of reflectance with the internal photomultiplier, scattering effects tend to balance out. This comes about because the separation of the internal photomultiplier from the spherical mirror in the incident position, is very nearly equal to its separation from the specimen in the reflected position.

* Recorded data (Figures 15 and 16) were corrected to radiance ratios by dividing by 2.81 to correct for the size difference between entrance and scanning apertures.

5.2 LiF/Aluminum Coated Mirrors

Typical radiation effects data on LiF/Al-coated mirrors are discussed in this section. The irradiation procedures and experiments on these mirrors were similar to that used on MgF_2/Al-coated mirrors.

5.2.1 Integrated Flux Dependence - Typical effects of proton irradiation on the LiF/Al-coated fused silica mirrors are shown in Figures 18 and 19. Figure 18 is a plot of the specular reflectance versus wavelength and Figure 19 shows the percentage change-in-reflectance ($\Delta R/R$) versus wavelength. Irradiation with protons resulted in production of a rather complex, broad absorption band in the wavelength region from about 105 nm to 600 nm, and narrow absorption bands at about 94.5 nm and 100 nm. The growth of the various absorption bands with increased irradiation can be noted in Figure 19. After the initial exposure increment (5×10^{14} protons-cm^{-2}), subpeaks were apparent at 120, 145 and 190 nm. The 120 and 190 nm peaks were of comparable heights until an exposure of 2×10^{15} protons-cm^{-2} was exceeded.

The growth rate of peaks at 95, 120 and 200 nm can be compared in Figure 20. The percentage change-in-reflectance at the three respective wavelengths is plotted versus the integrated proton flux. Data from two identically irradiated specimens were used. Test results show that the 95 and 200 nm peaks continued to grow with increasing integrated flux up to 1×10^{16} protons-cm^{-2}, whereas, the 120 nm peak approached saturation above 10^{15} protons-cm^{-2}.

Scattered light measurements made before irradiation and after 1×10^{16} protons-cm^{-2} showed that no measurable change in scattered light occurred at either 253.7 nm or 500 nm wavelengths.

5.2.2 Flux Dependence - The validity of testing LiF/Al-coated mirrors at accelerated rates was evaluated by irradiating at fluxes of 1.2×10^{10}, 1.3×10^{11}, and 1.2×10^{12} protons-cm^{-2} sec^{-1}. The effects of exposing specimens at different rates are shown in Figure 21. The percentage change-in-reflectance of three specimens, irradiated at different fluxes to an integrated flux of 10^{15} protons-cm^{-2}, is plotted versus wavelength. The most significant observation to be made from the curves is that the amount of radiation damage is both flux dependent and wavelength dependent. For example, at the 200 nm wavelength peak a large flux-dependence occurred between fluxes of 1.3×10^{11} and 1.2×10^{12} protons-cm^{-2} sec^{-1}, with little dependence between 1.2×10^{10} and 1.3×10^{11} protons-cm^{-2} sec^{-1}. On the other hand, at the 120 nm peak a small flux-dependence was noted between 1.3×10^{11} and 1.2×10^{12} protons-cm^{-2} sec^{-1}, and a large flux-dependence between 1.2×10^{10} and 1.3×10^{11} protons-cm^{-2} sec^{-1}.

5.2.3 Post-Irradiation Reflectance Changes.- The LiF/Al-coated mirrors were evaluated for post-irradiation reflectance changes similarly to the MgF_2/Al-coated mirrors. Specimens were stored in ambient air, vacuum ($\sim 5 \times 10^{-7}$ torr), and argon (99.996 percent label purity) for various periods of time after irradiation. It was found that the reflectance changed with time after irradiation and that changes occurred in both air and argon environments. The rate of change in air was considerably higher than in argon. The specimen retained in vacuum after irradiation showed no significant reflectance changes after 16 hours.

Results of the experiment in which a mirror was exposed to ambient air after irradiation with 10^{16} protons-cm^{-2} are shown in Figure 22. The percentage change-in-reflectance is plotted versus wavelength for conditions immediately after irradiation, after 14 minutes in air, and after 38 hours in air. The 14 minute air exposure was accomplished by backfilling the chamber with air to atmospheric pressure and then immediately pumping down. The time required for backfilling and pumping down to 10^{-3} torr pressure was 14 minutes. It can be noted in the figure that degradation continued in the wavelength region below 110 nm and at wavelengths longer than about 130 nm. A small increase in reflectance (or recovery) occurred between about 110 nm and 130 nm. The width of the band in which recovery occurred widened by progressing to longer wavelengths as time increased.

Data from the LiF/Al-coated mirror which was allowed to stand in argon for 62 hours after irradiation are shown in Figure 23. It can be noted that the reflectance degraded in the wavelength regions below 108 nm and above 130 nm, similar to the specimen which was exposed to air (Figure 22). The rate of degradation observed in argon, however, was considerably lower than that which occurred in air. Contrary to results obtained for exposure to air, no reflectance increase occurred in the region between 108 and 130 nm.

Results of the above experiments showed that the magnitude of post-irradiation reflectance changes is dependent upon the environment to which the specimen is exposed. The question as to whether an oxygen or water vapor reaction is involved cannot be answered with available knowledge.

5.3 Discussion of Results

It was suspected early in the program that proton-induced contamination effects were the dominant cause of observed reflectance degradation. The suspected mechanism involved was radiation cross-linking or polymerization of organic molecules which impinge on the mirror surface from the vacuum system. To verify this suspicion a rather extensive investigation of the contamination phenomena was undertaken. The approach involved: (1) experiments and calculations to determine whether a contaminant film was deposited during irradiation; (2) cleaning experiments to determine the extent to which such contaminant films affected the data; and (3) calculations to predict the spectral reflectance changes produced by a contaminant film.

Much emphasis was placed on the investigation of contamination because such phenomena can occur in space or during environmental tests of optical mirrors. In the following discussion the term "contaminant film" is used rather loosely to explain the increase in surface height on the irradiated area. It should be noted, however, that a chemical analysis of the film was not made and therefore the possibility exists that different phenomena occurred. A discussion of results of experiments aimed at determining whether a contaminant film was deposited on the mirrors follows:

5.3.1 Contaminant Detection Experiments.- Evidence that a contaminant film formed during irradiation came from several observations and experiments. First, it was noted that a water-break-free film would not form on irradiated test specimens. This suggested the presence of an organic film. Second, an experiment in which changes in interference characteristics of a specially prepared mirror were evaluated indicated deposition of a contaminant film during irradiation. The special mirror was coated with aluminum and overcoated with vacuum-deposited fused silica (2 microns thick) to produce adequate interference modulations on the reflectance curve throughout the visible wavelength region*. This technique for detecting contamination (ref. 12) involves measuring the reflectance before irradiation, after irradiation, and after cleaning with finely-divided calcium carbonate. The nature of changes in interference characteristics produced by irradiation and cleaning provided information for concluding whether a contaminant film was deposited during irradiation.

The contamination detection specimen was exposed to 10^{16} protons-cm^{-2} at a flux of 10^{11} protons-cm^{-2} sec^{-1}. Reflectance data before and after irradiation and after cleaning are shown in Figure 24. Data were plotted as straight line segments between interference maxima and minima positions. It can be noted that the irradiation produced

---

* After preparation, the mirror was exposed to ultraviolet radiation in air for about 18 hours to reduce the absorption in the ultraviolet wavelength region. A General Electric UA-3 low pressure mercury-arc lamp was used.

both a shift in wavelength of maxima and minima to shorter values and a decrease in reflectance of interference minima at wavelengths below about 500 nm. The magnitude of the changes at minima positions became progressively greater as wavelengths decreased. A slight decrease in reflectance at maxima positions was apparent in the region below 380 nm. An estimate of the contaminant film thickness, from calculations performed in ref. 12 assuming optical constants of n = 2 (refractive index) and k = 2 (extinction coefficient), showed it to be less than 0.5 nm thick. It may be recalled that interferometer measurements (Sec. 5.1.4) on a similarly irradiated specimen indicated a film thickness of 4.5 nm. This difference in thickness suggests that one or both of the above assumed optical constants is too large.

After the post-irradiation reflectance measurements had been made, the fused silica/Al-coated mirror was evaluated for water wetting characteristics. It was found that the irradiated area would not wet with water, whereas, surrounding unirradiated areas formed a break-free film. This was a good indication that an organic film had been affixed to the irradiated area. The surface was then scrubbed with $CaCO_3$ on a wet cotton pad. Scrubbing was continued until the irradiated area formed a water break-free film. An interesting observation made during scrubbing was that the $CaCO_3$ was preferentially attracted to the irradiated area such that it could not be flushed off with water. Scrubbing with a camel-hair brush under running water removed the $CaCO_3$ from that area. The implication of this effect was that the irradiated area may have become sufficiently rough to trap the $CaCO_3$ particles. This observation is substantiated with electron micrograph results (Figure 14).

Following cleaning, the reflectances at interference maxima and minima positions were restored to their pre-irradiation values, thus, indicating the removal of a thin surface film from the fused silica. Since no change in the wavelength position of maxima and minima occurred during cleaning, it was concluded that no fused silica was removed in that operation. The permanent shift of interference maxima and minima wavelength positions is evidence of radiation effects in the fused silica film.

The general conclusion from this contamination detection experiment was that a very thin contaminant film was formed on the surface during irradiation.

A third contamination detection experiment was conducted with a platinum coated mirror. The platinum film was irradiated with protons, similarly to other mirrors, and measured for reflectance changes. It was assumed that the optical properties of platinum would not change during irradiation, therefore, if a change in reflectance occurred it could be related to the presence of a contaminant film. The platinum mirror, furnished by the Naval Research Laboratory (NRL), comprised

10 nm of platinum deposited on plate glass. The platinum was applied using standard procedures. The mirror was irradiated with 10^{16} protons-cm^{-2} at a flux of 1.4×10^{11} protons-cm^{-2} sec^{-1}. Reflectance and $\Delta R/R$ data are shown in Figures 25 and 26, respectively. Data are given in Figure 26 for various integrated fluxes, after 16 hours standing in vacuum, and after standing in air for 68 hours. The proton irradiation caused a rather large decrease in reflectance over the entire wavelength region (95 to 250 nm). The plot of $\Delta R/R$ shows that the decrease in reflectance reached a maximum of -40 percent at about 120 nm wavelength. Post-irradiation reflectance measurements on the platinum coated mirror showed continued decreases in reflectance throughout the wavelength region. It should be noted that the largest post-irradiation reflectance changes occurred in the region where maximum changes occurred during irradiation.

In comparing the post-irradiation reflectance changes observed on MgF_2, LiF, and platinum coated mirrors, certain differences in behavior are apparent. Results obtained on MgF_2 and LiF overcoated mirrors showed recovery in one wavelength region and continued degradation in others, whereas, platinum continued to degrade at all wavelengths measured. A possible explanation for these post-irradiation reflectance changes is the presence of an unstable polymer film which reacts with oxygen or water vapor over a long period of time. The resulting optical property changes in the contaminant film in conjunction with optical properties of the mirror coatings, could explain the difference in behavior between coating types.

A fourth experiment which indicated the presence of a contaminant film involved irradiation and subsequent cleaning of a quartz window. The quartz window was irradiated with 10^{16} protons-cm^{-2} at a flux of about 10^{12} protons-cm^{-2} sec^{-1}. The transmittance at 200 nm wavelength decreased from 89 to 82 percent (ref. 16). Subsequent cleaning with finely-divided calcium carbonate restored the transmittance to 89 percent, thus, indicating that the loss in transmittance was caused by absorption in a contaminant film.

The above experiments strongly indicated that a contaminant film was applied to the surface during irradiation. Based on the assumption that the mechanism of deposition involved polymerization of organic molecules on the surface, further studies were conducted to attempt to verify such a mechanism. These studies included: (1) residual gas analyses in the test chamber to determine the gases present; (2) calculations to predict contaminant film growth rate and an irradiation experiment to determine whether the contaminant film deposition rate is controlled by the vacuum environment or radiation parameters (flux and integrated flux); (3) cleaning experiments to measure the residual optical damage after removal of the contaminant films; and (4) calculations to predict reflectance changes induced by the presence of a contaminant film. Discussions of results of these various studies are given in the following sections.

5.3.2 Residual Gas Analyses.- Residual gas analyses were made in the test chamber using a magnetic, sector instrument*. Mass spectra were obtained with the chamber blanked off from both the accelerator and monochromator, during the reflectance measurement mode of operation, and during the irradiation mode of operation. All conditions were similar to actual mirror tests with the exception that the proton rf source could not be operated during the irradiation mode because of electrical noise problems.

Mass analysis data for the three modes of operation were adjusted for comparable output at atomic mass unit (amu) 14 (assuming the isolated chamber to be baseline condition) and are plotted in Figures 27, 28 and 29. Determination of the actual gas composition and sources of contaminants was not undertaken because it was not within the scope of the present program. However, cursory evaluation revealed the following information:

1) The dominant gas species for any mode of operation was hydrogen. Operation of the system with either the monochromator or low energy accelerator (both of which inject hydrogen gas) produced essentially 100 percent hydrogen in the chamber. Pumping on the chamber for three days only reduced the hydrogen concentration to about 50 percent.

2) A relatively high concentration of hydrocarbon molecules with masses up to about 90 amu was present in both the isolated test chamber, and the chamber when open to the monochromator. Although a silicone spectrum was anticipated (due to DC-704 oil in the diffusion pump), it was not detected;

3) The hydrocarbon molecules were not effectively trapped-out with the liquid nitrogen trap in the test chamber;

4) A substantial decrease in the proportion of hydrocarbons present in the chamber was observed during operation with the accelerator.

* VEECO Instruments Inc. Model GA-4R

In regard to sources of hydrocarbon molecules, several interesting observations can be made. It was noted that the cylindrical cold trap in the chamber was not effective in trapping out organic molecules. This may indicate that the source of the hydrocarbons was semi-infinite. (Backstreaming from a pump would be a semi-infinite source, whereas, outgassing molecules from O-rings would decrease with time as the volatile molecules were depleted.) The observation that the hydrocarbon molecules appear to come from a semi-infinite source correlates with the fact that reflectance degradation on mirror specimens was reproducible throughout the program.

The proportional decrease of hydrocarbons during operation with the accelerator indicates that: (1) the ion pump (on the accelerator) is more effective in pumping hydrocarbons than is the turbomolecular pump; and (2) the source of hydrocarbons in the test chamber may have been the vacuum pumping system.

5.3.3 Contaminant Film Deposition Rate.- To verify the hypothesis that a hydrocarbon film was deposited on the mirror surfaces during irradiation, a calculation was made using kinetic gas theory. It was assumed that hydrocarbon molecules impinge on the surface at a rate (ν) given by the following equation (ref. 17):

$$\nu = 3.513 \times 10^{22} \frac{P}{(MT)^{1/2}} \text{ molecules-cm}^{-2} \text{ sec}^{-1}$$

where:

P = pressure, mm Hg (torr)

M = molecular weight

T = surface temperature, ^{o}K

It was also assumed that the partial pressure of the hydrocarbon molecules was 1×10^{-9} torr, the hydrocarbon species was CH_4, the specimen temperature was $300^{o}K$, and the time required for irradiation was 22 hours.

Results showed that if all impinging molecules were permanently affixed to the surface by protons, a film thickness of about 30 nm could be accumulated in 22 hours. In this case the rate of deposition would be controlled by the arrival rate of the molecules. If it is assumed that the rate of deposition is limited by the proton flux* (10^{11} protons-cm^{-2} sec^{-1}), a film thickness of about 6 nm would be accumulated in 22 hours. This latter value is in reasonable agreement with the measured increase in surface height of 4.5 nm (Sec. 5.1.4), suggesting that the accumulation is primarily limited by proton flux for this case.

---

* This assumption implies that one molecule is affixed for each arriving proton. Hence, the contaminant film thickness is proportional to the integrated flux.

On the other hand, an increase of the flux to 10^{12} protons-cm^{-2} sec^{-1} reduces the exposure by a factor of ten (to 2.2 hours) for the same integrated flux of 10^{16} protons-cm^{-2}. If every impinging molecule adheres to the surface, this shorter exposure permits accumulating only 3 nm of contaminant. This value is clearly less than the thickness predicted by assuming the contaminant build-up to be proton flux limited; since accumulation is proportional to integrated flux, this prediction is - as before - 6 nm. Thus, for the higher flux it must be concluded that contaminant deposition is limited by the contaminant partial pressure, and that the lesser accumulation will result in less reflectance degradation. This much is confirmed by experiment (Sec. 5.1.2).

To attempt to verify this conclusion, a mirror was irradiated at the higher flux in an atmosphere of reduced hydrocarbons. This should have resulted in reduction in contaminant accumulation and proportionally less reflectance change. Irradiation was carried out in the accelerator beam tube (see Figure 2) isolated from the test chamber; flux was 2.3×10^{12} protons-cm^{-2} sec^{-1}. Residual gas analysis data (Figures 27 and 29) indicated that this vacuum environment would have a lower partial pressure of hydrocarbons. Results of the beam tube experiment showed that the amount and spectral character of the reflectance changes were approximately the same as those induced at similar flux and dosage in the test chamber. The most likely explanation for the inconsistency of this result is that the assumption of fewer hydrocarbons in the beam tube, is invalid. In this connection it should be noted that the residual gas analyses were atypical of irradiation conditions in that ion gun could not be operated during the time of analysis.

5.3.4 Cleaning Experiments.- Since results of contamination detection experiments strongly indicated that a contaminant film was deposited during irradiation, it was imperative to delineate the changes in reflectance caused by contamination from those caused by proton damage. To accomplish this, cleaning experiments were undertaken. It was hoped that by noting the reflectance before and after removal of the contaminant film, the permanent radiation damage to the reflective coatings could be ascertained*. A discussion of the results of cleaning experiments follows.

Observations of irradiated MgF_2/Al-coated mirrors prior to cleaning revealed that an unusual breath pattern (diffuse appearance caused by condensed breath vapors) occurred in the irradiated zone. It was also noted that a water-break-free film would not form anywhere on the surface.

An unsuccessful attempt was made to remove the contaminant film from a MgF_2/Al-coated mirror by a Freon and Collodion treatment. The surface was flushed with Freon prior to application of Collodion. No change in reflectance occurred in the vacuum ultraviolet wavelength

* The majority of protons will pass through the reflective films regardless of the presence of a thin contaminant film. The projected range of 10 keV protons in LiF, MgF_2 and aluminum was calculated to be 105, 99 and 120 nm, respectively.

region. The same mirror was then scrubbed with finely-divided $CaCO_3$ using a wet surgical cotton pad. The calcium carbonate was carefully decanted to obtain only the smallest particles for scrubbing. After several light passes with the cotton it was noted that the surface wet better, however, the unusual breath pattern was still present in the irradiated zone. The scrubbing was then continued until fine scratches appeared on the mirror. The unusual breath pattern could still be produced in the irradiated zone after cleaning. Reflectance data after cleaning is shown in Figure 30. The effect of the abrasive cleaning was to: (1) eliminate the strong absorption bands at 108 and 210 nm; (2) increase the reflectance above pre-irradiation values in the wavelength region below 116 nm; and (3) only partially restore the reflectance in the wavelength region from 160 to 350 nm (the limit of measurement)*. These latter changes indicate that the abrasive cleaning may have reduced the thickness of the MgF_2 film. Visual observations indicate that the scattered light from the surface should have increased, however, the effect of such losses on specular reflectance was not determined. It was generally concluded that the calcium carbonate cleaning technique was too harsh.

An attempt was made to remove the contaminant film by soaking in carbon tetrachloride. It was found that no change in reflectance occurred after soaking for 11 hours at ambient temperature. These results are consistent with those of other experimenters in attempting to remove radiation-polymerized organic films (refs. 7, 18, 19 and 20).

It was theorized that if the contaminant film was hydrocarbon (in contrast to silicon), it might be possible to remove it by oxidation with fluorine or atomic oxygen. Oxidation should produce gaseous or volatile compounds. It was anticipated that the MgF_2 or LiF overcoatings would not be decomposed because they already are stable fluorine compounds.

Exposure of pieces of contaminated aluminum and stainless steel to fluorine was attempted first. These metals had been irradiated over about a six month period and were discolored to a yellow-brown appearance. The specimens were placed in small bell-jars which were evacuated and purged twice with dry nitrogen before introducing the fluorine. This minimized the possibility of forming hydrofluoric acid from residual water vapor. The bell jars were then filled with fluorine to a pressure of about one atmosphere. It was noted that the fluorine caused the yellow film to disappear over about a 45 minute period. A similar fluorine exposure was then given to an irradiated, MgF_2/Al-coated mirror except that the exposure time was reduced to 35 minutes. It was noted that the entire mirror surface wet with water after exposure to fluorine, but that the unusual breath pattern was still visible in the irradiated area. Subsequent reflectance measurements showed that substantial changes in reflectance had occurred in the vacuum-ultraviolet wavelength region.

*The ultraviolet reflectometer was initially designed for operation at wavelengths shorter than 250 nm. It was demonstrated later that reasonably accurate measurements could be made out to wavelengths of 350 to 400 nm.

Specular reflectance and $\Delta R/R$ data are shown in Figures 31 and 32, respectively. It can be noted in Figure 32 that the fluorine nearly eliminated the absorption band centered at 210 nm, and increased the absorption in the wavelength region below 113 nm. Examination of this mirror with an interferometer showed that a 5.9 nm thick film was still present on the irradiated area. This suggests that the fluorine may not have removed the contaminant film, but only changed its optical properties. Three other irradiated MgF_2/Al-coated mirrors were also exposed to fluorine with varying results. In all cases the fluorine nearly eliminated the absorption band centered at 210 nm, however, below about 130 nm data was conflicting. It was noted that two of the MgF_2/Al-coated mirrors turned slightly hazy (or diffuse) in the irradiated area as a result of exposure to fluorine.

An unirradiated MgF_2/Al-coated mirror was exposed to fluorine to ascertain whether reflectance changes discussed above, could have been caused by changes in the MgF_2 or aluminum films. It was found that the reflectance increased in the wavelength region from 106 to 180 nm. The maximum increase noted was 9 percent ($\Delta R/R \times 100$) at 110 nm (Figure 33). Possible explanations for this increase in reflectance of the unirradiated mirror include: (1) optical property changes in the MgF_2 film resulting from elimination of an inherent fluorine deficiency; and (2) a thickness change of the MgF_2 film. If an inherent deficiency does exist, the results suggest that mirrors of this type should be treated with fluorine after coating.

Lithium fluoride overcoated mirrors were also exposed to fluorine in an attempt to remove the contaminant film by oxidation. The results were completely unsatisfactory because of etching.

In general, the fluorine cleaning technique did not provide satisfactory results, therefore, experiments were initiated to evaluate atomic oxygen as a cleaning agent. The oxygen cleaning technique involved exposing mirror specimens in an atomic oxygen plasma created by an rf source. The mirror specimen was placed in a vacuum chamber which was evacuated to about 5×10^{-2} torr pressure. The chamber was then back-filled with oxygen to a pressure of 4.5×10^{-1} torr. An rf antenna, operated at one end of the chamber, provided sufficient excitation energy to ionize oxygen throughout the chamber. No accelerating potentials were applied in the chamber.

Results of oxygen cleaning an irradiated MgF_2/Al-coated mirror are given in Figure 34. The mirror was exposed for only 5 minutes. The reflectance at wavelengths above about 140 nm was restored to within 2 percent of its value before irradiation. In the region below 120 nm the reflectance exceeded the pre-irradiation value by as much as 20 percent ($\Delta R/R \times 100$). No visible effects were present on the mirror surface. Interferometric examination of the surface showed that the contaminant film was not present after cleaning.

The oxygen cleaning technique was then evaluated on an irradiated LiF/Al-coated mirror. Results are shown in Figures 35 and 36. It was found that a 5 minute exposure restored the reflectance to within 7 percent of its pre-irradiation value at all wavelengths. An additional 5 minute exposure, however, began to degrade the reflectance again in the region from 99 nm to 112 nm and initiated crazing on the mirror surface in one small patch. This result suggests that a 5 minute exposure is sufficiently long, or too long for removing the contaminant film. Interferometric examination revealed that the contaminant film was not present after cleaning.

In general, the atomic oxygen cleaning technique was highly successful in demonstrating that the bulk of the damage observed during irradiation was caused by the contaminant film. The small net change which remained after cleaning could be the result of proton damage to the reflecting coatings, the result of residual contamination, or the result of removing a small amount of the MgF_2 coating. Analysis on a theoretical basis (as in Section 5.3.5) favors interpretation as removal of a small amount of MgF_2 coating. A cleaning technique of this type may be of great value for both commercial and space applications. For example, in commercial applications it may be useful for cleaning hydrocarbons from optical mirrors and prisms, and from surfaces which are to be prepared for bonding. A possible space-program application is restoring the reflectance or transmittance of optics which have been contaminated in space or during Earth tests. Since contamination of this type is a significant problem facing space optical systems, it is recommended that the oxygen technique be developed and evaluated for such uses.

5.3.5 Prediction of Contaminant Film Induced Reflectance Changes.- Calculation of reflectance values from classical electromagnetic theory forms the basis for an exacting test of the hypothesis that mirror degradation resulted from the deposition of a contaminant film. For light of zero polarization, incident normally, the calculation requires only a knowledge of the thicknesses and optical constants (refractive index, n, and extinction coefficient, k) of the various layers which make up the reflecting boundary. These conditions on the incident light are sufficiently approximated in the experiment (7.5 deg. of arc incidence in monochromator, 6.0 in reflectometer) so as to involve negligible error in comparing measured and calculated reflectances.

For the work described below, solutions of the electromagnetic equations, based on a transmission line model of the boundary value problem, were programmed for a digital computer. Reflectances were calculated at 2.5 nm intervals from 95 to 345 nm, for a structure of opaque aluminum overcoated with magnesium fluoride.* A contaminant layer was then added and reflectances were recalculated. It was desired that the calculations predict: (1) reflectances before and after proton irradiation, that is with and without the contaminant film; (2) changes in the damage spectrum ($\Delta R/R$ vs λ) as the dosage (or contaminant film thickness) is increased; and (3) changes which result when a mirror with increased thickness of magnesium fluoride is irradiated.

* See Appendix C for optical constants for MgF_2 and aluminum.

A basic difficulty encountered was the lack of optical constants data for the contaminant film. Following a suggestion (ref. 21) that maximum change of reflectance should occur at interference minima and minimum change at interference maxima, a series of preliminary calculations were performed* to relate reflectance to optical constants and thickness of a contaminant film at selected wavelengths (see Appendix D for additional detail). These results were compared with typical observed reflectance changes and contaminant film thickness data to obtain n and k values at two wavelengths. By drawing dispersion-like curves through each pair of points, these data were extrapolated to other wavelengths.

With this simple, first approximation, the spectral dependence of reflectance was explored throughout the wavelength region showing large changes during radiation. The success achieved shows that all major changes observed in the test program are explainable in terms of contamination. The salient features of the predicted changes - all confirmed by relation to observed effects - are the following:

1) For the mirrors coated with 25 nm of magnesium fluoride, the change in reflectance occurs in two degradation peaks - a relatively narrow band centered near 110 nm and a broad band near 220 nm;

2) Between these degradation peaks the change in reflectance drops effectively to zero at 130 nm;

3) With increasing dosage, each of the three main features described above shifts to longer wavelength and shows increased degradation;

4) For a mirror coated with 43 nm of magnesium fluoride, these same three features appear, but shifted to longer wavelengths.

The behavior described in (1), (2) and (3) can be observed in the curves of Figure 37, which show degradation as a function of wavelength for several thicknesses of contaminant. The agreement between predicted and observed degradation is shown in Figure 38.

The experimental data for a fused silica mirror served as input data for determining the contaminant optical constants (Appendix D). As a result, exact agreement was expected between the experimental degradation at 200 nm and that calculated for a thick contaminant layer. Approximate agreement was expected at 121.6 nm. Agreement was realized within the consistency of the optical constants for aluminum and magnesium fluoride used in the preliminary calculations and the present calculations. The agreement at other wavelengths is, of course, the substance of the argument for the contaminant theory. The excellent agreement of the short-wavelength degradation peak and the intermediate

---

* By Mr. W. R. Hunter of the Naval Research Laboratory

minimum at about 130 nm with experimental results, should be particularly noted in Figure 38. At wavelengths shorter than 110 nm, agreement between calculated and measured values is less convincing than at longer wavelengths. This is largely a result of uncertainty in the optical constants of magnesium fluoride which is resonant at wavelengths near 110 nm. The experimental curve of Figure 38 in this region has been drawn in consonance with the calculated shape, but it should be noted that the density of experimental points is insufficient to render the detail shown.

To test the theory for a case of a thicker contaminant film, calculated reflectance changes were compared to data from a mirror which was irradiated with more than 10^{16} protons-cm^{-2}* (Specimen T-19). It was found that changes produced by a 15 nm-thick contaminant film, provided the best fit to experimental data (Figure 39). A significant observation to be made in the figure is the ability of the theory to predict the shift of maxima and minima positions to longer wavelengths (compared to those shown in Figure 38). Although calculated data shown in Figure 39, assumes a 15 nm-thick contaminant film, interferometric film thickness measurements** and the maximum degradation experienced at the long-wavelength absorption peak, suggest a slightly thinner film.

The calculated effect of depositing a 5 nm-thick contaminant film on a mirror overcoated with 43 nm of MgF_2 ***, is shown in Figure 40. Experimental data for an exposure of 10^{16} protons-cm^{-2} are also shown. In comparing experimental and predicted damage curves, reasonable agreement is seen between the order and magnitude of the maxima and minima. However, all features on the theoretical curve occur at longer wavelengths than their experimental counterpart. Here again, analysis of a trend proves useful. The change in predicted and measured behavior caused by increasing the magnesium fluoride coating thickness from 25 nm to 43 nm can be observed by correlating Figures 38 and 40. As can be seen, the trend of change predicted by calculation is confirmed in experiment.

The basic agreement between calculated and measured reflectance is shown in Figures 41 and 42. Figure 41 compares the calculated reflectance for a 25 nm MgF_2 coating with the reflectance values obtained for the specimens of Figures 38 and 39 before proton irradiation. Figure 42 provides similar information for the mirror coated with 43 nm of MgF_2 whose damage spectrum is shown in Figure 40. For both MgF_2 thicknesses, the agreement is generally good for long wavelengths (> 140 nm), fair at the onset of MgF_2 absorption (110 to 140 nm), and rather indifferent at wavelengths shorter than the absorption edge (< 110 nm).

---

* This mirror was used for checkout of the system and received an unknown integrated flux above 10^{16} protons-cm^{-2}.

** An area weighted mean of 13.6 nm

*** This mirror was provided by Dr. J. F. Osantowski, Goddard Space Flight Center; the 43 nm thickness quotation was supplied with the mirror.

Analysis of the residual disagreement between theory and experiment is not easy. A partial analysis indicates that better agreement would be obtained for the thick MgF_2 coating with an assumed MgF_2 thickness about 10 percent less. Similarly, an increase of 5 to 10 percent in the assumed 25 nm MgF_2 coating thickness would improve agreement of the basic reflectance curve at the absorption edge and could improve the damage spectrum match.

At wavelengths shorter than 110 nm, better agreement with experiment might be achieved by tailoring the optical constants of magnesium fluoride. It is not immediately apparent that a unique description suitable for all specimens of magnesium fluoride could be achieved; that is, each crystal from which coatings are prepared might have slightly varied absorption characteristics.

5.3.6 Degradation In Space.- The primary objective of this study was to determine the effects of the synchronous-orbit proton environment on mirror surfaces. This section is therefore devoted to discussing program results with respect to that objective. As developed in the foregoing sections, the primary mechanism of damage was proton-induced deposition of a contaminant film onto the mirror surfaces. Results of cleaning experiments and theoretical predictions of reflectance changes on MgF_2/Al-coated mirrors, quite conclusively show that the contaminant film accounted for essentially all of the observed damage. Furthermore, since the contaminant film was sufficiently thin ($\sim$ 5 nm the irradiation of mirror coatings proper was not inhibited. Thus, the normal proton radiation effects such as color center production, sputtering, and blistering are apparently of negligible consequence for these surfaces and radiation exposures (10^{16} protons-cm^{-2})*. The same conclusion cannot yet be made for LiF/Al-coated mirrors because reflectance changes have not been theoretically predicted. Cleaning experiments on those mirrors indicated, however, that the majority of damage could be accounted to the contaminant film.

It may be recalled from Section 2.0 that at synchronous orbit a mirror surface with 2π geometry will encounter about 5.5×10^{15} protons-cm^{-2} $year^{-1}$, with roughly 70 percent having energies less than 30 keV. Assuming no dependence of damage on proton energy, (i.e., 10 keV protons adequately simulate the energy spectrum in space), an integrated flux of 10^{16} protons-cm^{-2} represents about two years in synchronous orbit. The overall program results thus lead to the conclusion that negligible degradation will occur on MgF/Al-coated mirrors over a two year period in synchronous orbit. The same conclusion can probably be stated for LiF/Al-coated mirrors, with the reservation that contaminant-film induced effects have not yet been verified by theory.

* A cautionary note in this regard is consideration that the presence of a contaminant film may have interfered with mechanisms for loss of atoms from the fluoride coating during irradiation.

6.0 CONCLUSIONS AND RECOMMENDATIONS

As a result of experiments conducted in this program, the following conclusions have been reached:

1) Proton exposure, equivalent to about two-years of unshielded operation at synchronous orbit, induced no significant reflectance change in either MgF_2/Al or LiF/Al-coatings in the wavelength interval of 90 to 50,000 nm;

2) Mirrors coated with MgF_2/Al and LiF/Al (as well as other coatings) exhibit significant reflectance loss in the vacuum ultraviolet as a result of proton induced deposition of a contaminant film;

3) The reflectance of irradiated mirrors could be restored to nearly pre-irradiation values by removing the contaminant film in an atomic oxygen plasma;

4) Irradiation of mirrors with 10^{16} protons-cm^{-2} caused no measurable change in scattered light at either 253.7 or 500 nm wavelengths;

5) The necessity of in-situ reflectance measurements was not established since the mirror degradation was caused by contaminant film formation rather than by coating or substrate damage;

6) The type of mirror substrate (fused silica, Cer-Vit, or Kanigen-nickel plated beryllium) was immaterial to the radiation effects observed in the experiments;

7) Substrates of fused silica and Cer-Vit were polished to a better finish than the Kanigen-nickel surface;

8) Electron photomicrographs showed that application of vacuum deposited coatings to polished substrates did not significantly affect the microroughness of the surface.

The following recommendations are presented as a result of this research:

1) Additional proton radiation experiments should be conducted in ultra-high vacuum to study radiation effects in a cleaner environment. Such experiments are required to verify that radiation-induced contaminant deposition does not inhibit the coating damage mechanisms;

2) A feasibility/development study should be conducted on the oxygen cleaning technique to evaluate its use for restoring reflectance of mirrors contaminated in space or in large vacuum chambers;

3) A space flight experiment should be developed to measure degradation of ultraviolet-reflecting mirrors down to 100 nm wavelength. Since optical properties of these mirrors are extremely sensitive to thin contaminant films, the experiment should include exposures to both a "clean" and "outgassing-organic" environment;

4) Scattering experiments should be conducted with self-imaging test specimens so that absolute data can be obtained at wavelengths shorter than 253.7 nm;

5) A program should be conducted to determine the contaminant film deposition mechanism and to develop a suitable theory for predicting contaminant film growth from known environmental conditions.

7.0 APPENDIXES

APPENDIX A

MIRROR SAMPLE PROCUREMENT SPECIFICATIONS

Mirror Application.- These mirrors (of ultraviolet astronomical telescope quality) are to be used to determine the effects of charged particle irradiation on their reflectance and specularity in the far-ultraviolet to middle-infrared wavelength region.

Mirror Specification.-

1) Size

All samples shall be of dimensions:

Length of sides	2.00 $\pm$ 0.05 inches square	(5.08 cm)
Thickness	0.75 $\pm$ 0.10 inch	(1.9 cm)

2) Substrate Material

Beryllium-Kanigen - Grade HP-40 from Beryllium Corporation, Reading, Pennsylvania. All surfaces to be plated with Kanigen Nickel to a thickness of 0.006 inch (0.015 cm). Plating shall be continuous on all surfaces.

Fused Silica - Corning Fused Silica #7940 Mirror Blank Quality.

Cer-Vit - Premium Grade Mirror Blank Material C-101, Owens-Illinois, Toledo, Ohio.

3) Surface Figure

One of the 2- by 2-inch surfaces of each sample shall be polished flat over a 1.875-inch-diameter (4.76 cm) aperture to $\lambda/10$ for the mercury green line (546.1 nm).

4) Surface Quality

There shall be no evidence of gray or orange peel on the uncoated and finished mirror surface when viewed with a 5X eye loupe. Surface defects classified as pits, digs, or sleeks shall not exceed a 60-40 finish as generally defined by Mil Spec MIL-O-13830A.

5) Reflective Coatings

MgF_2/Al:

Coatings were applied by Optical Coating Laboratory, Inc., Santa Rosa, California. Samples to be coated shall be aluminized to a thickness of 60 to 120 nm (just visibly opaque) with fast evaporated, high purity Al and overcoated with approximately 25 nm of MgF_2 to produce a minimum reflectivity of 0.73 at 121.6 nm and a reflectivity versus wavelength curve similar to that obtained by Hass & Tousey (J. Opt. Am. 49, 601, Figure 17).

LiF/Al:

Coatings were applied by Dr. George Hass, U. S. Army Electronics Command, Night Vision Laboratory. Mirror samples shall be coated to a thickness of 60 to 120 nm with fast-evaporated, high-purity aluminum and overcoated with approximately 14 nm of LiF. A minimum nominal reflectivity of 72 percent at 102.6 nm shall be required. The mirror temperature shall be maintained at near ambient temperature during vacuum operations.

6) Uniformity

All mirror specimens of a given type shall be coated in the same batch. Uniformity of reflectance shall be within $\pm$ 0.05 at 102.6 nm and 121.6 nm for LiF and MgF_2 overcoated mirrors respectively.

7) A witness blank shall be included with the mirror batch during the coating process. A strip 0.08 to 0.13 cm wide shall be masked across the center of the witness blank. Commercial microscope slides are acceptable.

8) Supports for the mirrors during evaporation must not intrude more than 0.15 cm onto the mirror face.

9) All surfaces except the mirror surface shall be ground flat with an 80-grit finish.

10) Surfaces should be square with respect to each other and the mirror face to within 0.25 deg. of arc.

11) Each sample shall be permanently marked on the edge (vacuum proof) with a code showing material and sample number.

12) All sharp edges shall be removed by 45-deg. of arc beveling, 0.02 to 0.05 cm on the flat.

13) The substrate material shall be ordered from a specific and identifiable batch or lot. Mirror samples shall be accompanied by detailed information, including source and composition of material and the processes involved, so that duplication of procurement is possible. For example, data on vacuum coating conditions is desired.

14) Handling precautions

a) No contact on face of mirror after evaporation, except in support areas identified in Item 8.

b) No part of mirror to be handled without gloves, or otherwise contaminated with hydrocarbons after precoating cleaning.

c) The mirror samples shall be kept in an environment of relative humidity lower than 40 percent. Coated mirrors shall be stored and shipped in Boeing-supplied sealed containers.

APPENDIX B

MISCELLANEOUS DATA ON MIRROR SUBSTRATES AND COATINGS

MgF_2 and LiF Overcoated Test Specimens

Substrate Data.-

Beryllium

Manufacturer:	The Beryllium Corporation (Berylco)
Specification:	HP-40
Berylco Unit Nos.:	669K-1 through 16
Berylco Film No.:	HSB-2684
Heat No.:	669K
Purity Analysis:	
Beryllium	95.10 percent
BeO	6.68
Carbon	0.164
Iron	0.167
Aluminum	0.060
Magnesium	0.010
Silicon	0.061
Other Metallic	0.10 max.
Ultimate Tensile Strength:	4.96×10^8 newtons-m^{-2}
Precision Elastic Limit:	6.2×10^7 newtons-m^{-2}
Grain Size:	Less than 15 microns (15000 nm)
Density:	1.880×10^3 kg-m^{-3}
Kanigen-Nickel Plater:	Grunwald Plating Company Chicago, Illinois
Plating Specifications:	MIL-C-26074A-C1
Heat Treatment:	$463 \pm 5^{\circ}K$ for 4 hours
Nickel Plating Thickness:	0.015 cm (0.006 in.)

Cer-Vit

Manufacturer:	Owens-Illinois Company, Toledo, Ohio
Specification:	Premium Grade Mirror Blank Material, C-101
Chemical Analysis:	Meets Patent Requirements
Average Linear Thermal Expansion Coefficient:	$0.0 \times 10^{-7}/^{\circ}C$ at 0° to $38^{\circ}C$
Dimensions:	5.039-5.080 by 5.039-5.080 by 1.864-1.905 cm
Seed Count:	0 to 4 per specimen
Stress Analysis:	Stress retardation of 5 - 10 mμ/cm in the diffuse stress. Stress is mainly at sharp corners.

Fused Silica

Manufacturer:	Corning Glass Works, Bradford, Pa.
Specification:	#7940 (Mirror Blank Quality) Code No. 851056)
Corning Glass Order No.: (MgF_2 Overcoated Mirrors)	OZ 813326 December 28, 1967
Corning Glass Order No.: (LiF Overcoated Mirrors)	OZ 813788 March 6, 1968

Cleaning and Coating Data.-

MgF_2/Aluminum Coatings

1) Cleaned in a liquid detergent/water-solution;
2) Wiped dry with flannel cloth;
3) Glow discharge cleaned in vacuum chamber;
4) Vacuum deposited aluminum film applied in accordance with data published by Hass and Tousey (J. Opt. Soc. Am., Vol. 49, 593, 1959)

   Chamber pressure ---------- less than 10^{-5} torr

   Rate ---------- approximately 85 nm in less than 4 seconds

5) Magnesium fluoride film applied as follows:

Substrate temperature ------ ambient

Chamber pressure ---------- less than 10^{-5} torr

Rate ---------- 25 nm in less than 10 seconds

MgF_2 source ---------- procured per Mil Spec JAN-M-621

(Beryllium and Cer-Vit substrates coated in OCLI coating run No. 352-163 February 28, 1968. Fused silica substrates coated in batch 352-166, February 29, 1968.)

LiF/Aluminum Coatings

1) Glow discharge cleaned for 3 min;

2) Aluminum deposition

Chamber pressure ---------- $\approx 1 \times 10^{-5}$ torr

Time period ---------- 2 to 3 secs.

Thickness ---------- $\approx$ 80 nm

3) LiF deposition

Chamber pressure ---------- $\approx 2 \times 10^{-5}$ torr

Time period ---------- 10 secs.

Thickness ---------- 13.5 to 14 nm

(LiF source was random cuttings from Harshaw crystals. Evaporated from a tungsten boat.)

APPENDIX C

OPTICAL CONSTANTS OF ALUMINUM

Wavelength, nanometers	Refractive Index, n	Extinction Coefficient, k
90.0	0.0630	0.397
95.0	0.0549	0.535
100.0	0.0526	0.653
105.0	0.0526	0.757
110.0	0.0537	0.852
115.0	0.0555	0.940
120.0	0.0578	1.026
125.0	0.0605	1.105
130.0	0.0635	1.186
135.0	0.0667	1.262
140.0	0.0703	1.338
145.0	0.0740	1.410
150.0	0.0779	1.484
155.0	0.0823	1.555
160.0	0.0863	1.625
165.0	0.0907	1.694
170.0	0.0954	1.763
175.0	0.1000	1.830
180.0	0.1050	1.898
185.0	0.1090	1.964
190.0	0.1150	2.031
195.0	0.1210	2.096
200.0	0.1260	2.162
205.0	0.1320	2.227
210.0	0.1380	2.291
215.0	0.1440	2.356
220.0	0.1400	2.360
240.0	0.1600	2.600
253.6	0.1800	2.770
260.0	0.1900	2.850
280.0	0.2200	3.130
300.0	0.2500	3.330
320.0	0.2800	3.560
340.0	0.3100	3.800
360.0	0.3400	4.010
380.0	0.3700	4.250
400.0	0.4000	4.450
436.0	0.4700	4.840
450.0	0.5100	5.000
492.0	0.6400	5.500
546.0	0.8200	5.990
578.0	0.9300	6.330
650.0	1.3000	7.110

APPENDIX C (continued)

OPTICAL CONSTANTS OF MAGNESIUM FLUORIDE

Wavelength, nanometers	Refractive Index, n	Extinction Coefficient, k
90.0	1.5600	0.220
92.5	1.5600	0.265
95.0	1.5600	0.320
97.5	1.5600	0.372
100.0	1.3800	0.414
102.5	1.4300	0.430
105.0	1.9000	0.420
106.0	2.1000	0.402
107.0	2.2200	0.372
108.0	2.2300	0.318
109.0	2.2200	0.262
110.0	2.2000	0.210
111.0	2.0880	0.177
112.0	2.0220	0.152
113.0	1.9730	0.134
114.0	1.9310	0.120
115.0	1.8940	0.107
116.0	1.8610	0.095
117.0	1.8320	0.084
118.0	1.8050	0.073
119.0	1.7810	0.065
120.0	1.7590	0.055
121.0	1.7400	0.047
122.0	1.7250	0.043
123.0	1.7110	0.041
124.0	1.6990	0.039
125.0	1.6890	0.038
126.0	1.6810	0.037
128.0	1.6660	0.036
130.0	1.6530	0.035
132.0	1.6420	0.034
134.0	1.6320	0.033
136.0	1.6210	0.032
138.0	1.6120	0.031
140.0	1.6030	0.030
142.0	1.5950	0.029
144.0	1.5860	0.028
146.0	1.5780	0.027
148.0	1.5670	0.026
150.0	1.5540	0.025
152.0	1.5390	0.024
154.0	1.5230	0.023
156.0	1.5070	0.022
158.0	1.4930	0.021

APPENDIX C (continued)

OPTICAL CONSTANTS OF MAGNESIUM FLUORIDE

Wavelength, nanometers	Refractive Index, n	Extinction Coefficient, k
160.0	1.4820	0.020
162.0	1.4750	0.019
164.0	1.4720	0.018
166.0	1.4700	0.017
168.0	1.4700	0.016
170.0	1.4680	0.015
174.0	1.4590	0.013
178.0	1.4530	0.011
182.0	1.4480	0.009
186.0	1.4440	0.007
190.0	1.4420	0.005
195.0	1.4400	0.004
200.0	1.4390	0.002
404.6	1.3960	0.0
589.4	1.3895	0.0
706.5	1.3877	0.0

ASSUMED OPTICAL CONSTANTS FOR CONTAMINANT FILM

Wavelength, nanometers	Refractive Index, n	Extinction Coefficient, k
90.0	1.570	0.605
100.0	1.540	0.570
125.0	1.495	0.492
150.0	1.455	0.430
175.0	1.432	0.380
200.0	1.413	0.335
225.0	1.399	0.295
250.0	1.385	0.270
275.0	1.375	0.240
300.0	1.362	0.220
325.0	1.355	0.195
350.0	1.350	0.170

APPENDIX D

OPTICAL CONSTANTS FOR CONTAMINANT FILM

To demonstrate the effect of a contaminant film on a MgF_2/Al-coated reflective surface Mr. W. R. Hunter of the Naval Research Laboratory calculated the reflectance at 220 nm of a multilayer comprising opaque aluminum overcoated with 25 nm of magnesium fluoride plus the contaminant film. The calculations were carried out as a function of contaminant film thickness from zero to 10 nm. Drawing on previous experience, Mr. Hunter chose a value of 1.4 for the refractive index and carried out calculations for five values of extinction coefficient from 0.2 to 0.6. The curves generated are shown in Figure 43.

Following irradiation by 10^{16} protons-cm^{-2}, a MgF_2/Al-coated fused silica specimen showed a degradation, $\Delta R/R = 0.333$, at 220 nm. Interferometric measurement showed a mean accretion of 4.1 nm in the irradiated zone. As shown in Figure 43, these data are compatible with an extinction coefficient $k = 0.3$. Similar, but less detailed calculations by Hunter at 121.6 nm showed that the assumption of a refractive index $n = 1.5$ and an extinction coefficient $k = 0.5$, while not in good agreement with experimental data, were a fair approximation.

With these two pairs of points, dispersion like curves were constructed for n and k as functions of wavelength. These curves are shown in Figure 44, and data taken for the curves for calculation purpose are shown in the final table in Appendix C.

8.0 REFERENCES

1. A System Study of a Manned Orbital Telescope - Synchronous Orbit Study, NASA CR-66102, 1966.

2. A System Study of a Manned Orbital Telescope, NASA CR-66047, 1965.

3. Frank, L. A.: Several Observations of Low-Energy Protons and Electrons in the Earth's Magnetosphere with OGO-3. J. Geophys Res., vol. 72, 1967, pp. 1905-1916.

4. Frank, L. A.: On the Extraterrestrial Ring Current During Geomagnetic Storms. J. Geophys. Res., vol. 72, 1967, pp. 3753-3767.

5. Katz, L., et.al.: Low-Energy Particles Measured by OV1-9 (1966-11A). Earth's Particles and Fields, B. W. McCormac, ed., Reinhold Inc., 1968, p. 103.

6. Vette, J. I., and Lucero, A. B.: Models of the Trapped Radiation Environment, Volume III: Electrons at Synchronous Altitude. NASA SP-3024, 1967.

7. Gillette, Roger B.: Proton and Ultraviolet Radiation Effects on Solar Mirror Reflective Surfaces. J. Spacecraft Rockets, vol. 5, no. 4, April 1968, pp. 454-460. More detailed results were given in NASA CR-1024, Ultraviolet-Proton Radiation Effects on Solar Concentrator Reflective Surfaces, May 1968.

8. Fogdall, Lawrence B.; Cannaday, Sheridan S.; and Brown, Richard R.: In-Situ Electron, Proton, and Ultraviolet Radiation Effects on Thermal Control Coatings. Final report on NASA/Goddard contract NAS 5-9650, January 1969.

9. Hass, G.; Ramsey, J. B.; Heaney, J. B.; and Triolo, J. J.: Reflectance, Solar Absorptivity, and Thermal Emissivity of SiO_2 - Coated Aluminum. Applied Optics, vol. 8, no. 2, February 1969.

10. Greenberg, S. A.; Vance, D. A.; and Streed, E. R.: Low Solar Absorptance Surfaces with Controlled Emittance. A Second Generation of Thermal Control Coatings. Thermophysics of Spacecraft and Planetary Bodies. G. B. Heller, ed., Academic Press, 1967, pp. 297-314.

11. Reichard, Penelope J.; Triolo, Jack J.: Preflight Testing of the ATS-1 Thermal Coatings Experiment. Thermophysics of Spacecraft and Planetary Bodies. G. B. Heller, ed., Academic Press, 1967, pp. 491-513.

12. Hass, G.; Ramsey, J.P.; Triolo, J. J.; and Albright, H. T.: Solar Absorptance and Thermal Emittance of Aluminum Coated with Surface Films of Evaporated Aluminum Oxide. Thermophysics and Temperature Control of Spacecraft and Entry Vehicles. G. B. Heller, ed., Academic Press 1966, pp. 47-60.

13. Gillette, Roger B.; Brown, Richard R.; Seiler, Richard F.; and Sheldon, W. R.: Effects of Protons and Alpha Particles on Thermal Properties of Spacecraft and Solar Concentrator Coatings. Thermophysics and Temperature Control of Spacecraft and Entry Vehicles, G. B. Heller, ed., Academic Press, 1966, pp. 413-440.

14. Canfield, L. R.; Hass, G.; and Waylonis, J. E.: Further Studies on MgF_2 Overcoated Aluminum Mirrors with Highest Reflectance in the Vacuum Ultraviolet. Appl. Opt., vol. 5, no. 1, January 1966, pp. 45-50.

15. Cox, J. T.; Hass, G.; and Waylonis, J. E.: Further Studies on LiF-Overcoated Aluminum Mirrors with Highest Reflectance In The Vacuum Ultraviolet. Appl. Opt., vol. 7, no. 8, August 1968, pp. 1535-1539.

16. Personal communication with Dr. Georg Hass of the U. S. Army Electronics Command, Night Vision Laboratory, Fort Belvoir, Va., January 1969.

17. Dushman, S., and Lafferty, J.: Scientific Foundations of Vacuum Technique, Wiley and Sons, New York, 1962.

18. Ennos, A. E.: The Origin of Specimen Contamination in the Electron Microscope. Brit. J. Appl. Phys., vol. 4, April 1963, pp. 101-106.

19. Hillier, J.: On the Investigation of Specimen Contamination in the Electron Microscope. J. Appl. Phys., vol. 19, March 1948, pp. 226-230.

20. Ennos, A. E.: The Sources of Electron-Induced Contamination in Kinetic Vacuum Systems. Brit. J. Appl. Phys., vol. 5, January 1954, pp. 27-31.

21. Personal Communication with Dr. Georg Hass of the U. S. Army Electronics Command, Night Vision Laboratory, Ft. Belvoir, Va., and Mr. William Hunter of the Naval Research Laboratory, Washington, D.C., January 1969.

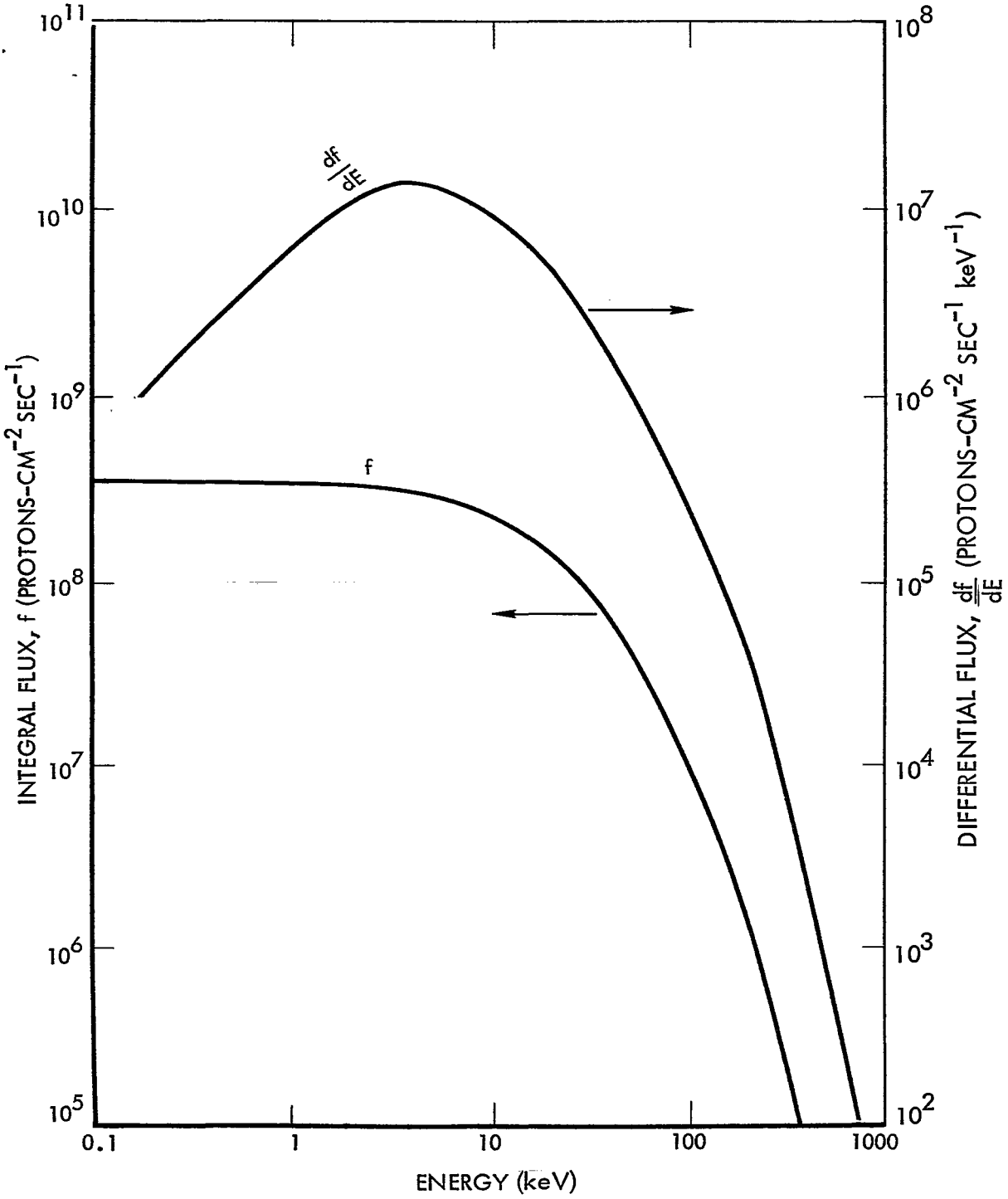

Figure 1 : TRAPPED PROTON SPECTRA AT SYNCHRONOUS ALTITUDE

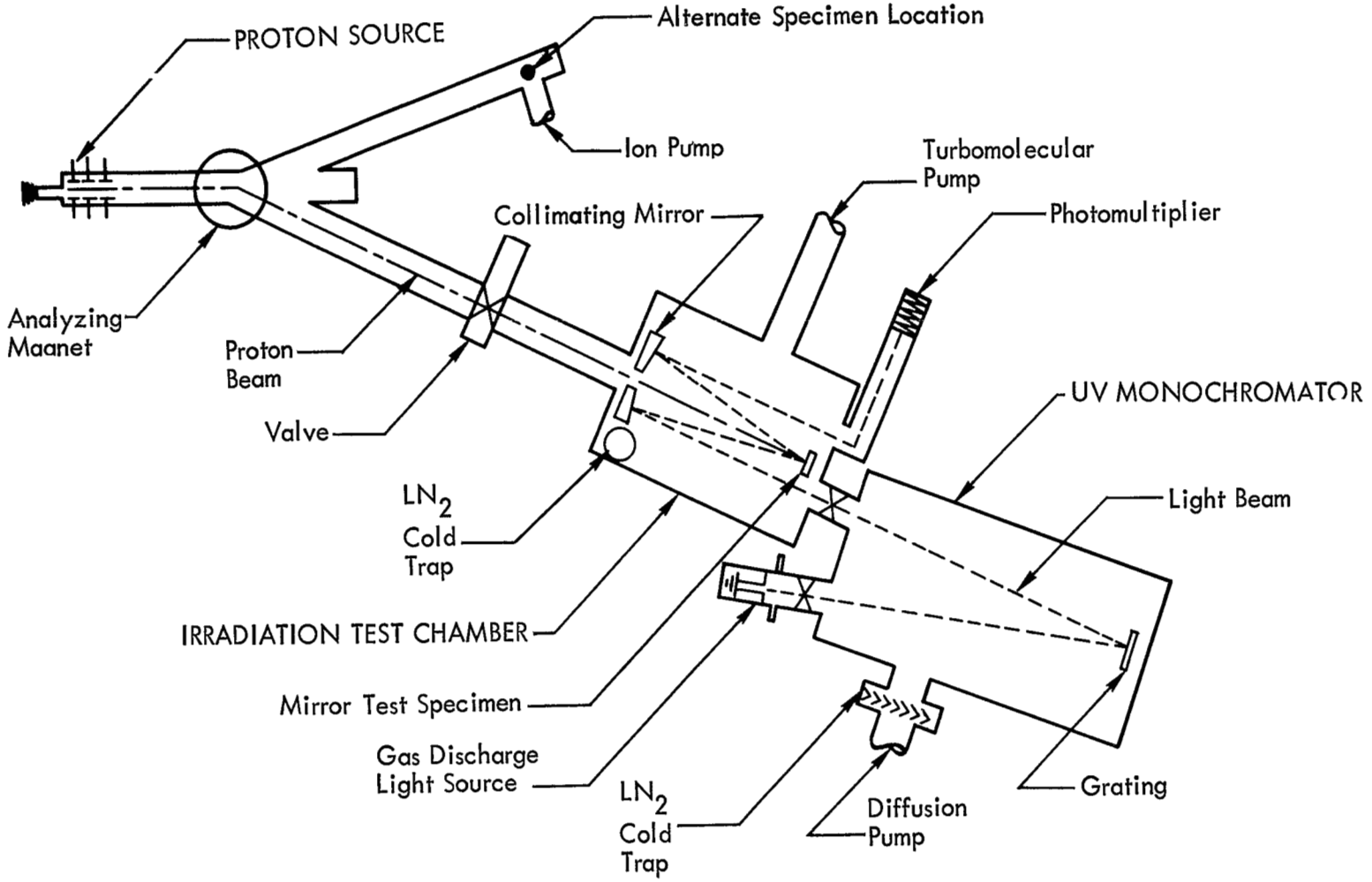

Figure 2 : SCHEMATIC OF PROTON RADIATION TEST FACILITY

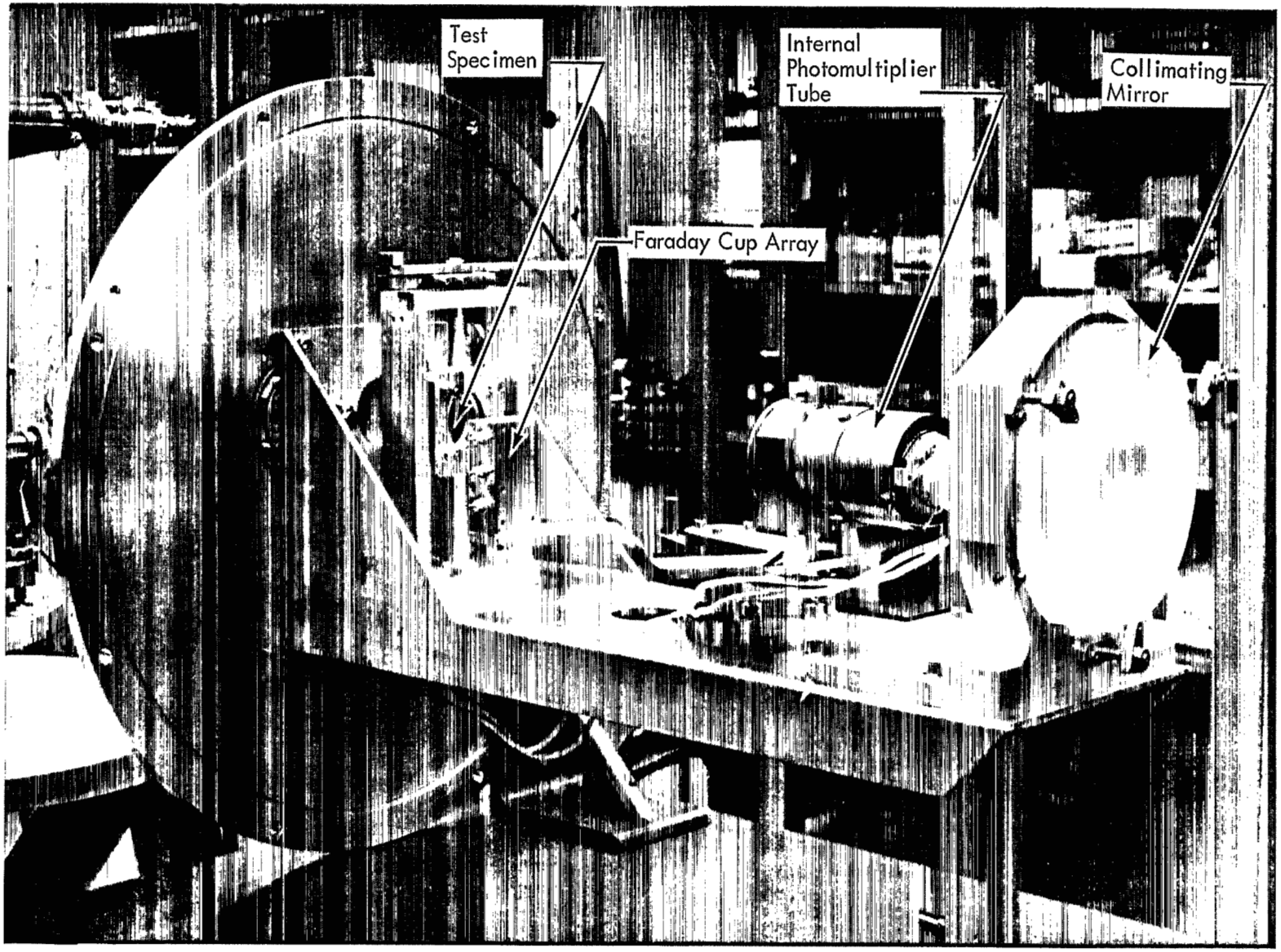

Figure 3: REFLECTOMETER INTERNAL CONSTRUCTION

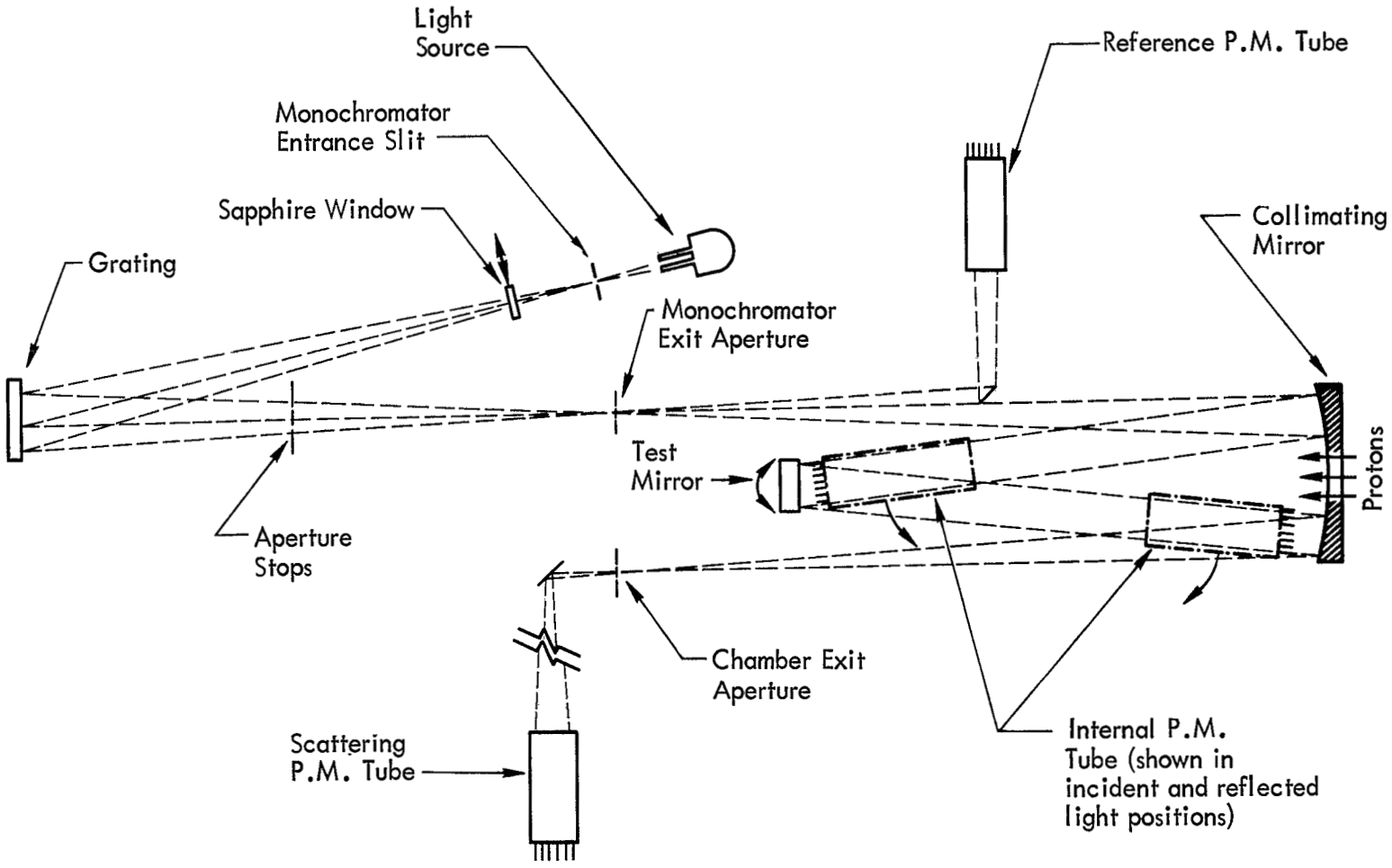

Figure 4: SCHEMATIC OF IN-SITU OPTICAL MEASUREMENT SYSTEM

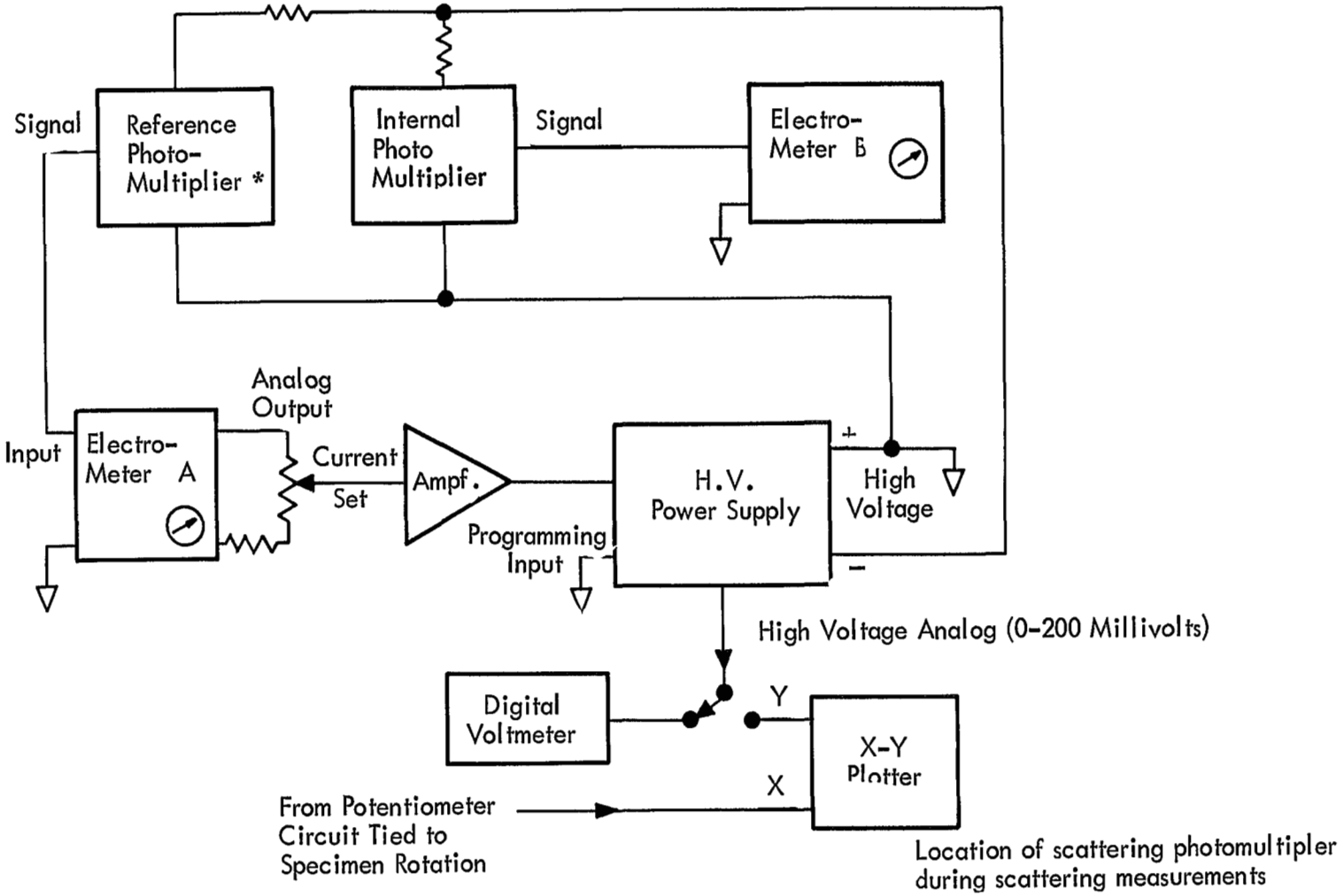

Figure 5: REFLECTOMETER/SCATTERING MEASUREMENT ELECTRONICS

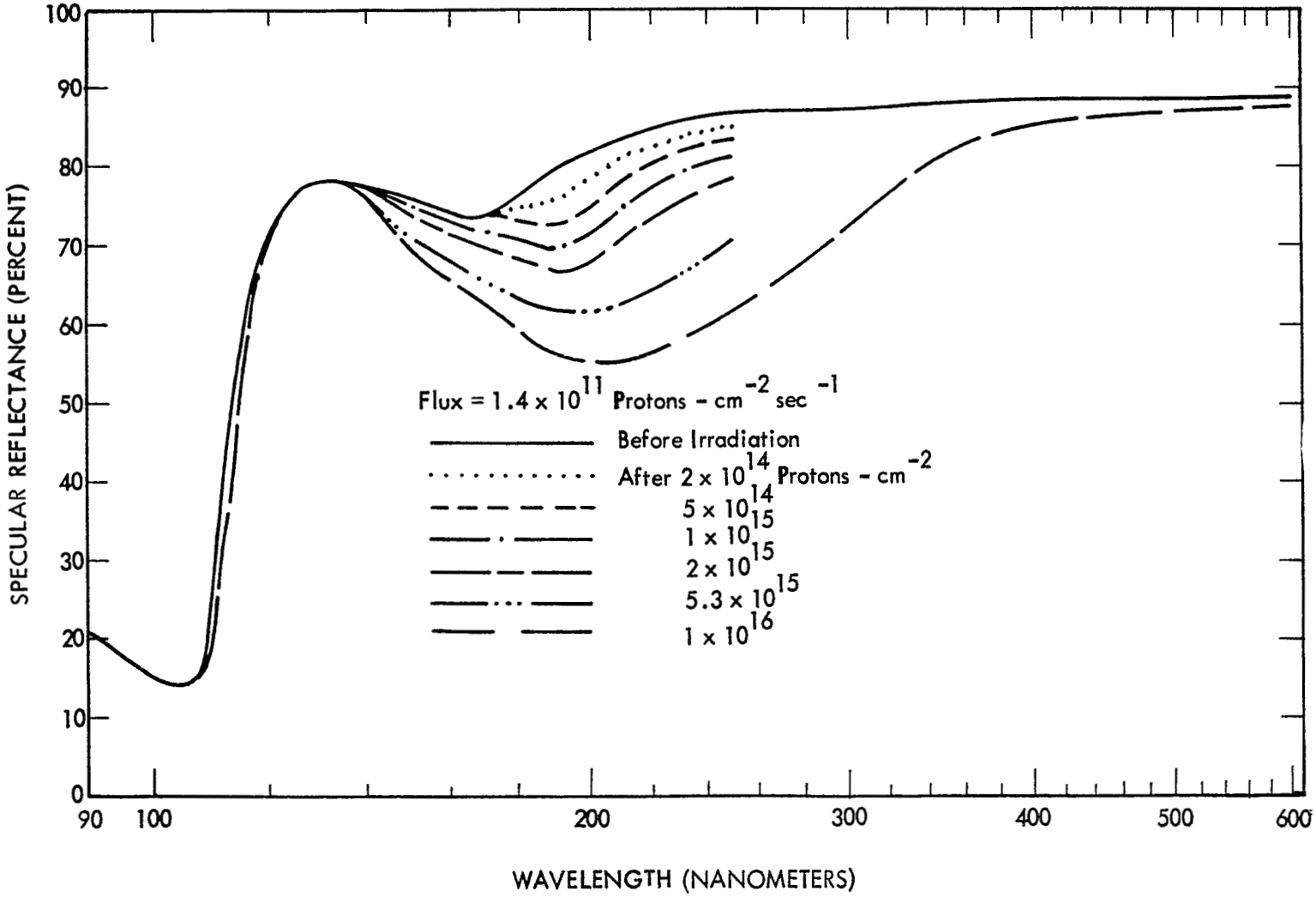

Figure 6: REFLECTANCE OF A MgF_2/Al-COATED CER-VIT MIRROR IRRADIATED BY 10 KEV PROTONS

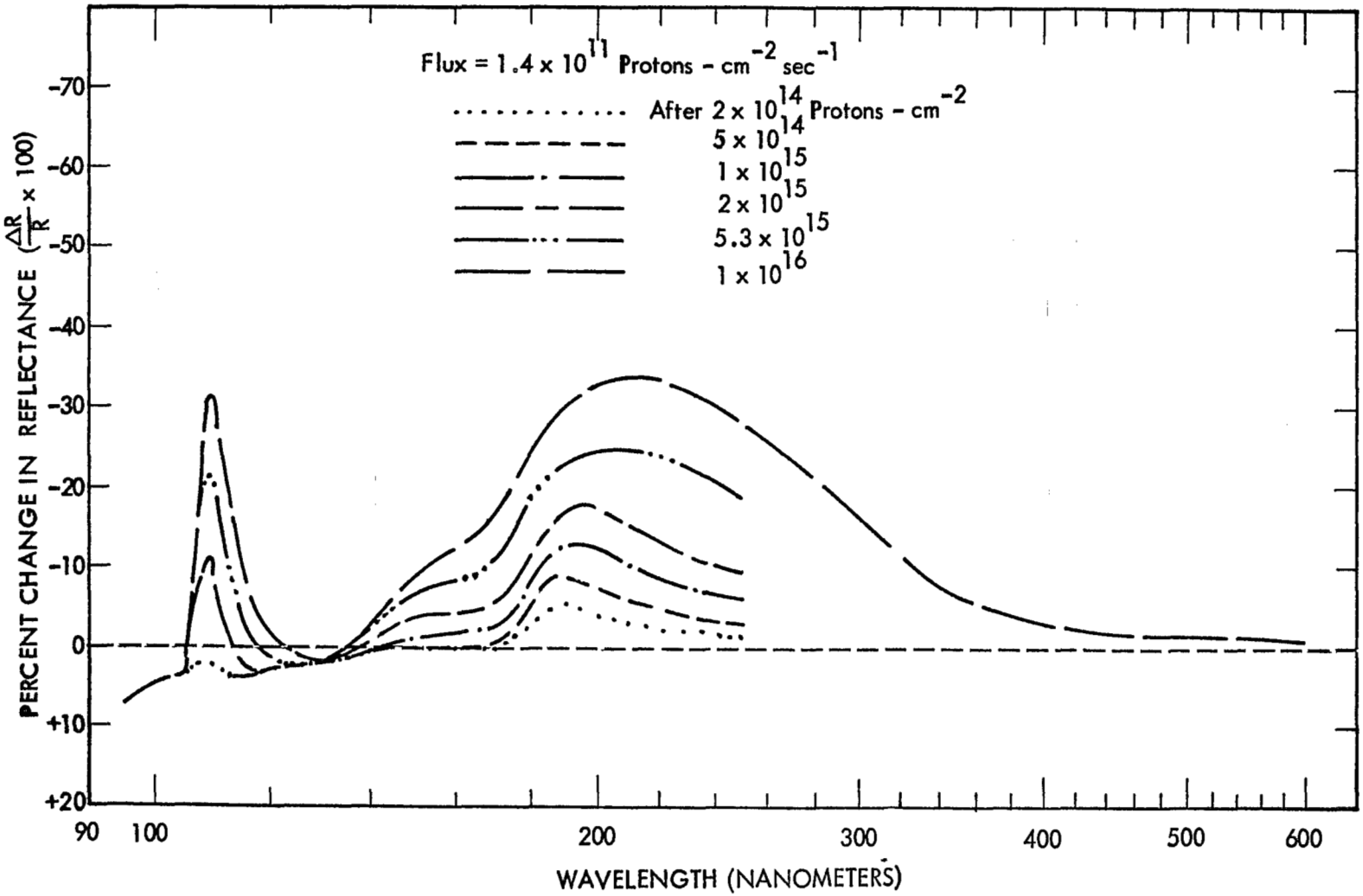

Figure 7: REFLECTANCE CHANGES OF A MgF_2/Al-COATED CER-VIT MIRROR IRRADIATED BY 10 KEV PROTONS

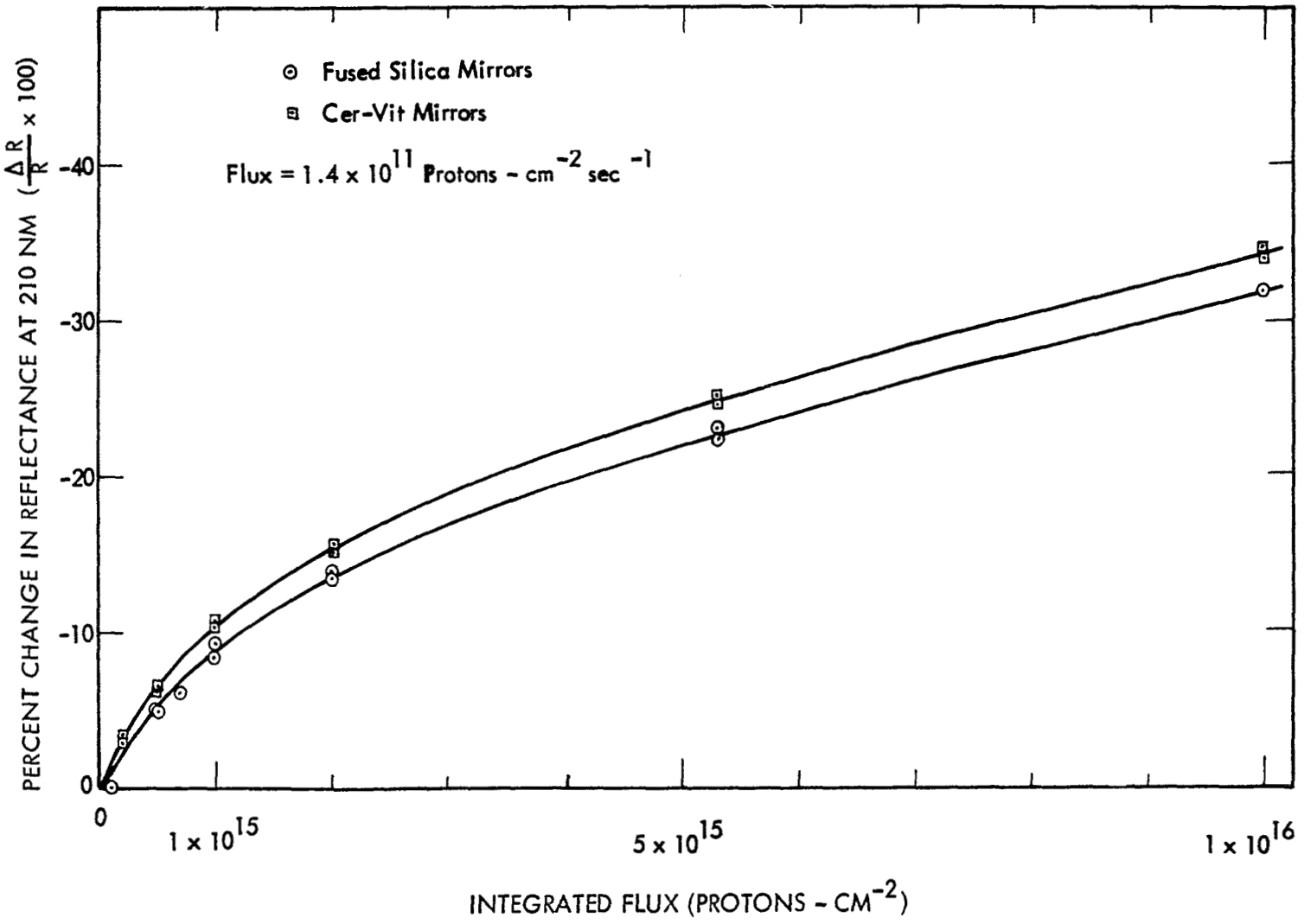

Figure 8: DIFFERENCE IN RADIATION DAMAGE OF MgF_2 / Al-COATED MIRRORS AS SHOWN BY REFLECTANCE CHANGES AT 210 NM

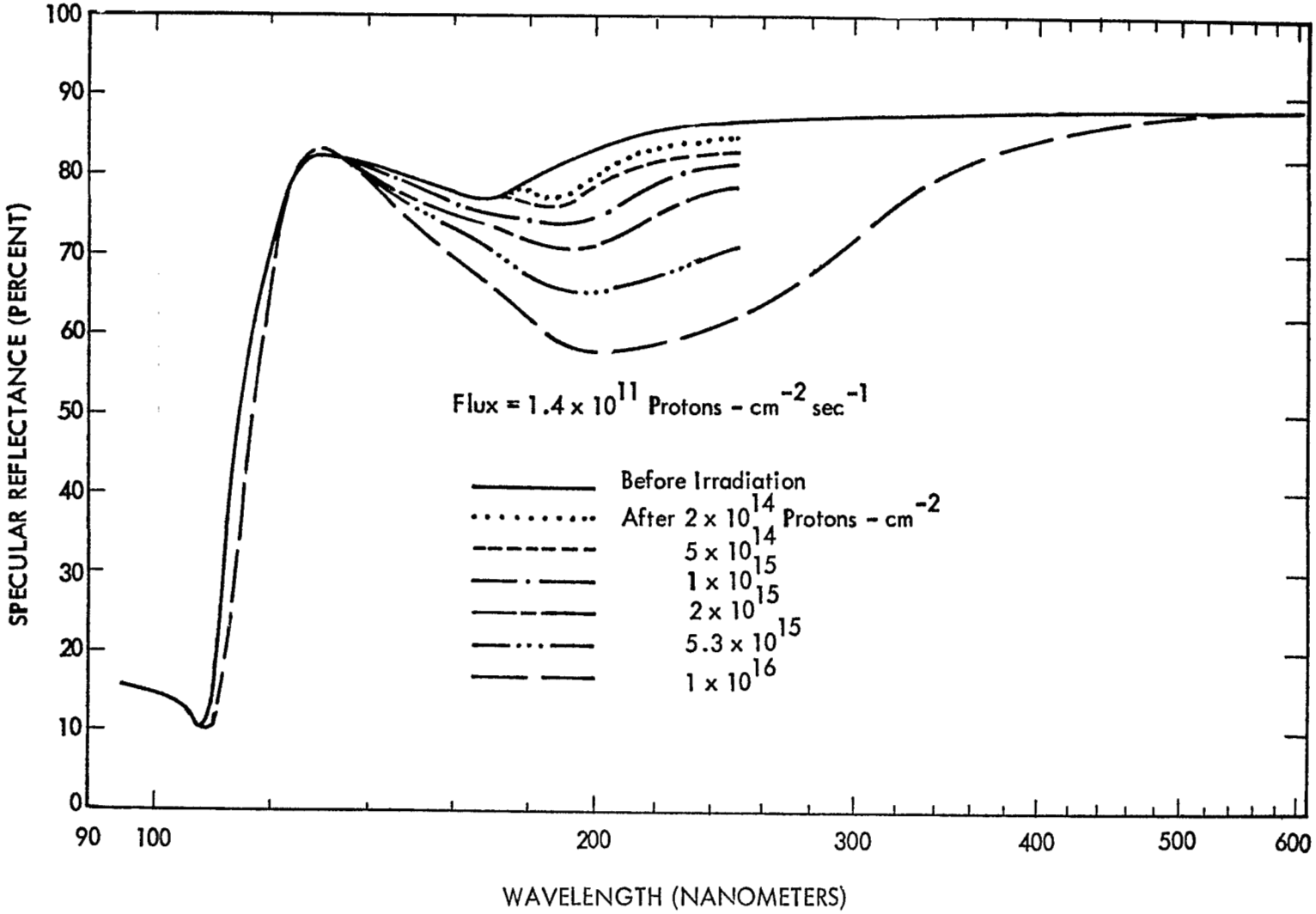

Figure 9: REFLECTANCE OF MgF_2/Al-COATED FUSED SILICA MIRROR IRRADIATED BY 10 KEV PROTONS

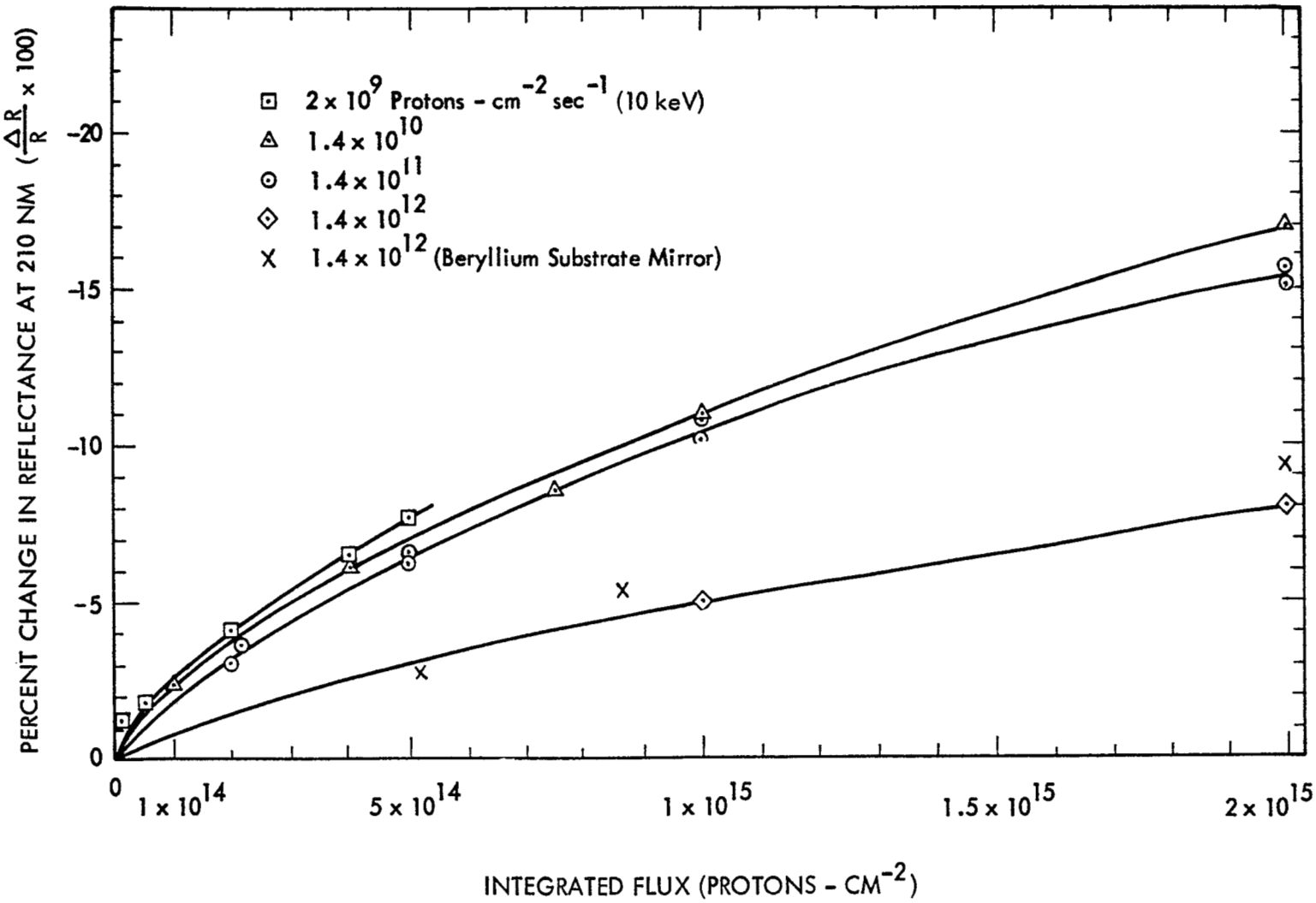

Figure 10: RATE EFFECT IN IRRADIATION OF MgF_2/Al-COATED CER-VIT MIRRORS AS SHOWN BY REFLECTANCE CHANGES AT 210 NM

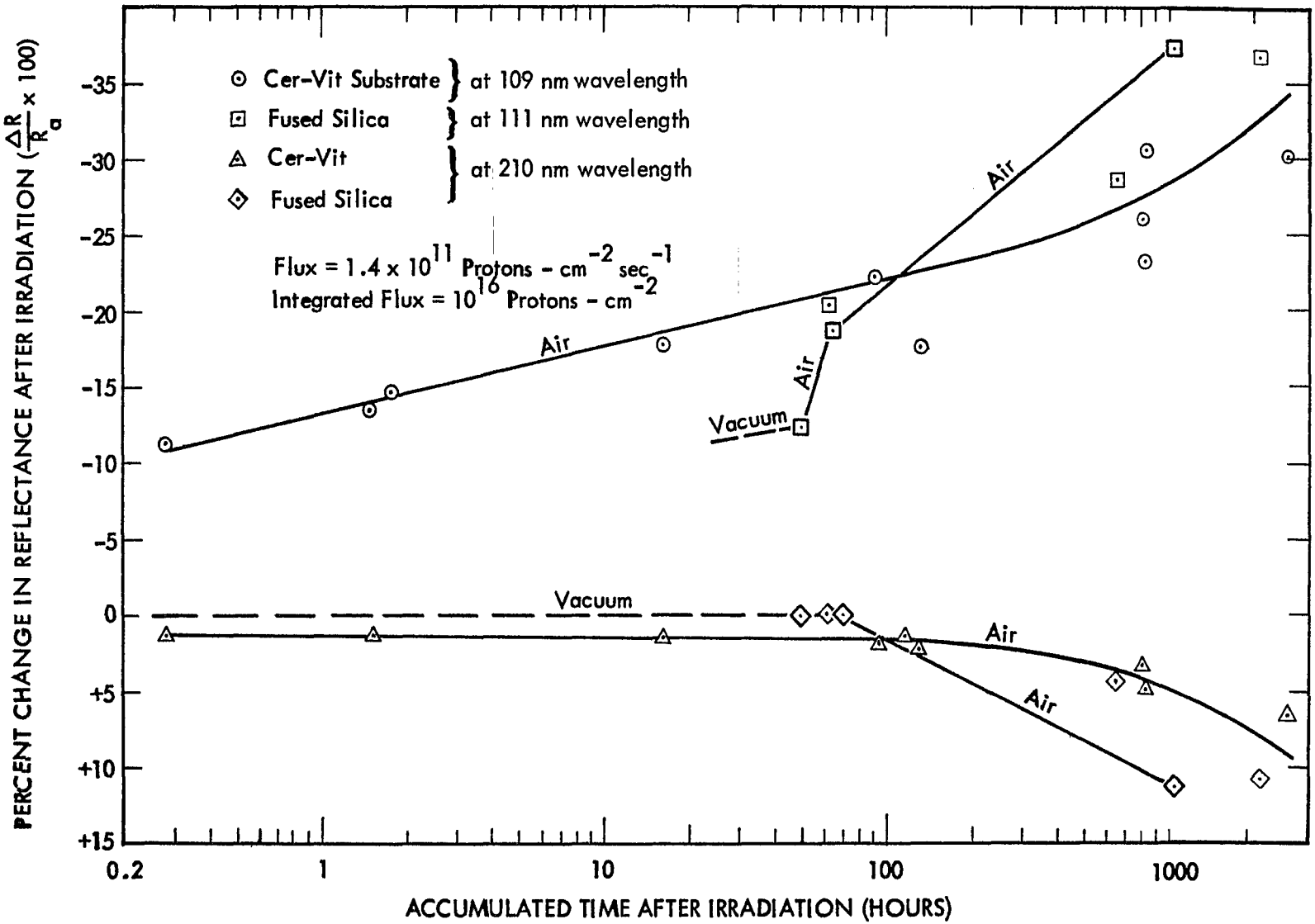

Figure 11: SUMMARY OF POST-IRRADIATION REFLECTANCE CHANGES FOR MgF_2/Al COATED MIRRORS

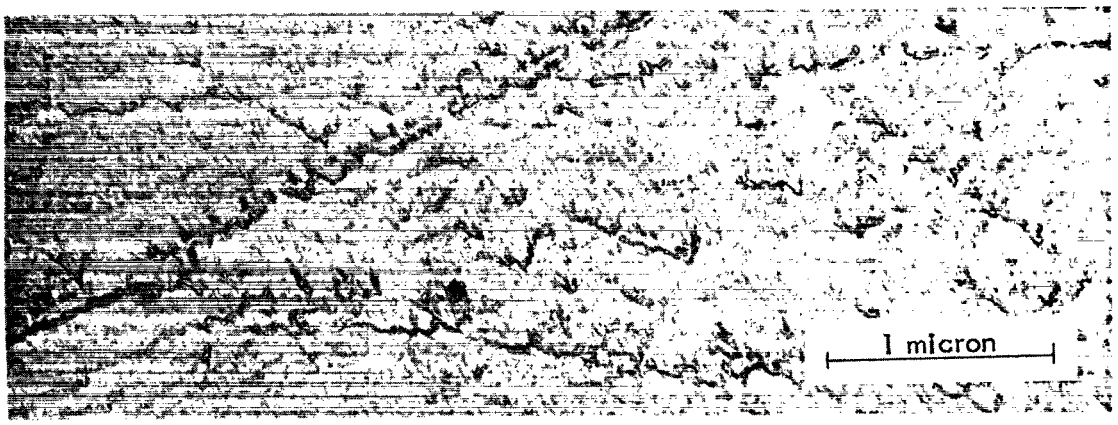

a) Kanigen Nickel (Beryllium Substrate)

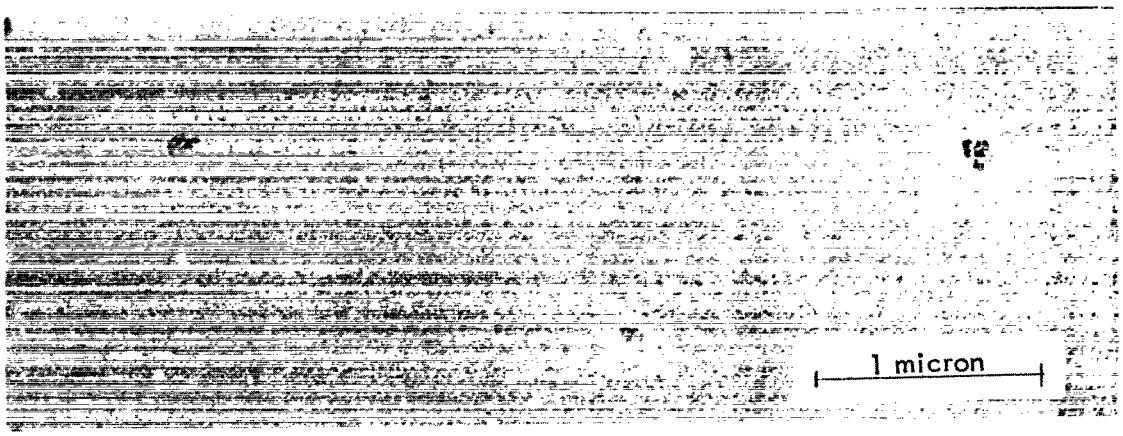

b) Fused Silica

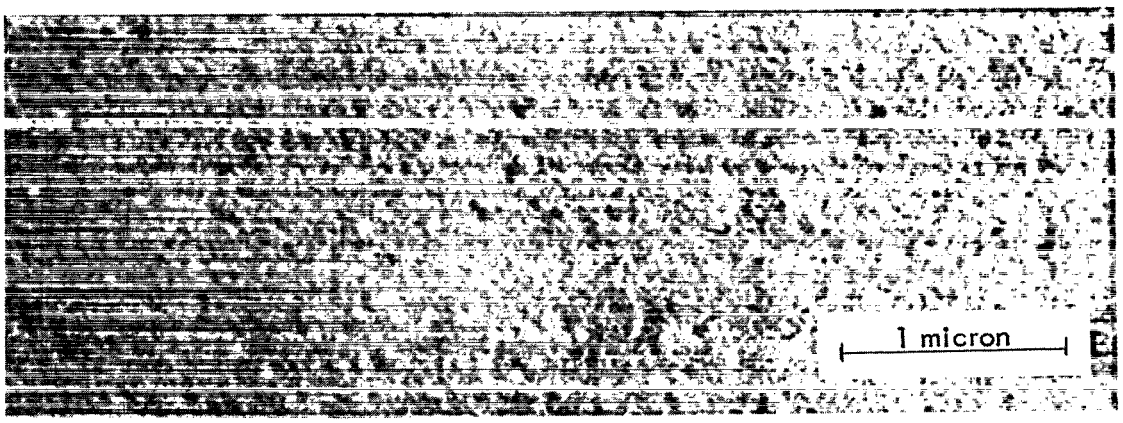

C) Cer-Vit

Figure 12: ELECTRON PHOTOMICROGRAPHS OF UNCOATED, POLISHED MIRROR SUBSTRATES

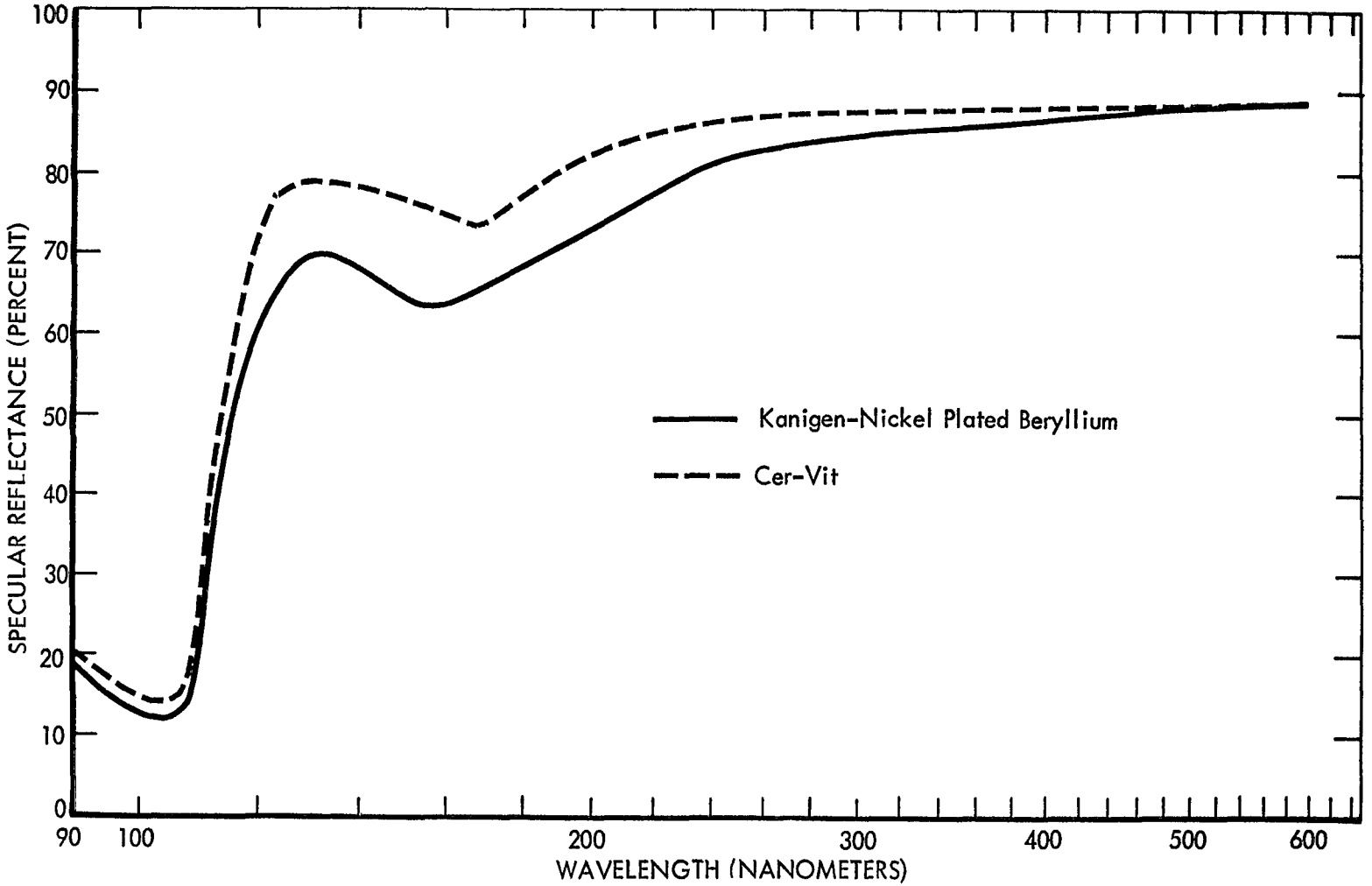

Figure 13: REFLECTANCE COMPARISON OF MgF_2/Al-COATED BERYLLIUM AND CER-VIT MIRRORS

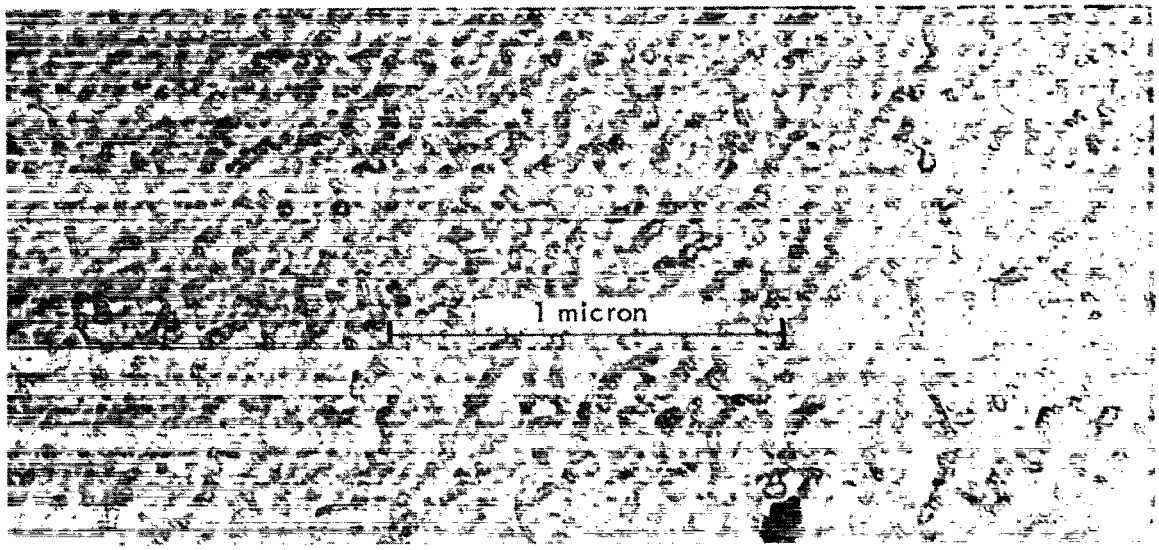

a) Irradiated With 10^{16} Protons - cm^{-2} At Flux of 10^{11} Protons - cm^{-2} sec^{-1} (10 keV)

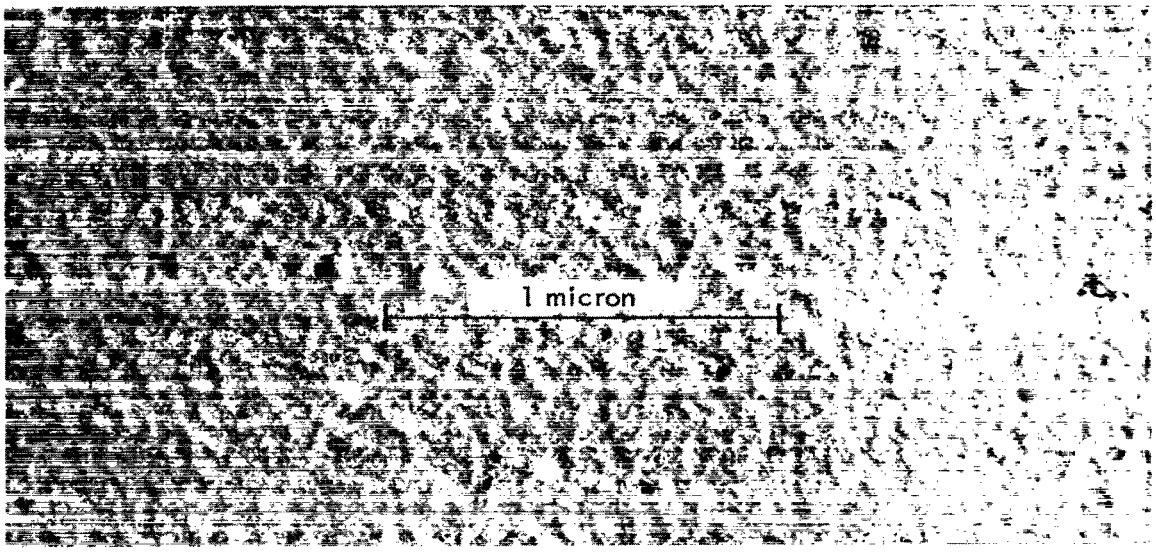

b) Unirradiated

Figure 14: ELECTRON PHOTOMICROGRAPHS OF IRRADIATED AND UNIRRADIATED MgF_2/Al-COATED FUSED SILICA MIRRORS

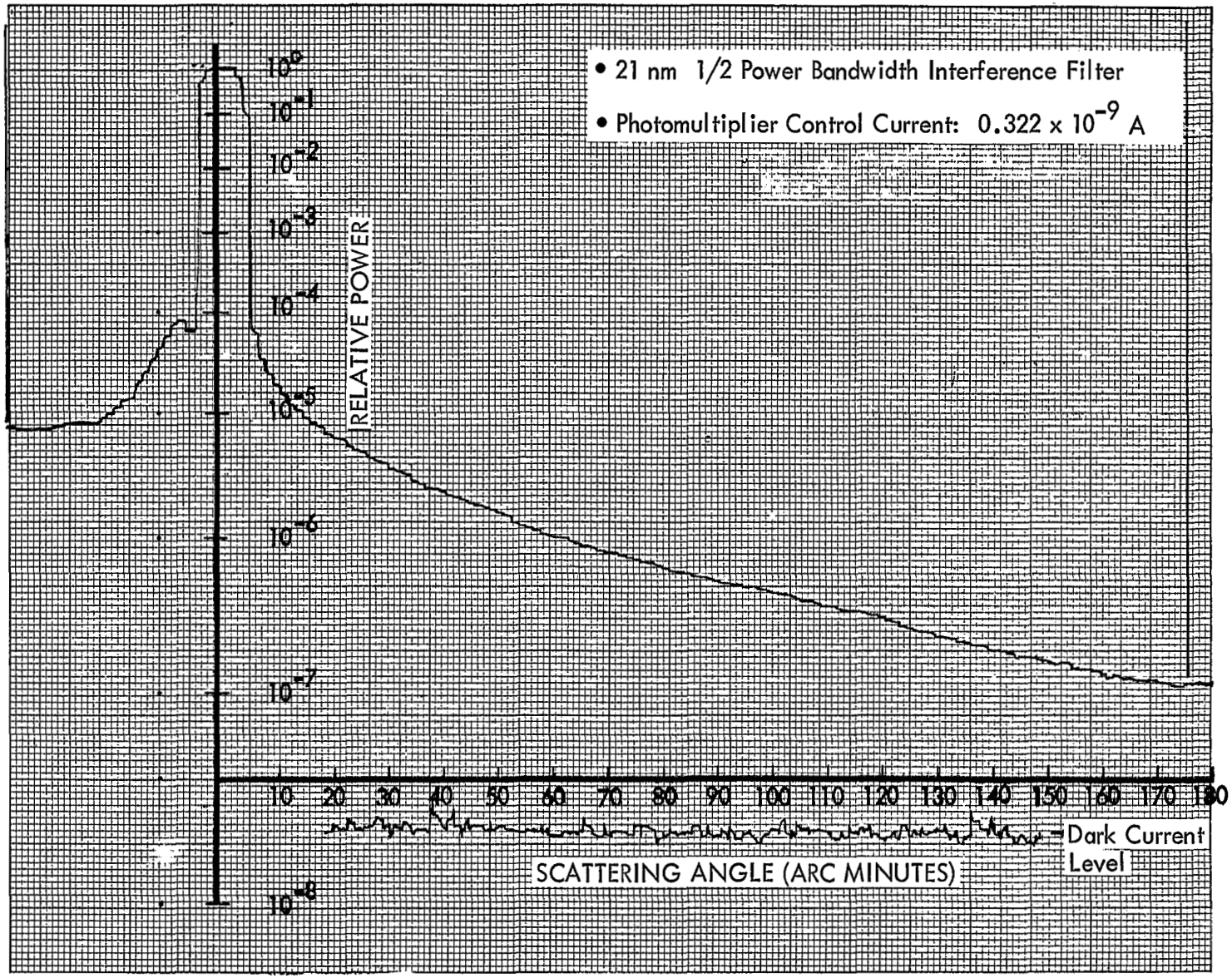

Figure 15: TYPICAL SCATTERED LIGHT DATA FOR AN UNIRRADIATED MgF_2/Al-COATED FUSED SILICA MIRROR AT 500 NM WAVELENGTH

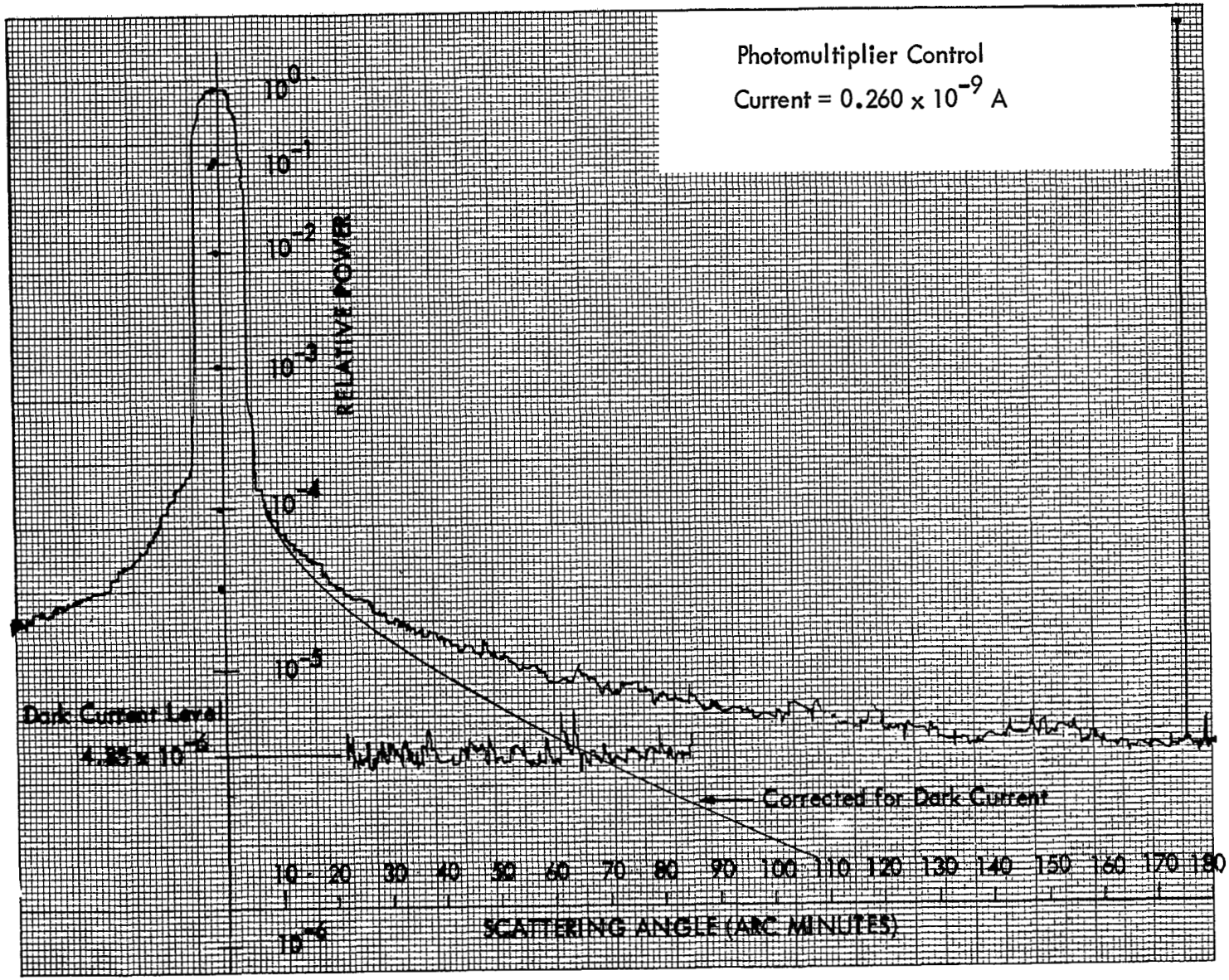

Figure 16: TYPICAL SCATTERED LIGHT DATA FOR AN UNIRRADIATED MgF_2/Al-COATED FUSED SILICA MIRROR AT 253.7 NM WAVELENGTH

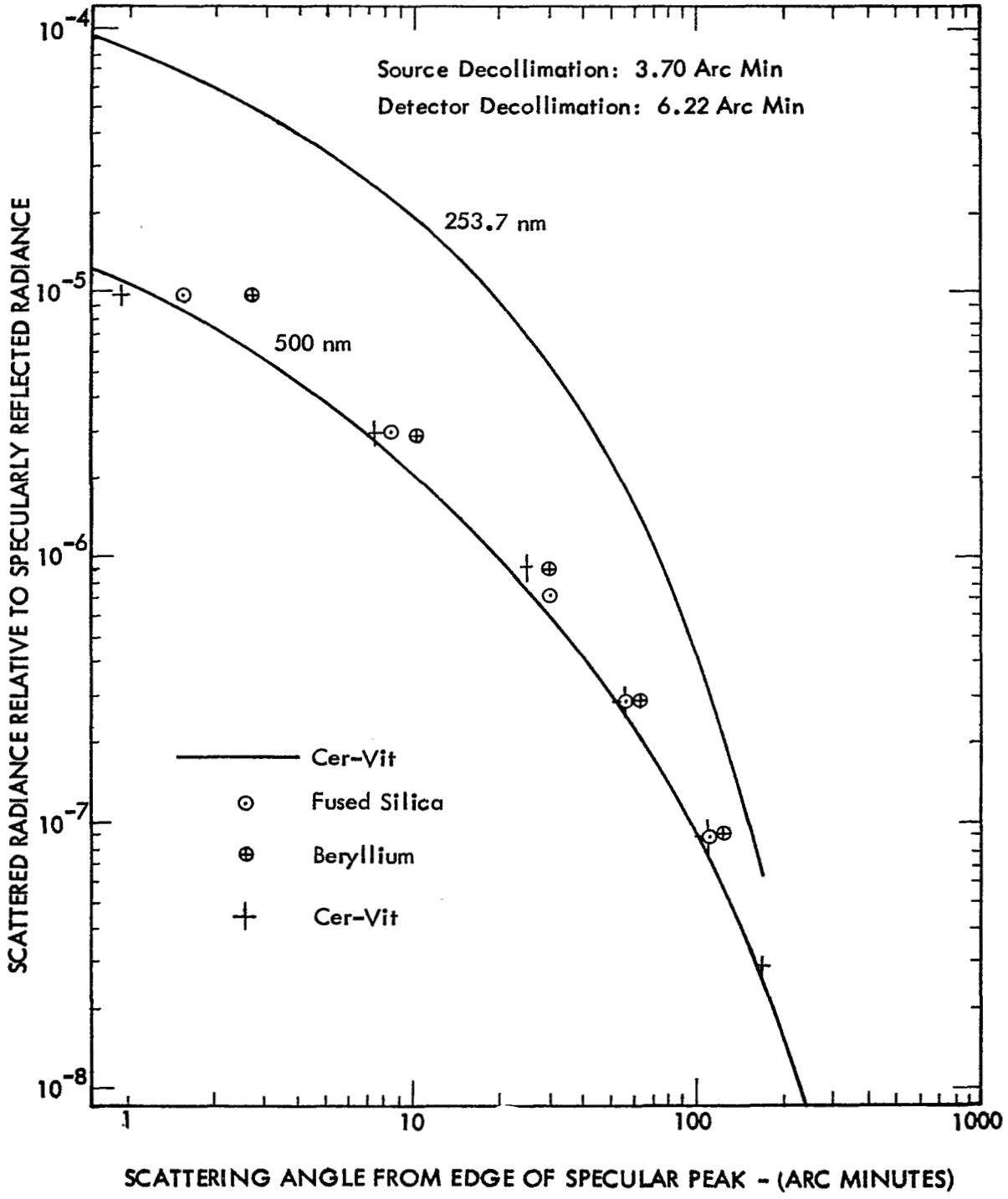

Figure 17: COMPARISON OF SCATTERING DATA AT 253.7 AND 500 NM WAVELENGTHS

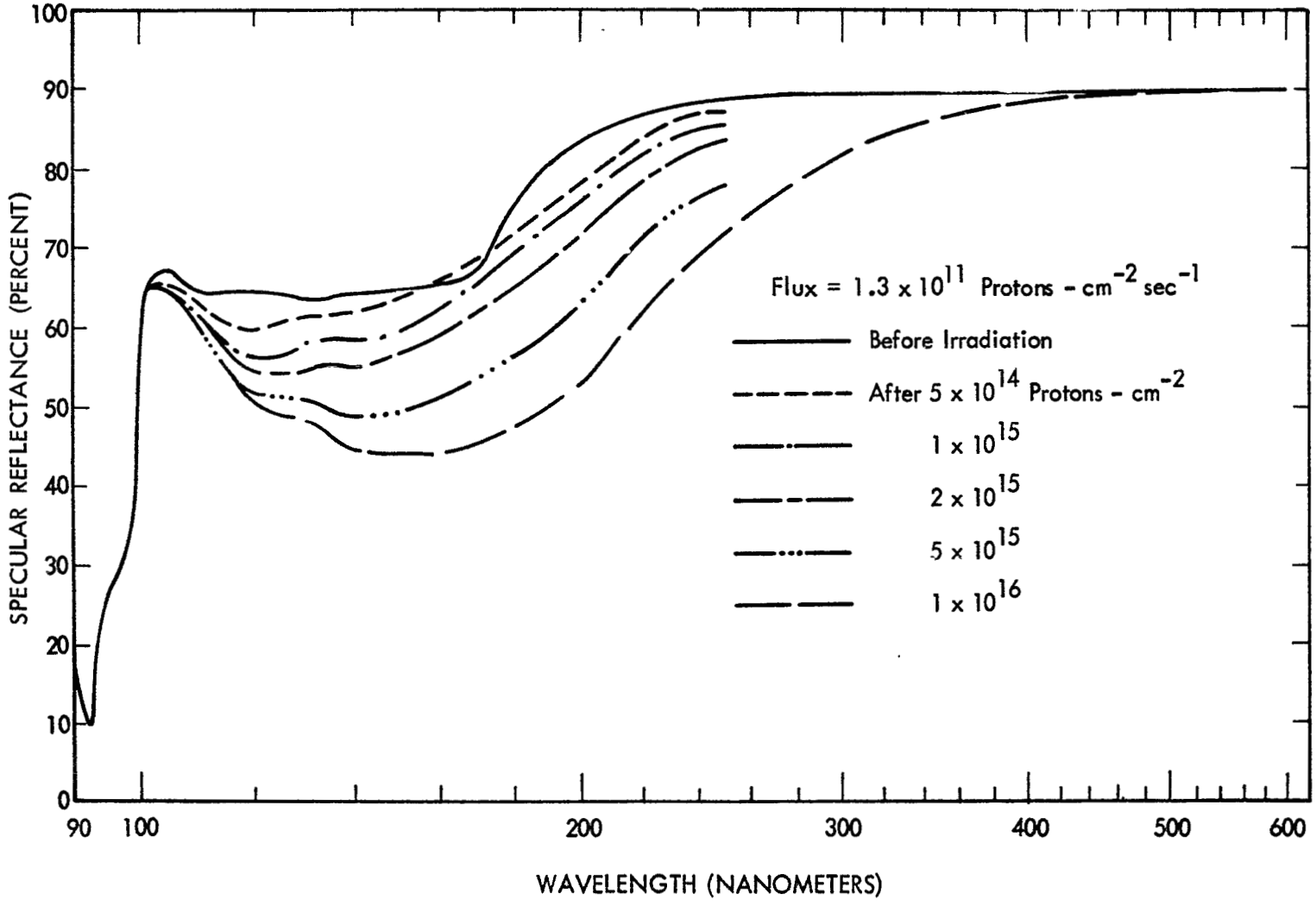

Figure 18: REFLECTANCE OF A LiF/Al-COATED FUSED SILICA MIRROR IRRADIATED BY 10 KEV PROTONS

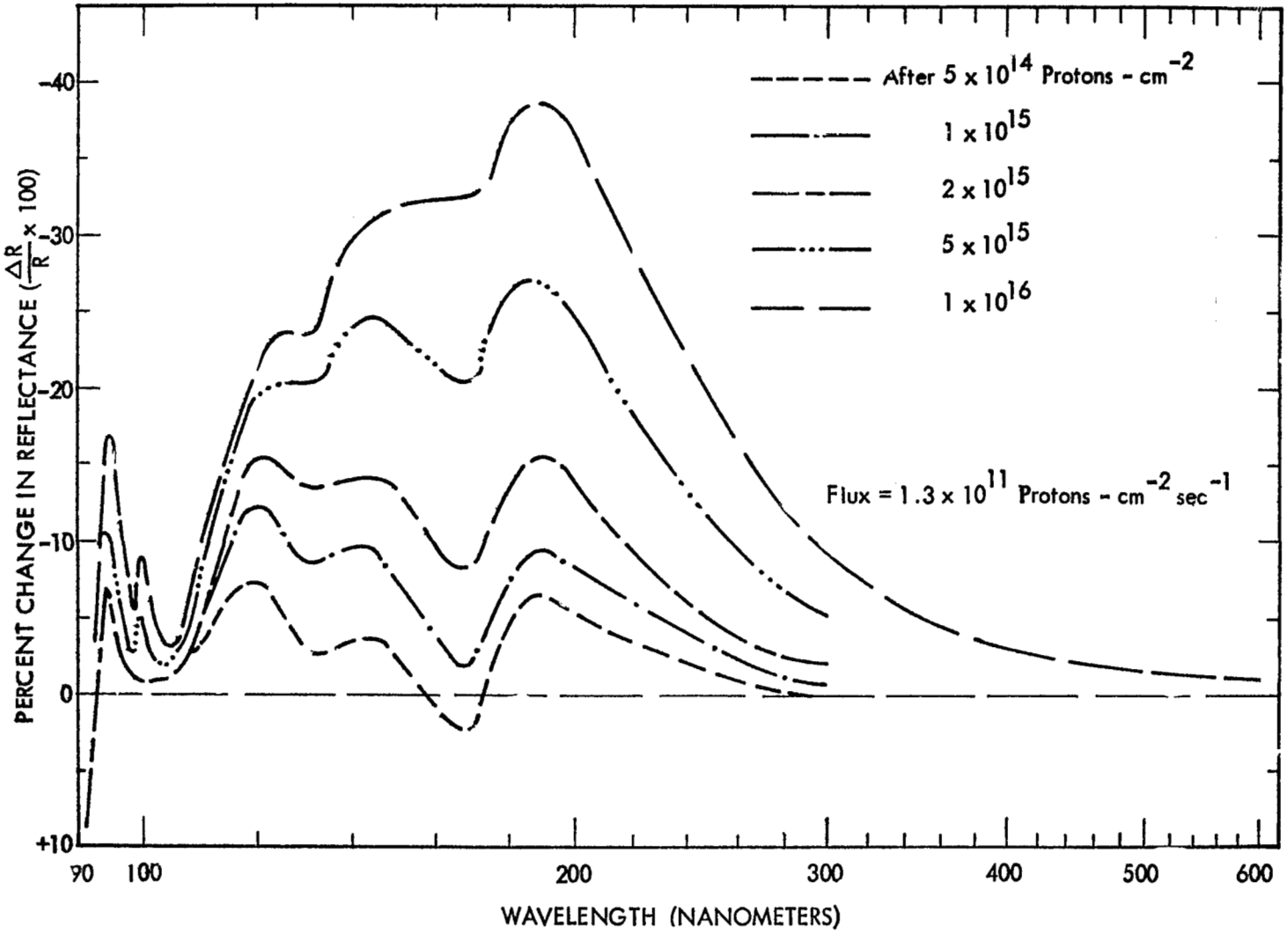

Figure 19: REFLECTANCE CHANGES OF A LiF/Al-COATED FUSED SILICA MIRROR IRRADIATED BY 10 KEV PROTONS

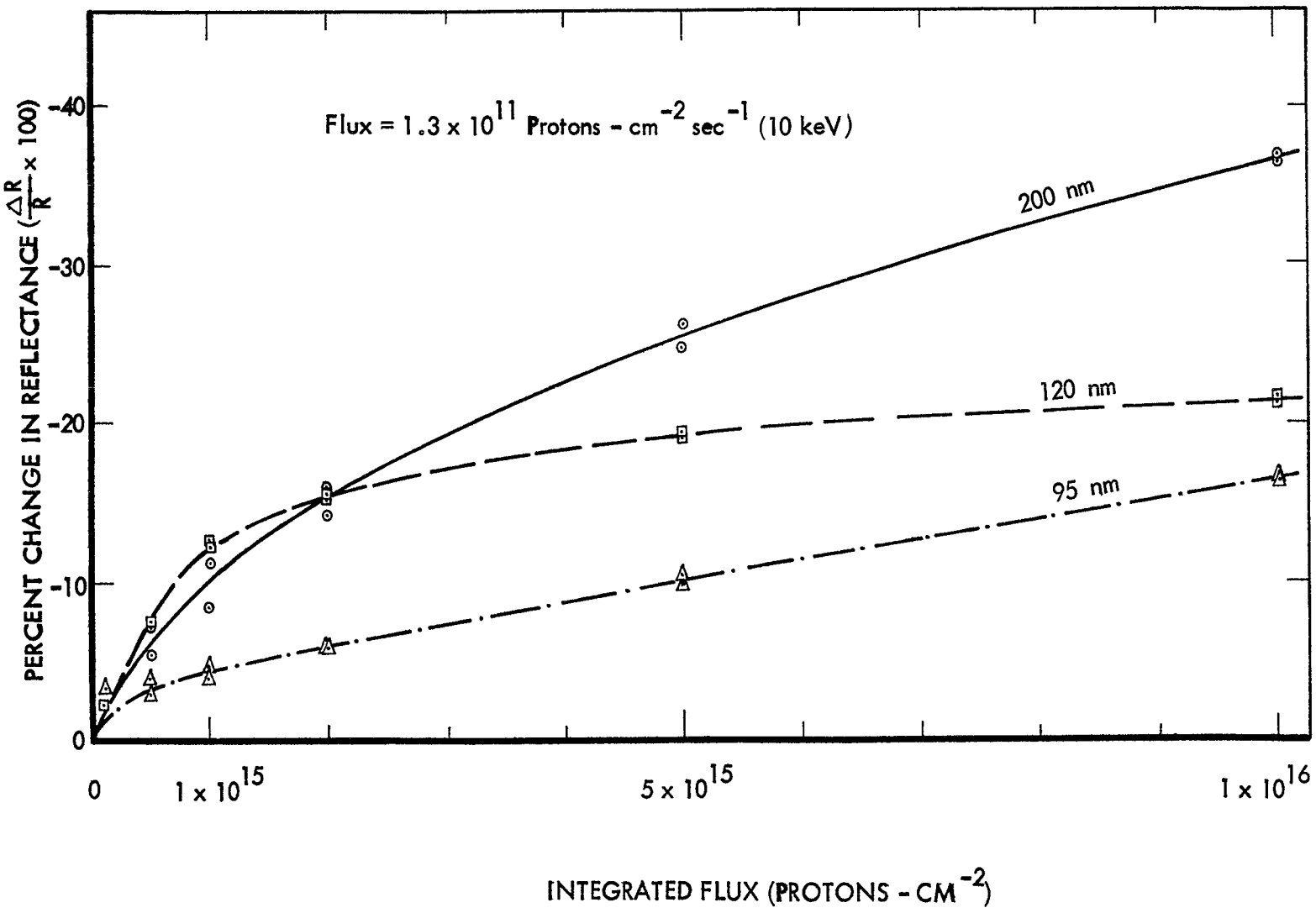

Figure 20: GROWTH RATE IN REFLECTANCE DAMAGE AT SELECTED WAVELENGTHS FOR PROTON IRRADIATED LiF/Al-COATED MIRRORS

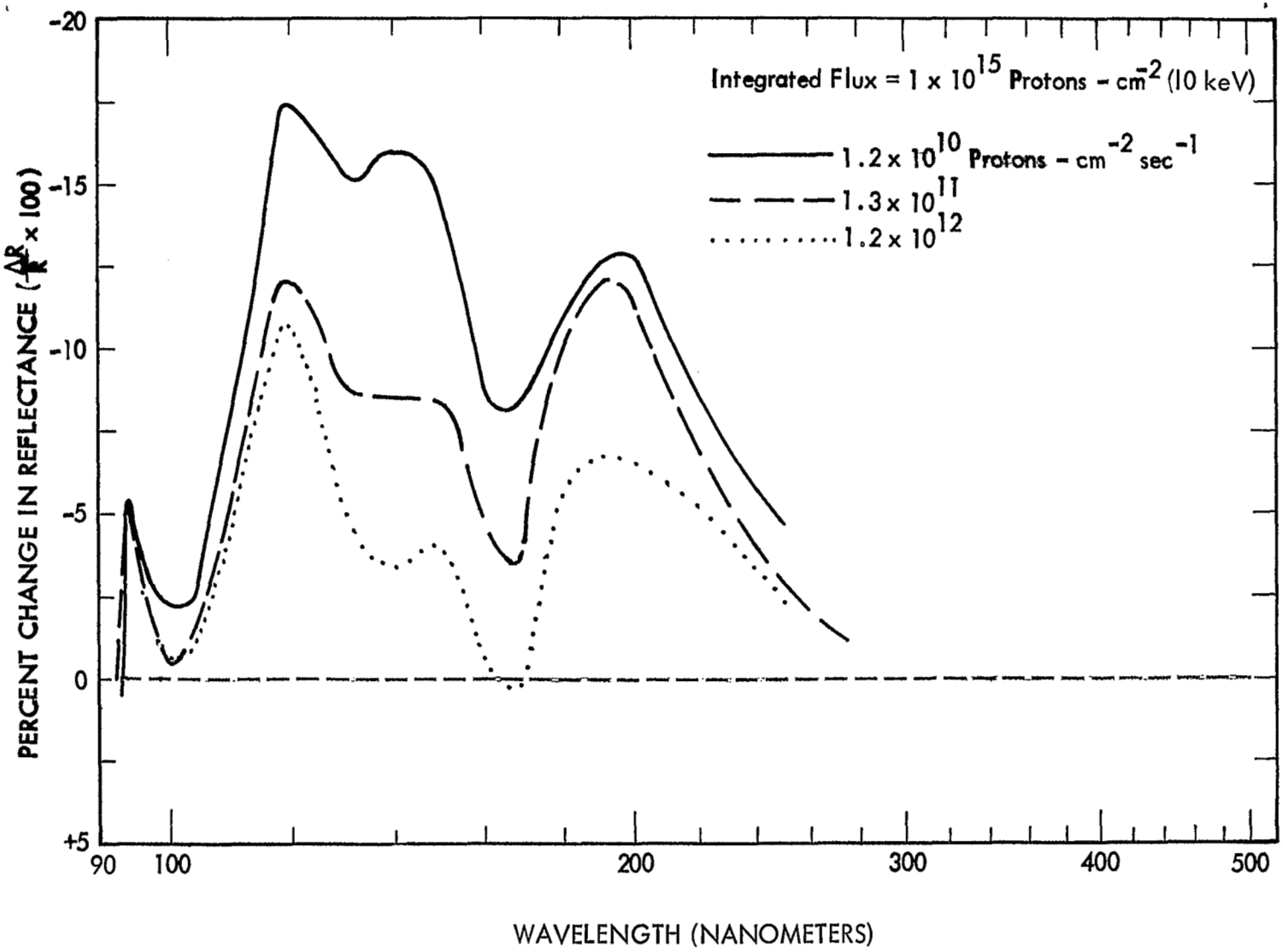

Figure 21: RATE EFFECT IN IRRADIATION OF LiF/Al-COATED FUSED SILICA MIRRORS

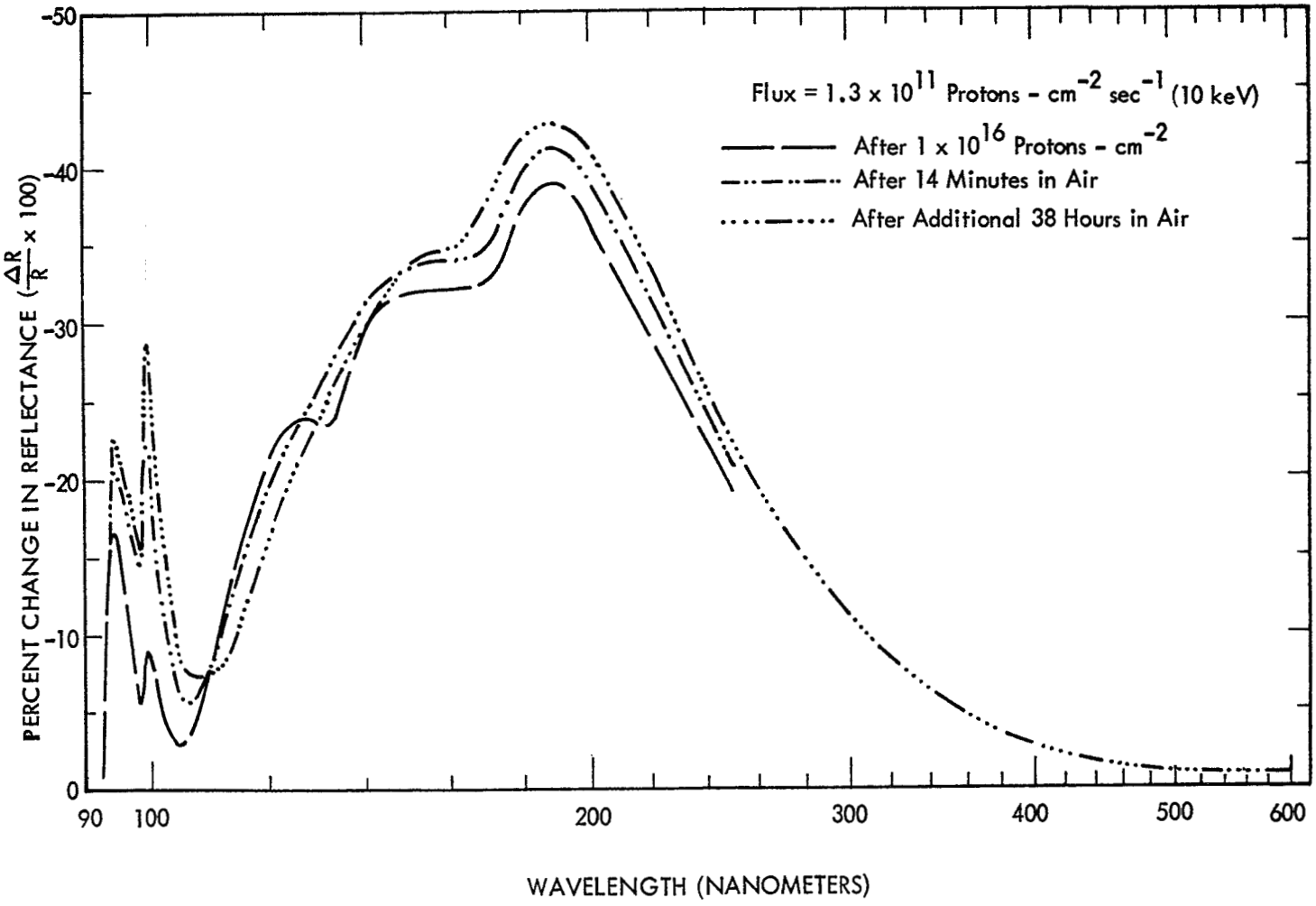

Figure 22: POST-IRRADIATION REFLECTANCE CHANGES OF LiF/Al-COATED MIRROR EXPOSED TO AIR

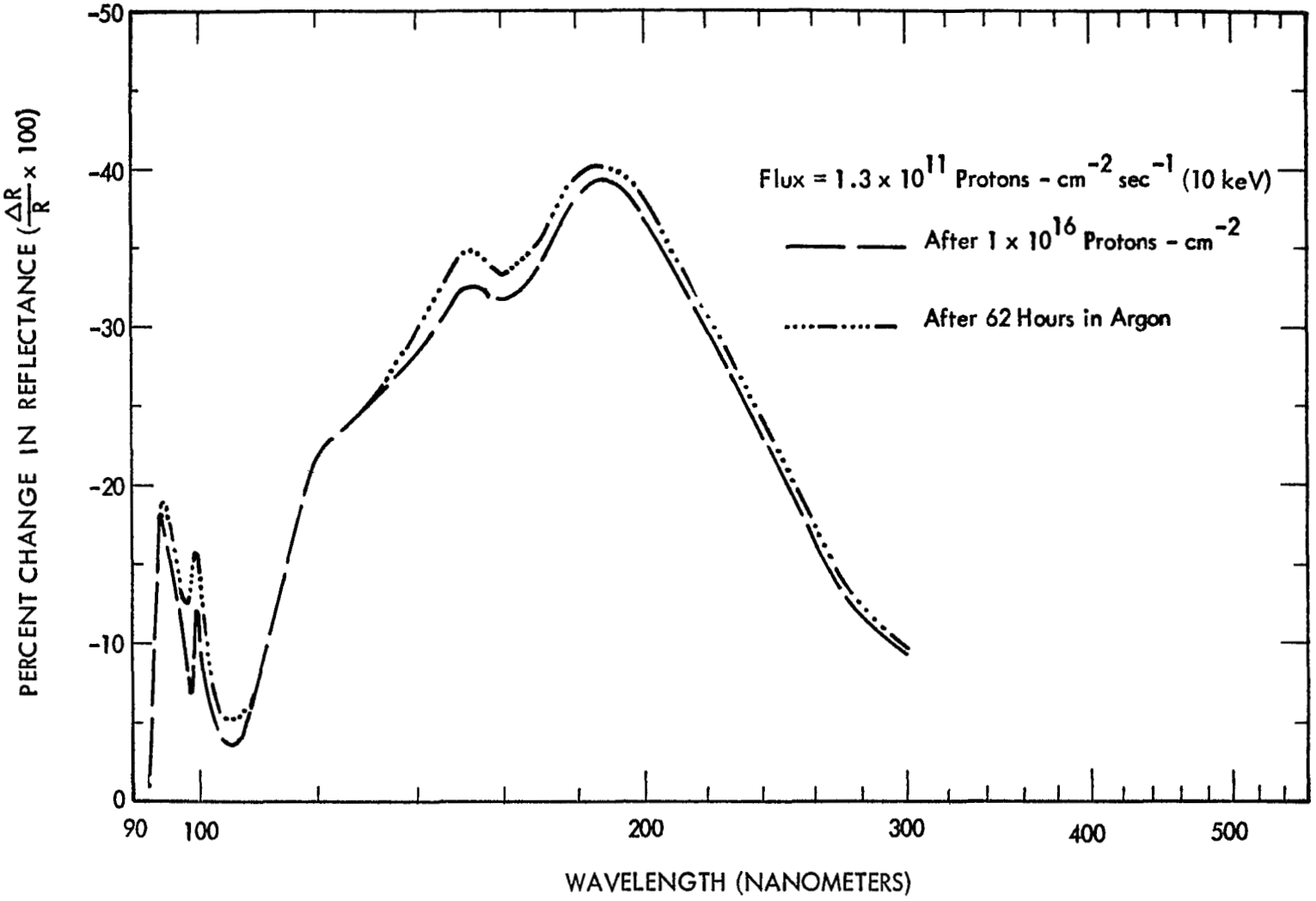

Figure 23: POST-IRRADIATION REFLECTANCE CHANGES OF LiF/Al-COATED MIRROR EXPOSED TO ARGON

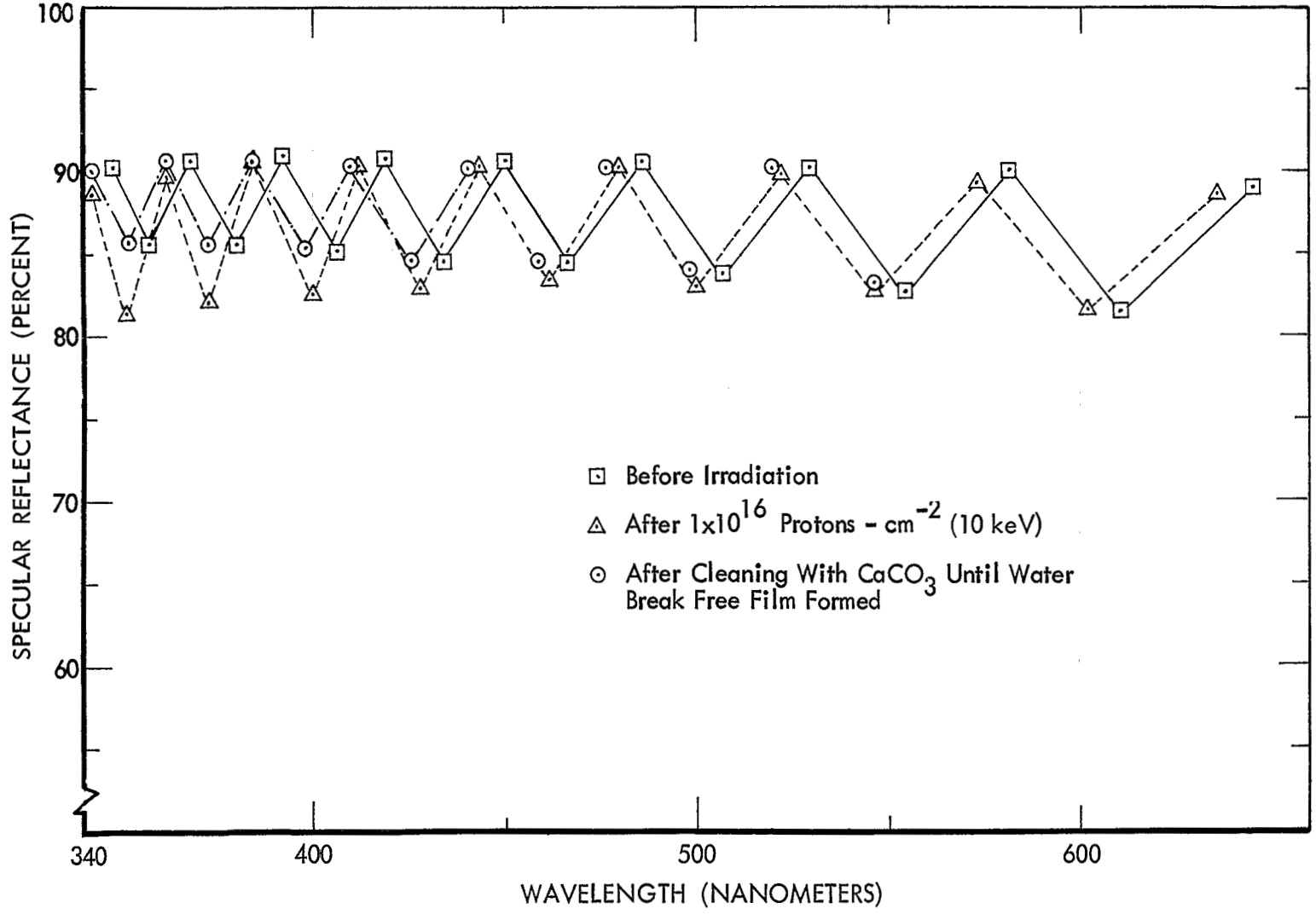

Figure 24: EFFECT OF IRRADIATION AND CLEANING ON INTERFERENCE CHARACTERISTICS OF SiO_2/Al-COATED MIRROR

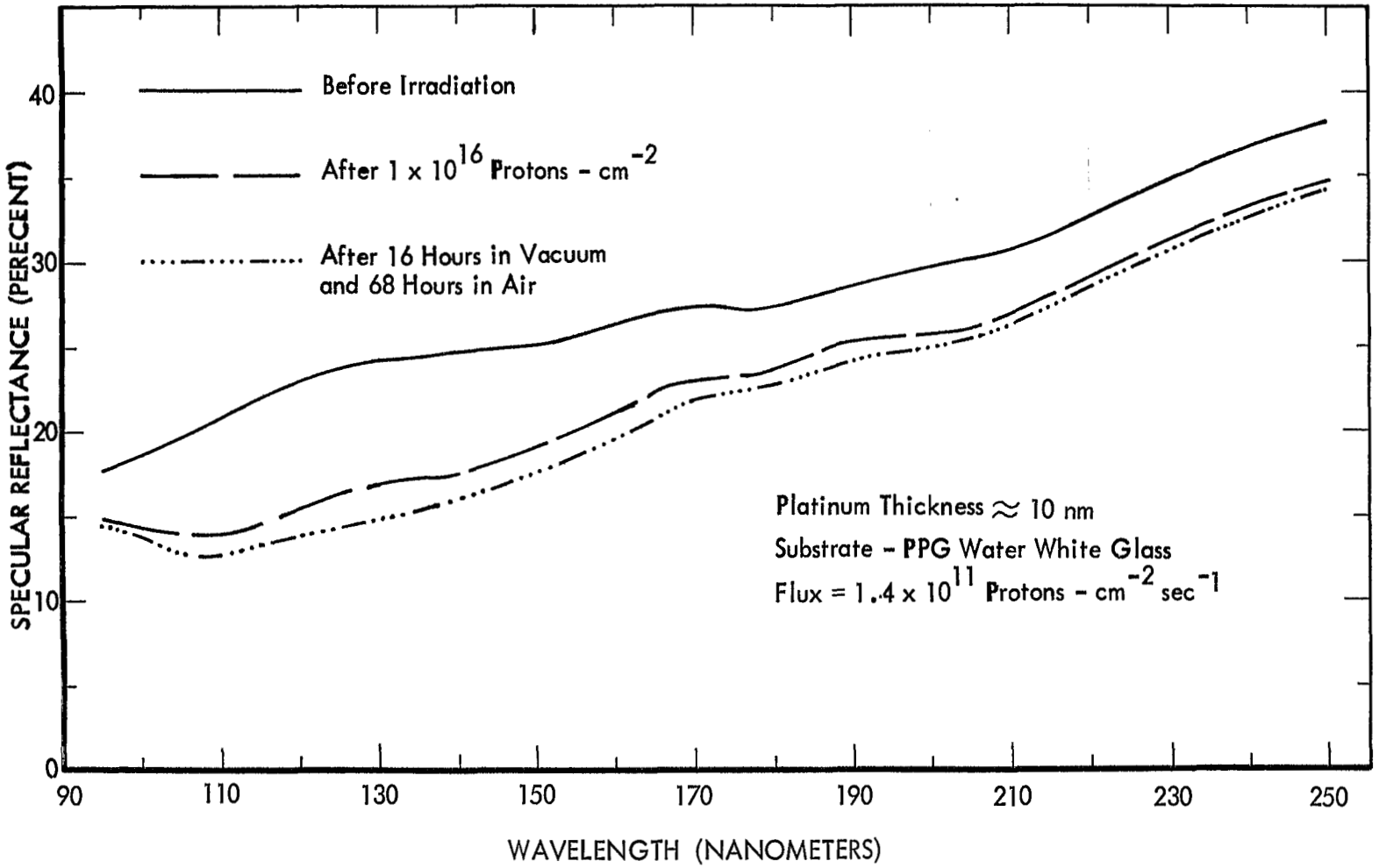

Figure 25: REFLECTANCE OF A PLATINUM COATED MIRROR IRRADIATED BY 10 KEV PROTONS

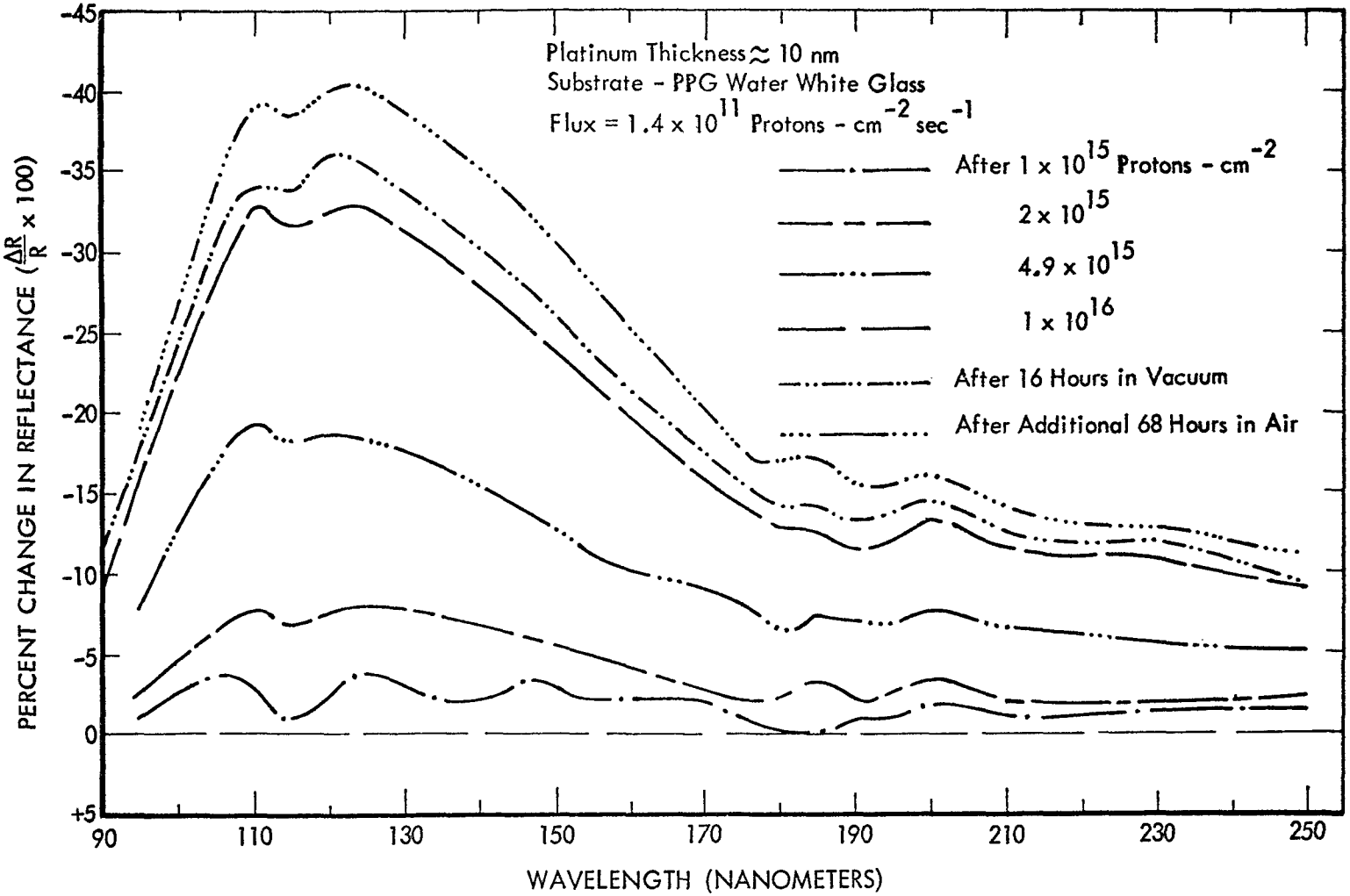

Figure 26: REFLECTANCE CHANGES OF A PLATINUM COATED MIRROR IRRADIATED BY 10 KEV PROTONS

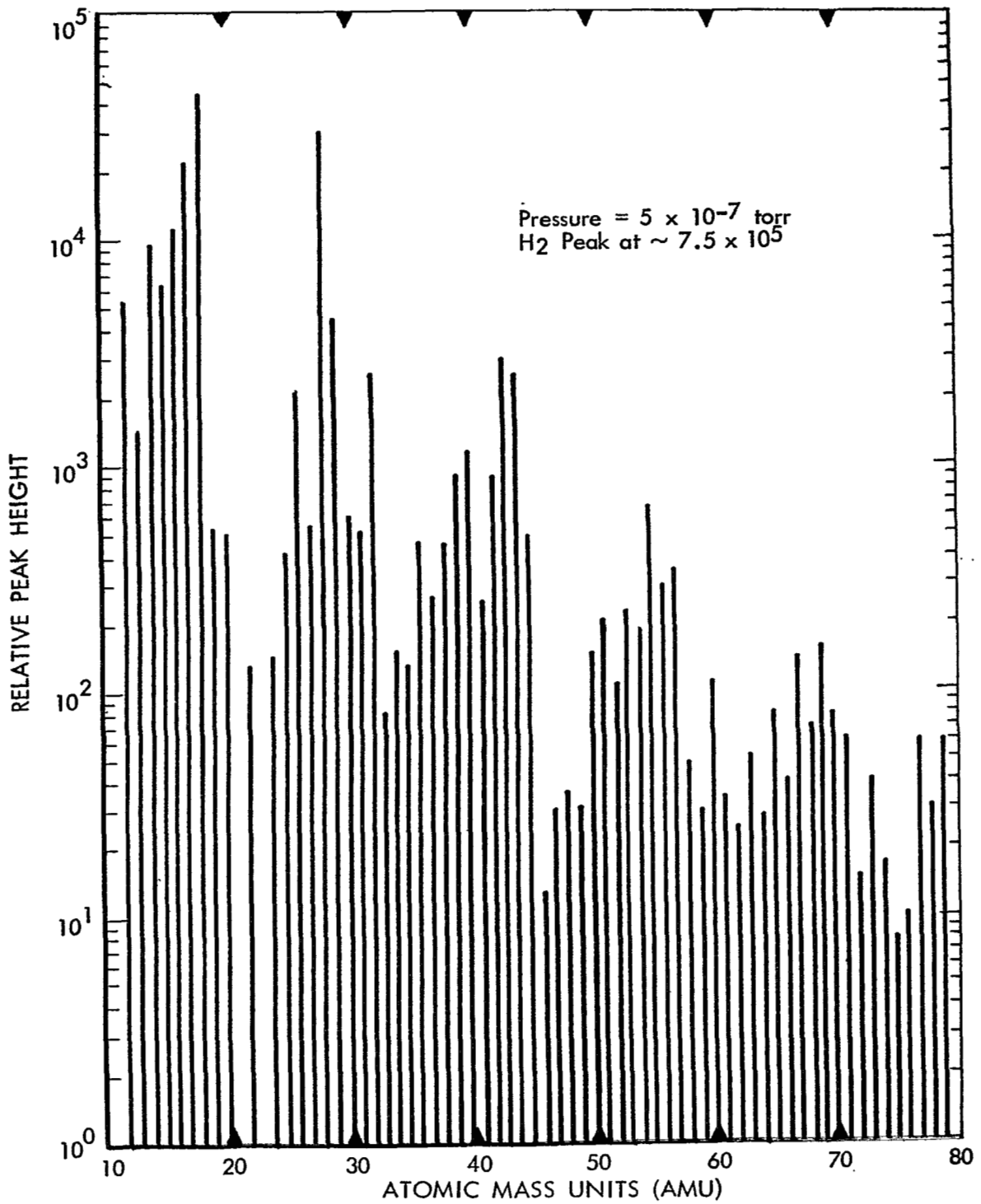

Figure 27: RESIDUAL GAS SPECTRUM FOR REFLECTOMETER CHAMBER-WITH TRAP FILLED (BASELINE SPECTRUM)

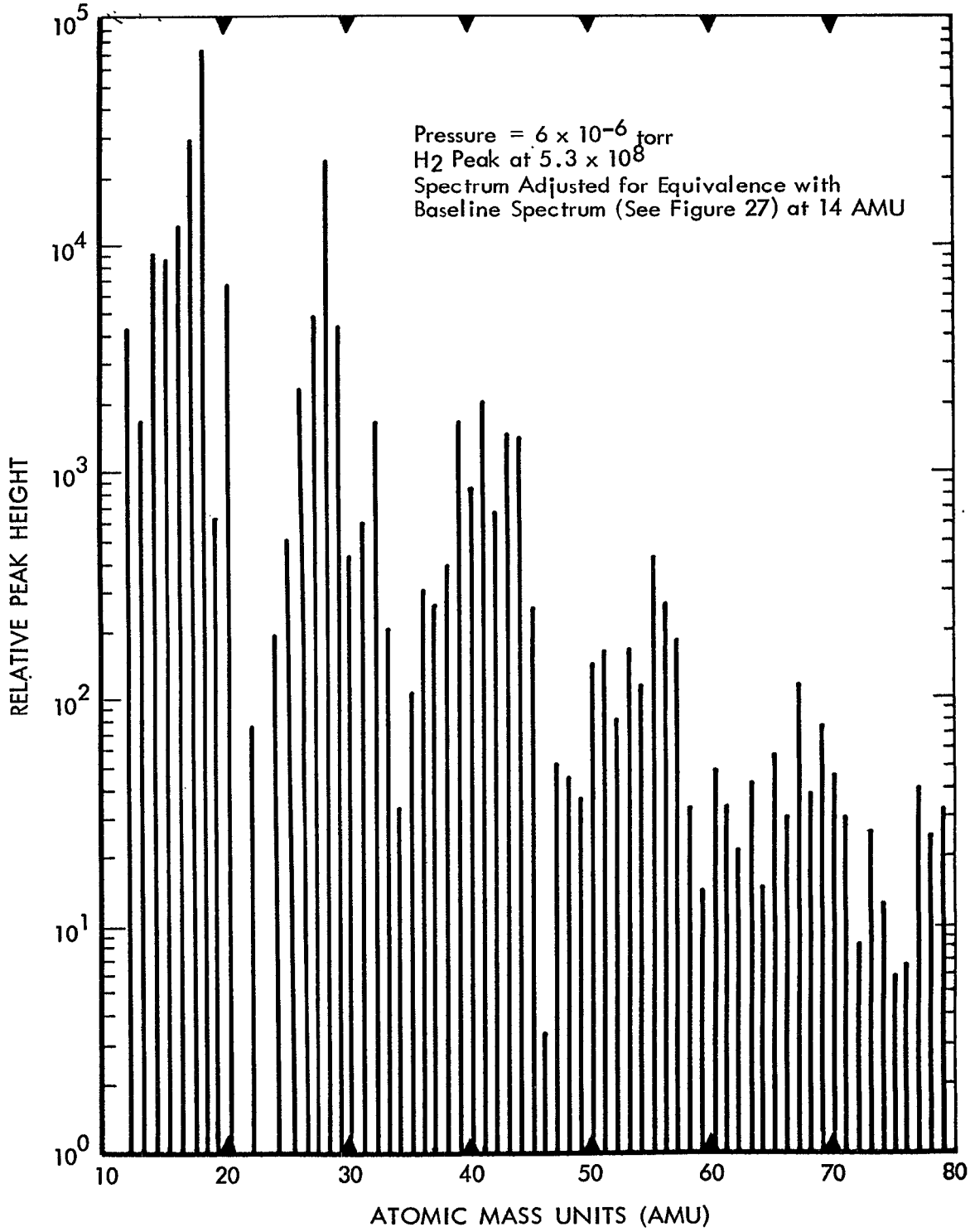

Figure 28: RESIDUAL GAS SPECTRUM FOR REFLECTOMETER CHAMBER + MONOCHROMATOR

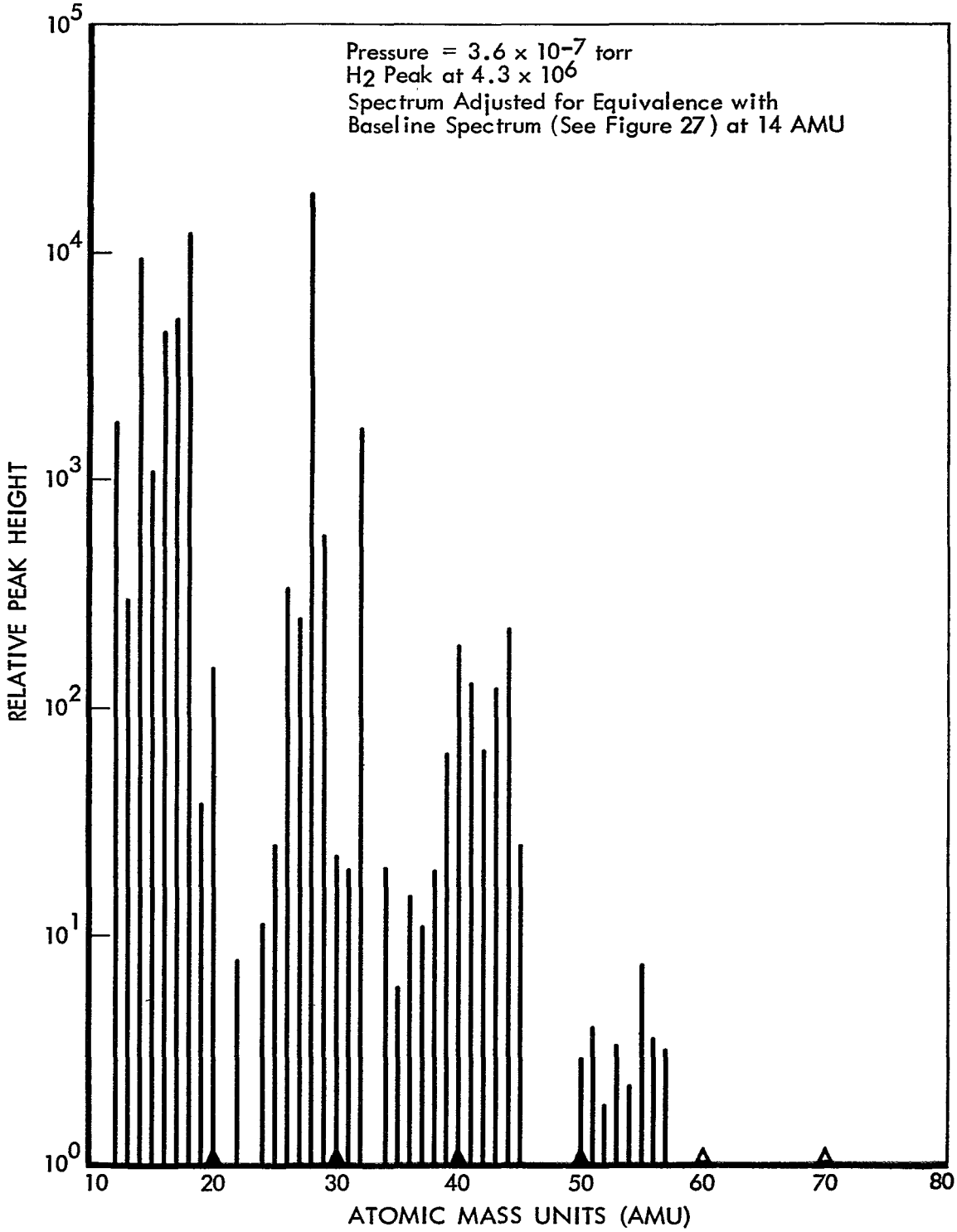

Figure 29: RESIDUAL GAS MASS SPECTRUM FOR REFLECTOMETER CHAMBER + ACCELERATOR BEAM TUBE (BEAM OFF)

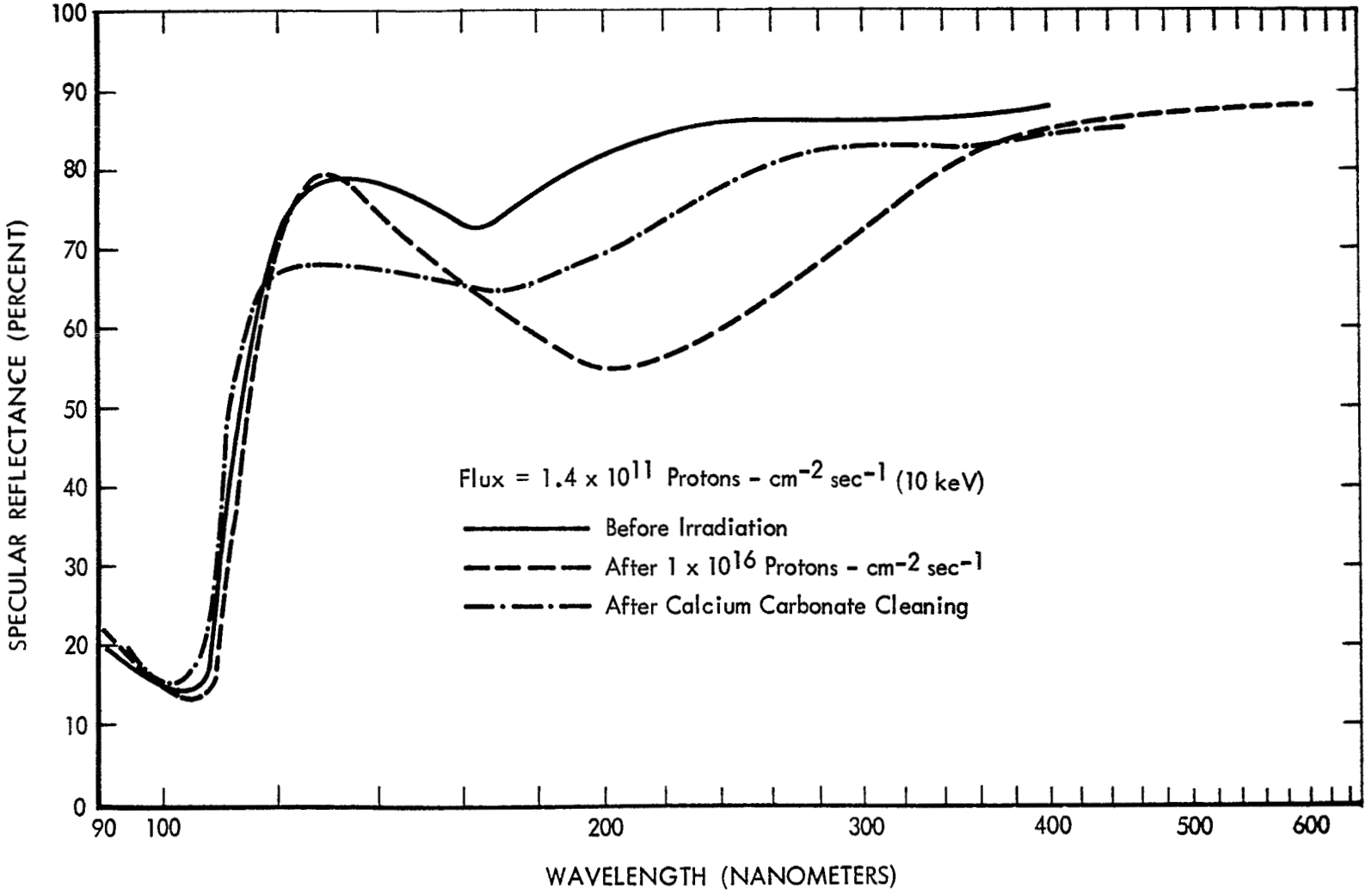

Figure 30: EFFECT OF ABRASIVE CLEANING ON REFLECTANCE OF AN IRRADIATED MgF_2/Al-COATED MIRROR

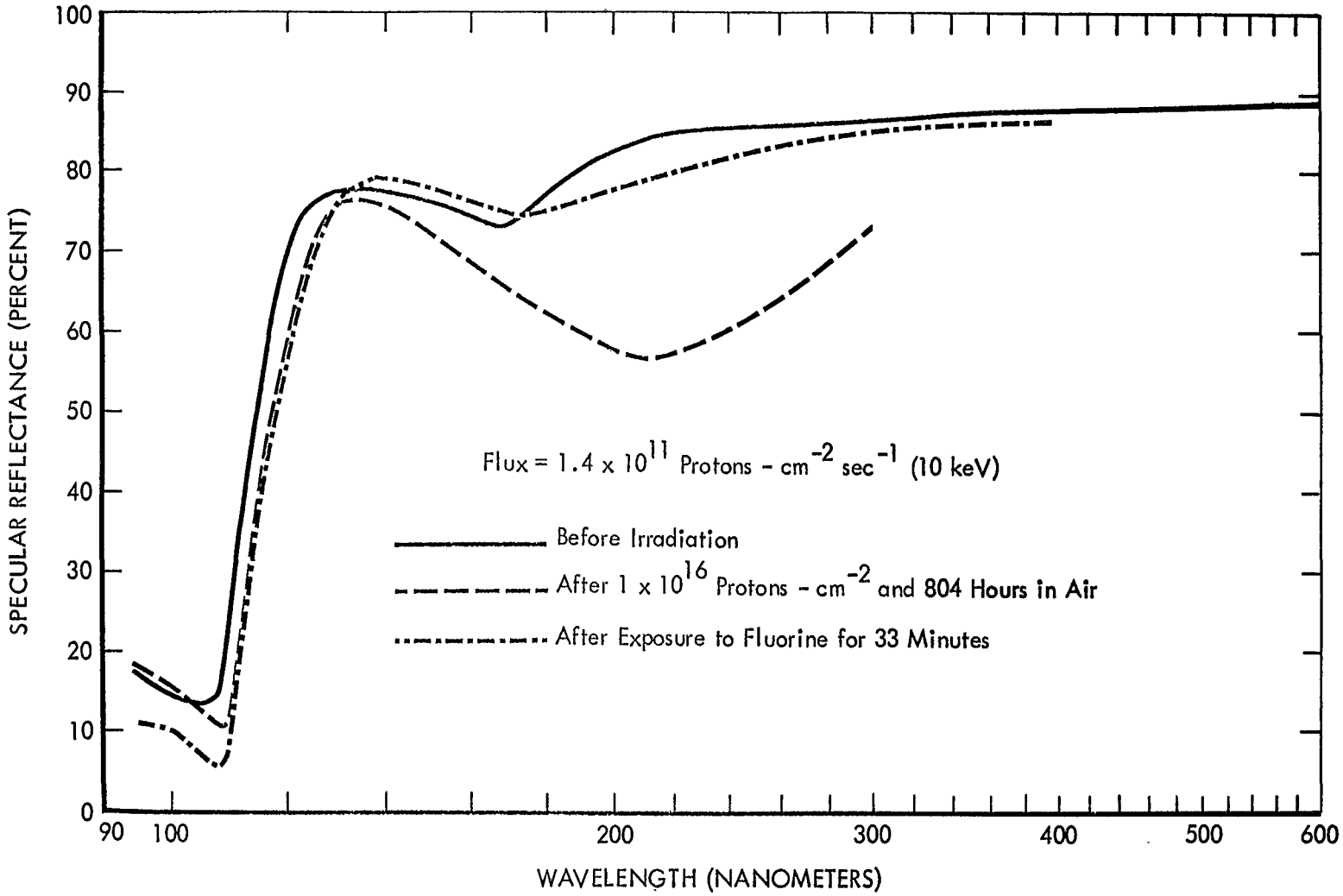

Figure 31: REFLECTANCE RECOVERY OF AN IRRADIATED MgF_2/Al-COATED CER-VIT MIRROR EXPOSED TO FLUORINE

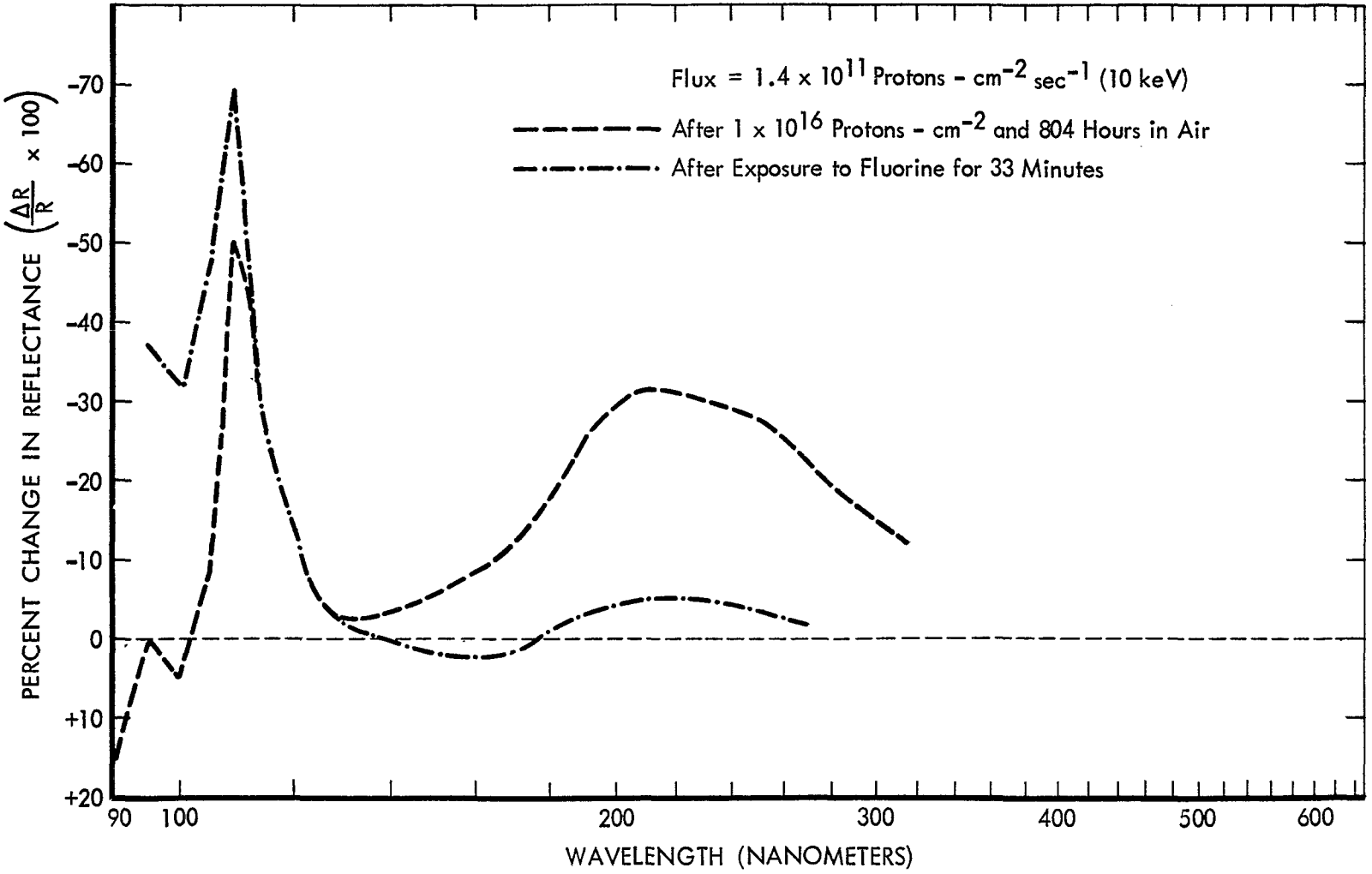

Figure 32: REFLECTANCE RECOVERY OF AN IRRADIATED MgF_2/Al-COATED CER-VIT MIRROR EXPOSED TO FLUORINE AS SHOWN BY CHANGE IN $\Delta R/R$

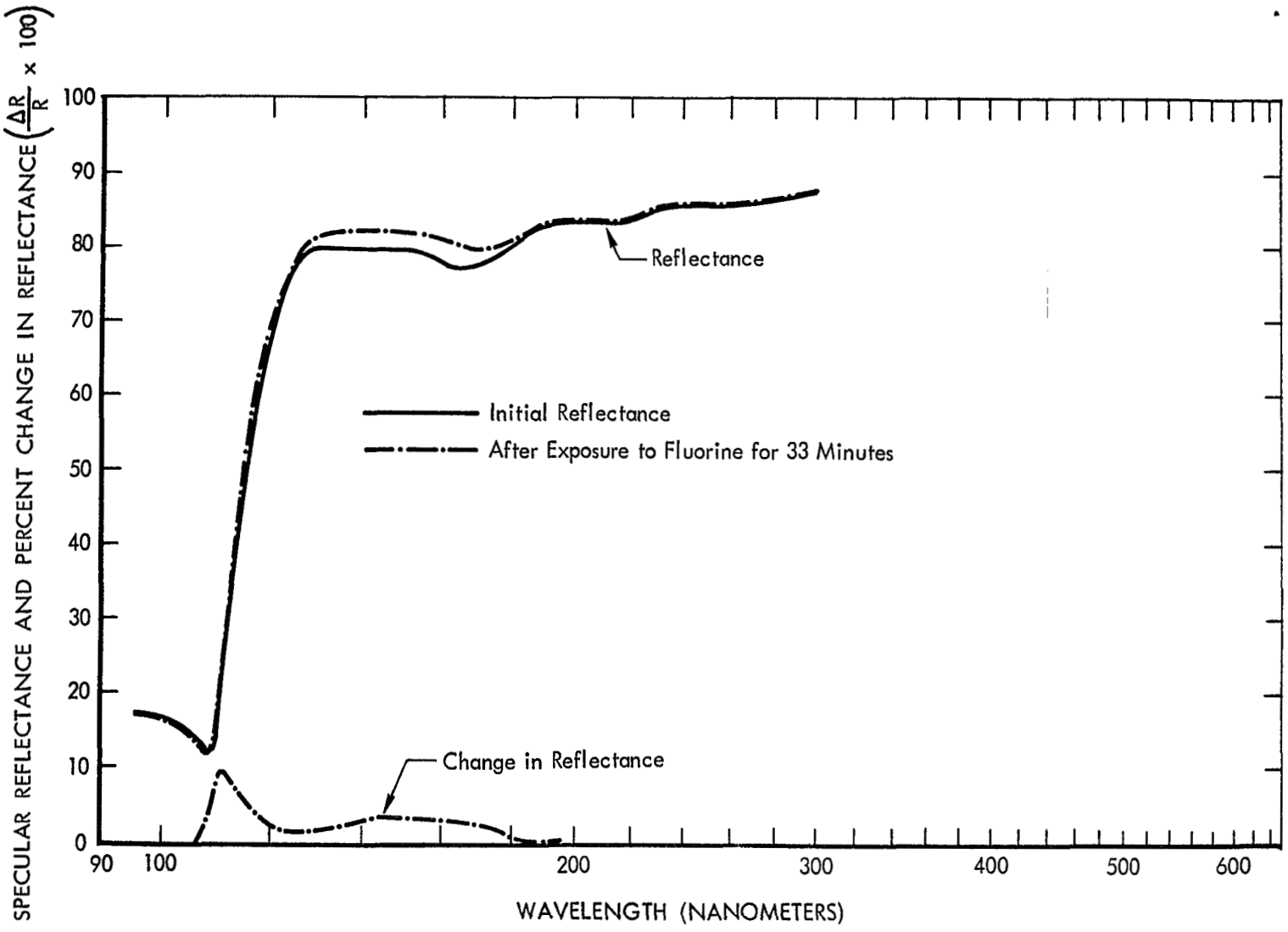

Figure 33: EFFECT OF FLUORINE EXPOSURE ON REFLECTANCE OF AN UNIRRADIATED MgF_2/Al-COATED MIRROR

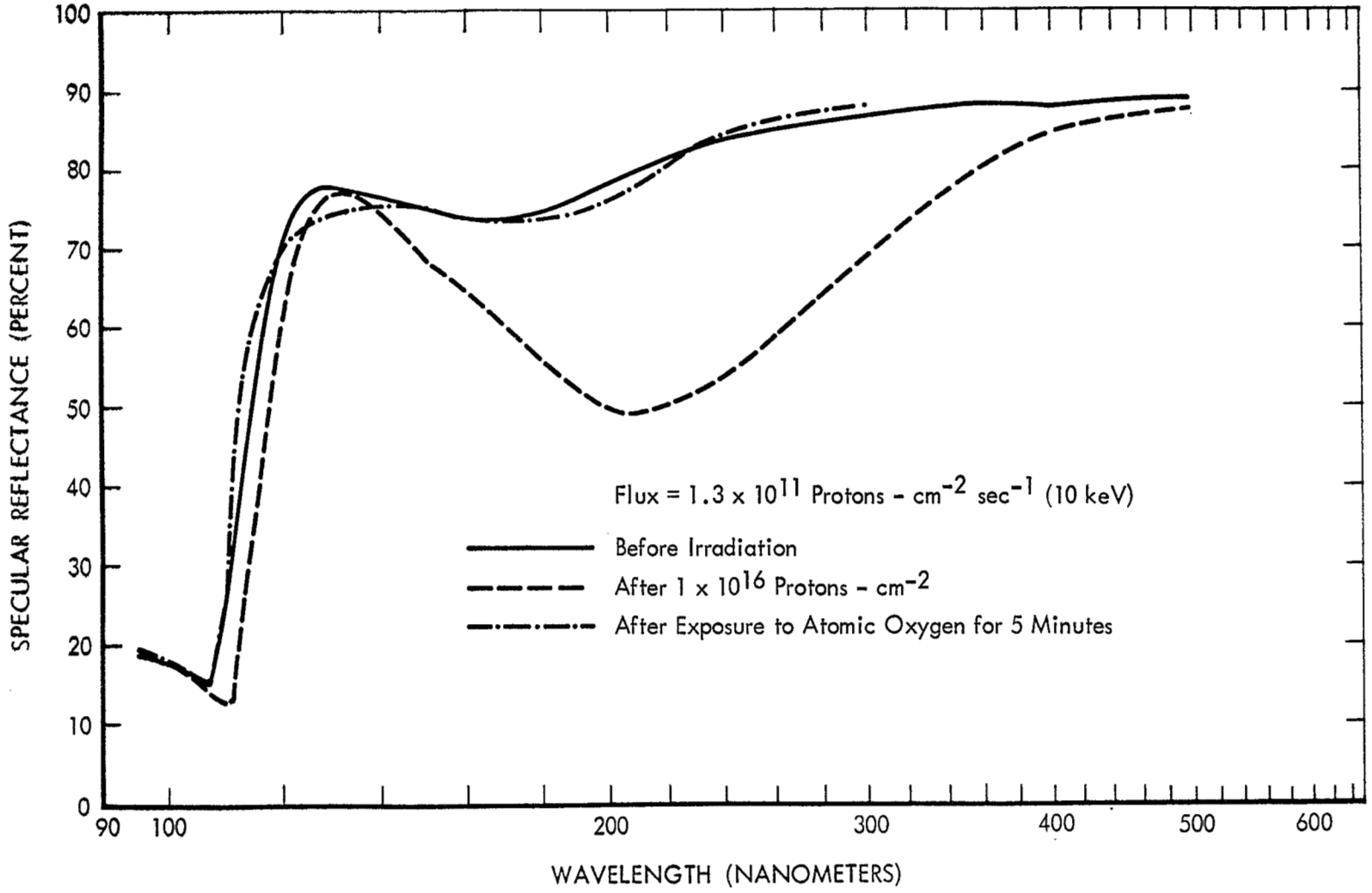

Figure 34: REFLECTANCE RECOVERY OF AN IRRADIATED MgF_2/Al-COATED CER-VIT MIRROR EXPOSED TO ATOMIC OXYGEN

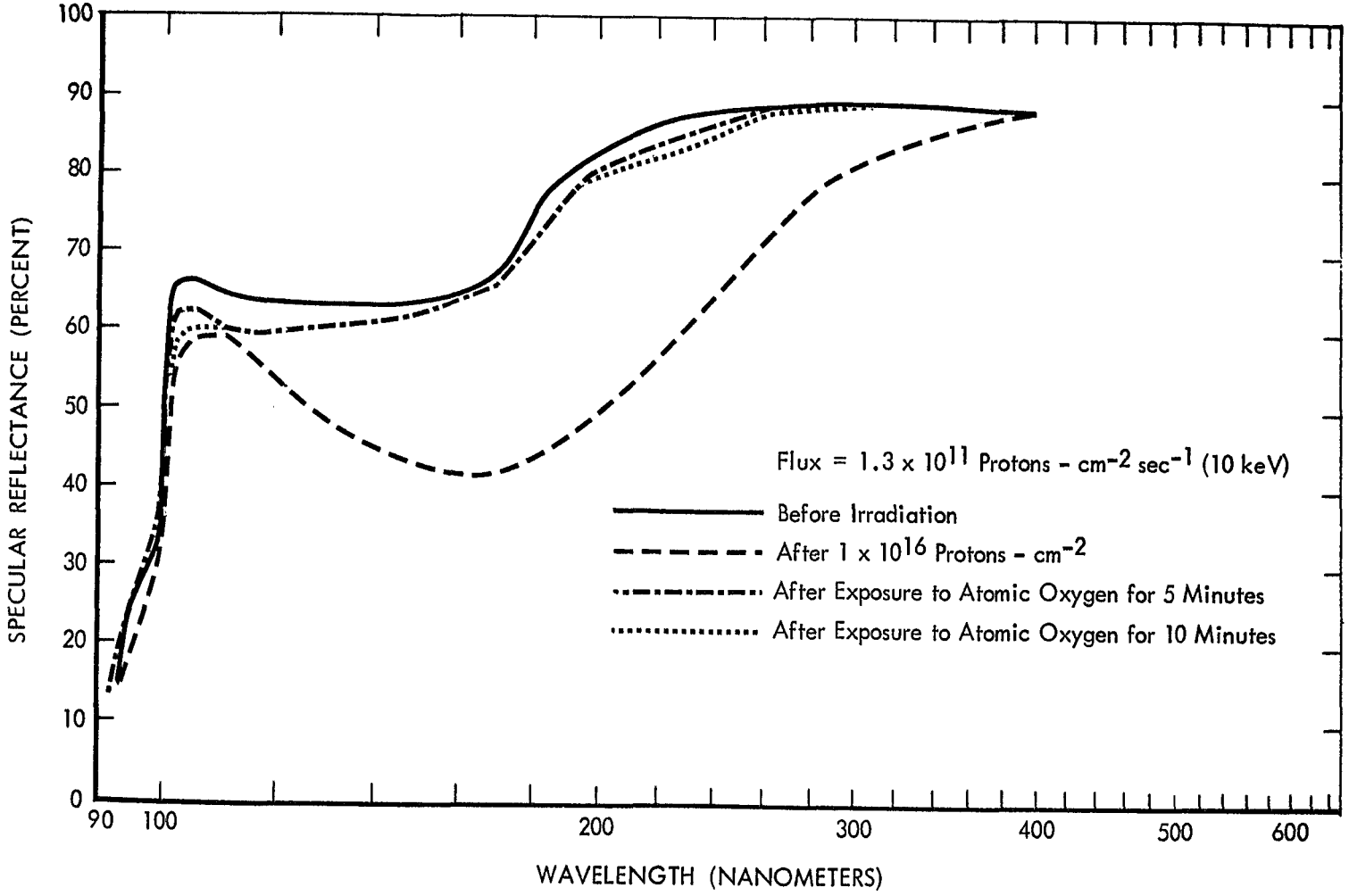

Figure 35: REFLECTANCE RECOVERY OF AN IRRADIATED LiF/Al - COATED FUSED SILICA MIRROR EXPOSED TO ATOMIC OXYGEN

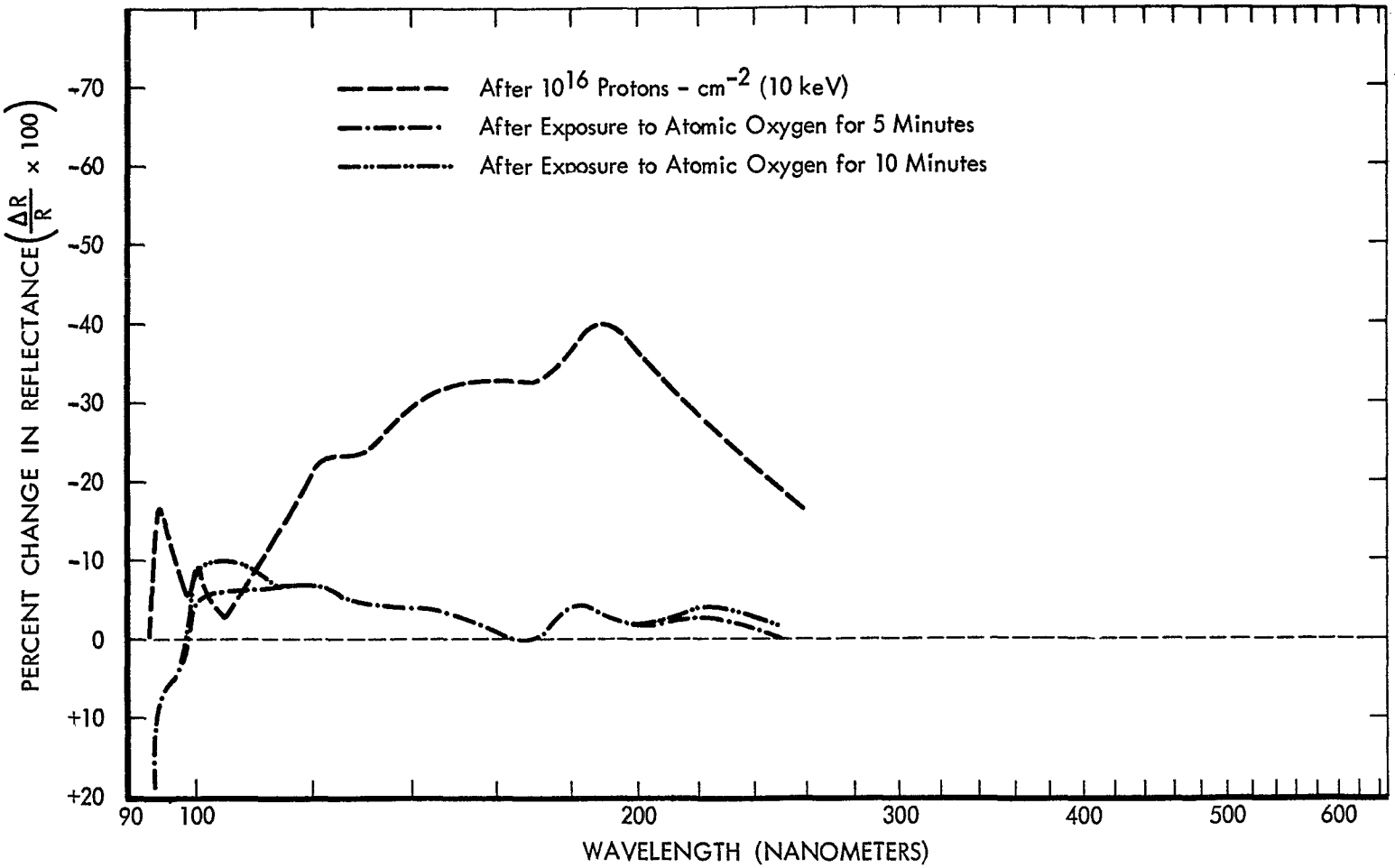

Figure 36: REFLECTANCE RECOVERY OF AN IRRADIATED LiF/Al-COATED FUSED SILICA MIRROR EXPOSED TO ATOMIC OXYGEN AS SHOWN BY CHANGE IN $\frac{\Delta R}{R}$

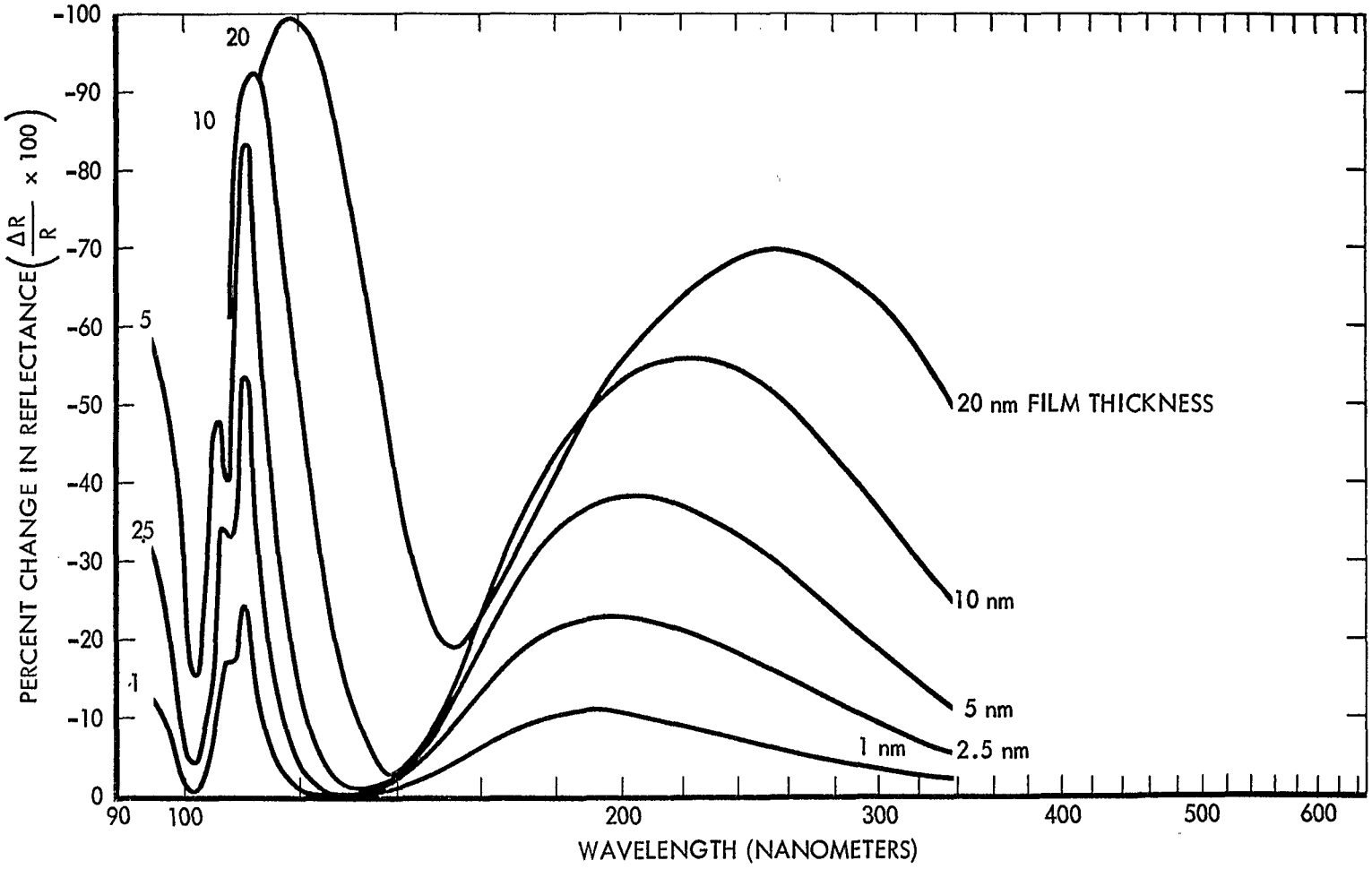

Figure 37: CALCULATED EFFECT OF CONTAMINANT FILM THICKNESS ON CHANGE IN REFLECTANCE OF MgF_2/Al-COATED MIRROR (25 NM OF MgF_2)

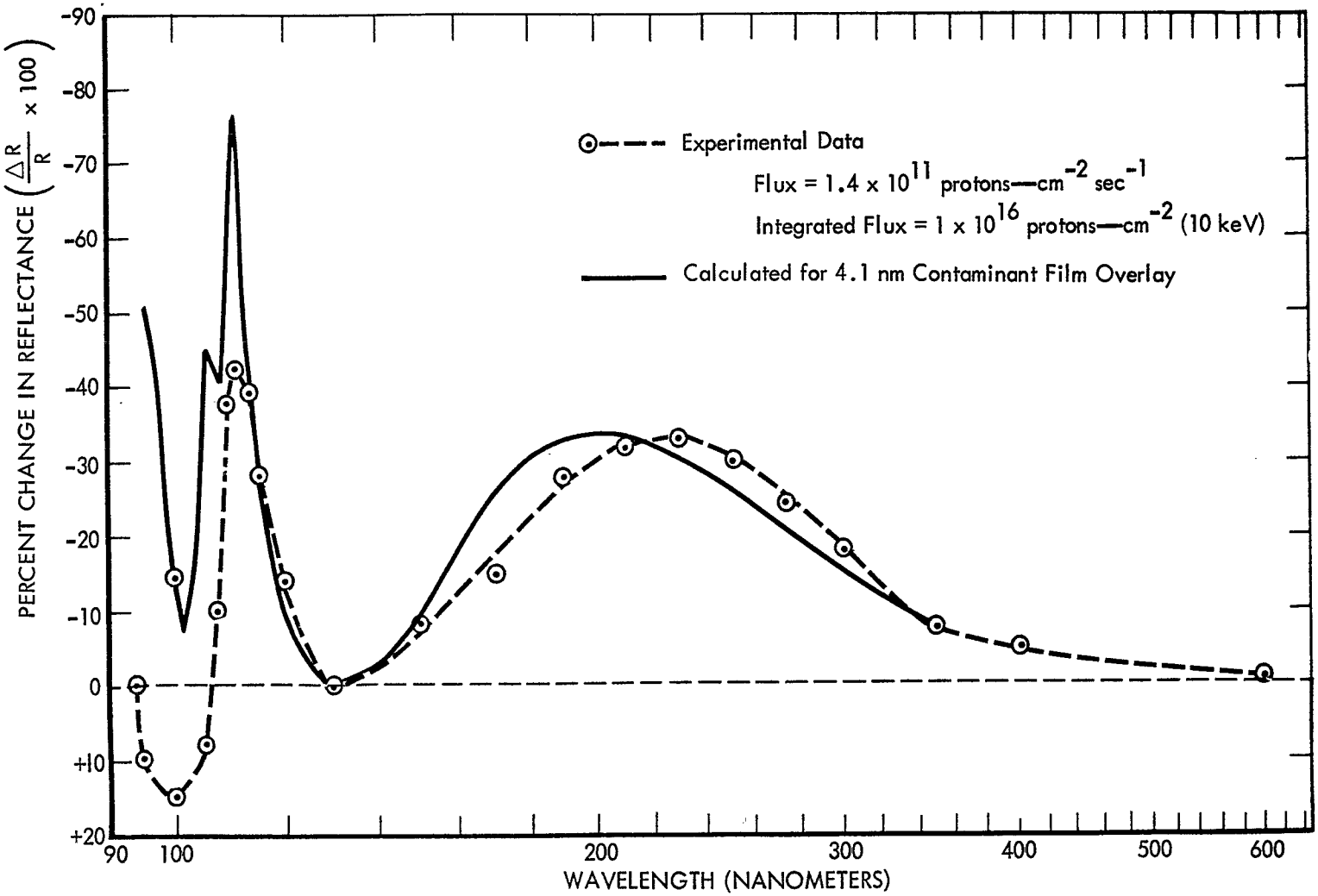

Figure 38: COMPARISON OF CALCULATED AND EXPERIMENTAL CHANGE IN REFLECTANCE FOR IRRADIATED, FUSED-SILICA MIRROR COATED WITH ALUMINUM AND 25 NM OF MgF_2

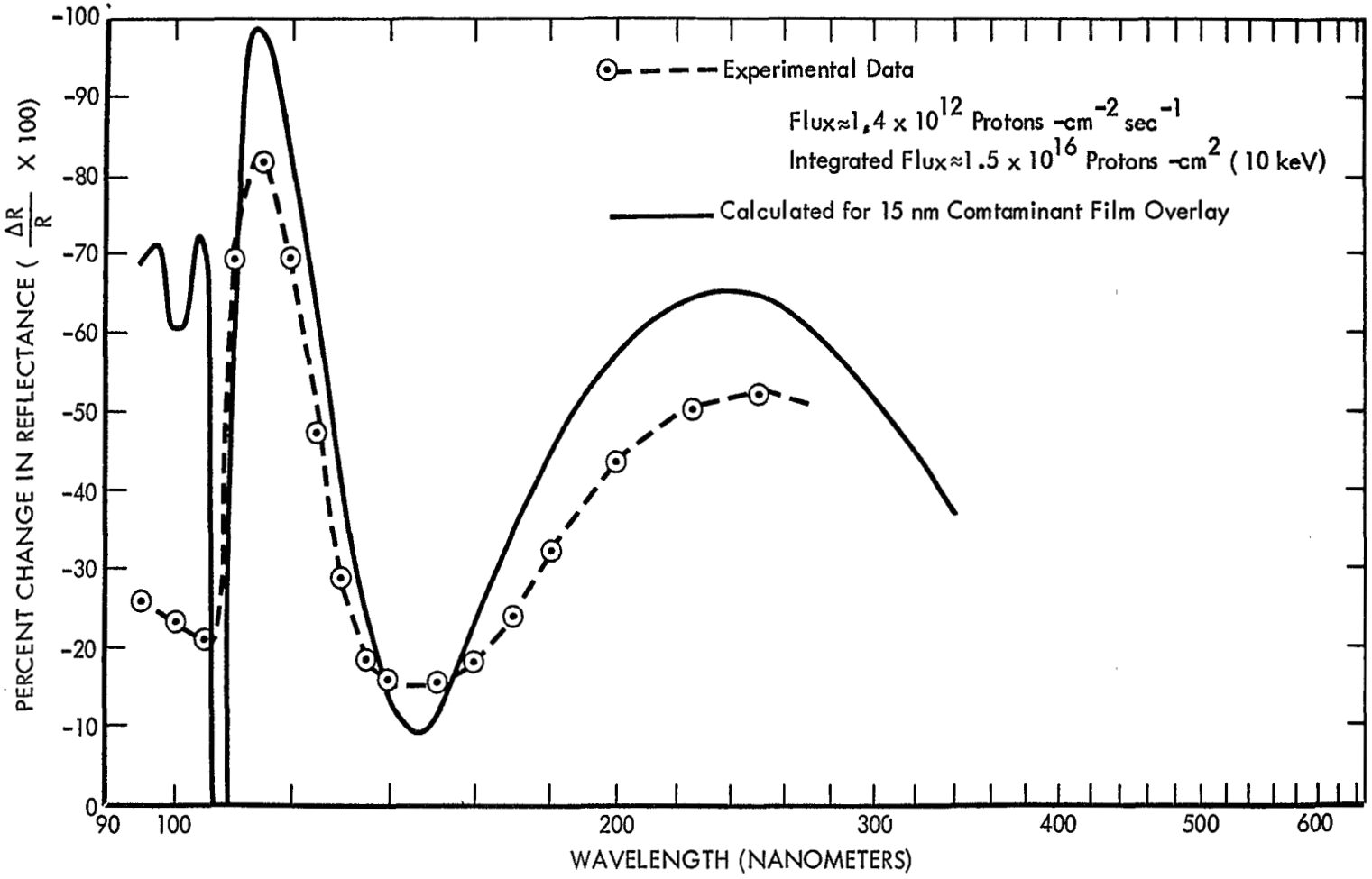

Figure 39: COMPARISON OF CALCULATED AND EXPERIMENTAL CHANGE IN REFLECTANCE FOR IRRADIATED CER-VIT MIRROR COATED WITH ALUMINUM AND 25 NM OF MgF_2

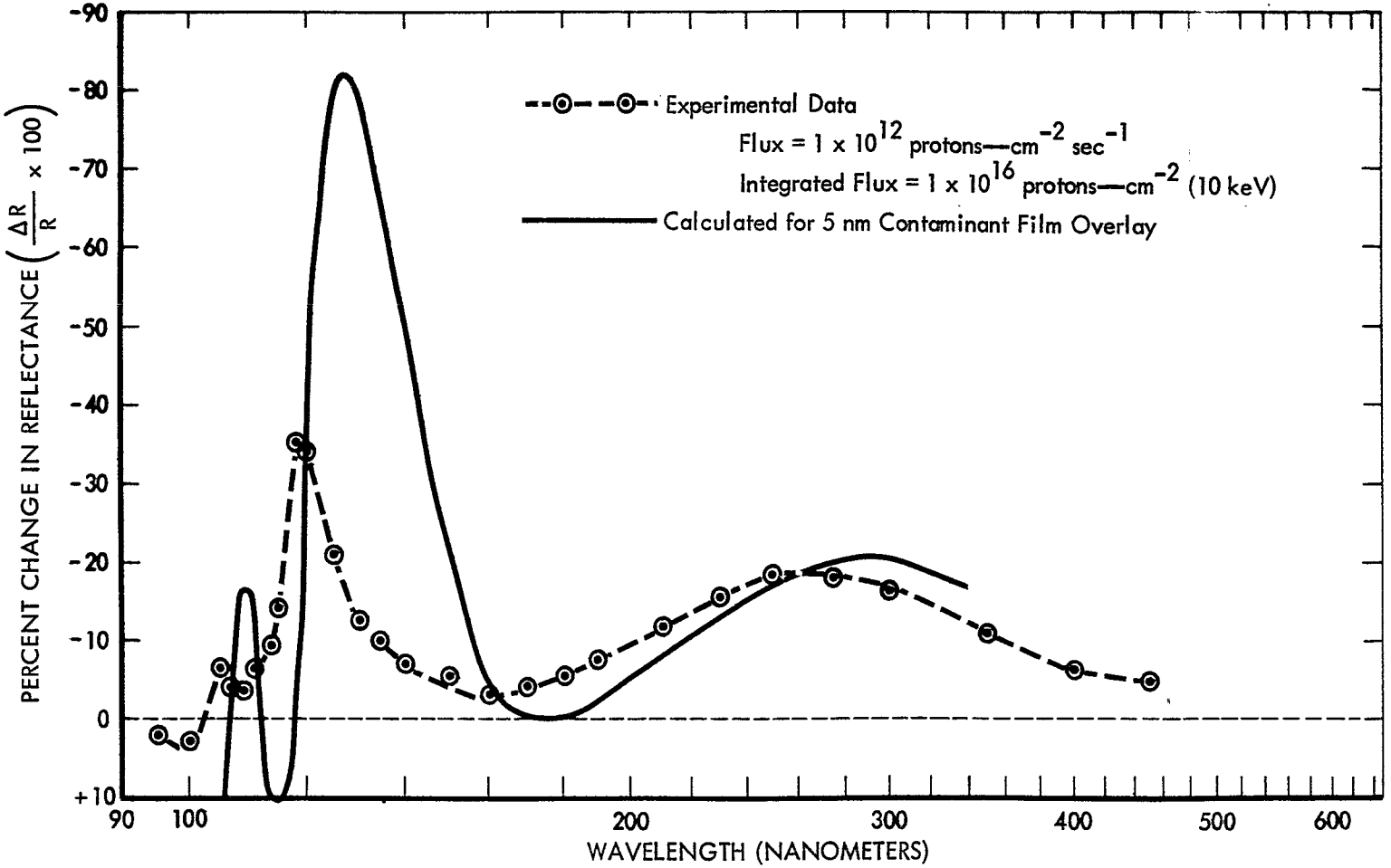

Figure 40: COMPARISON OF CALCULATED AND EXPERIMENTAL CHANGE IN REFLECTANCE FOR IRRADIATED PLATE-GLASS MIRROR COATED WITH ALUMINUM AND 43 NM MgF_2

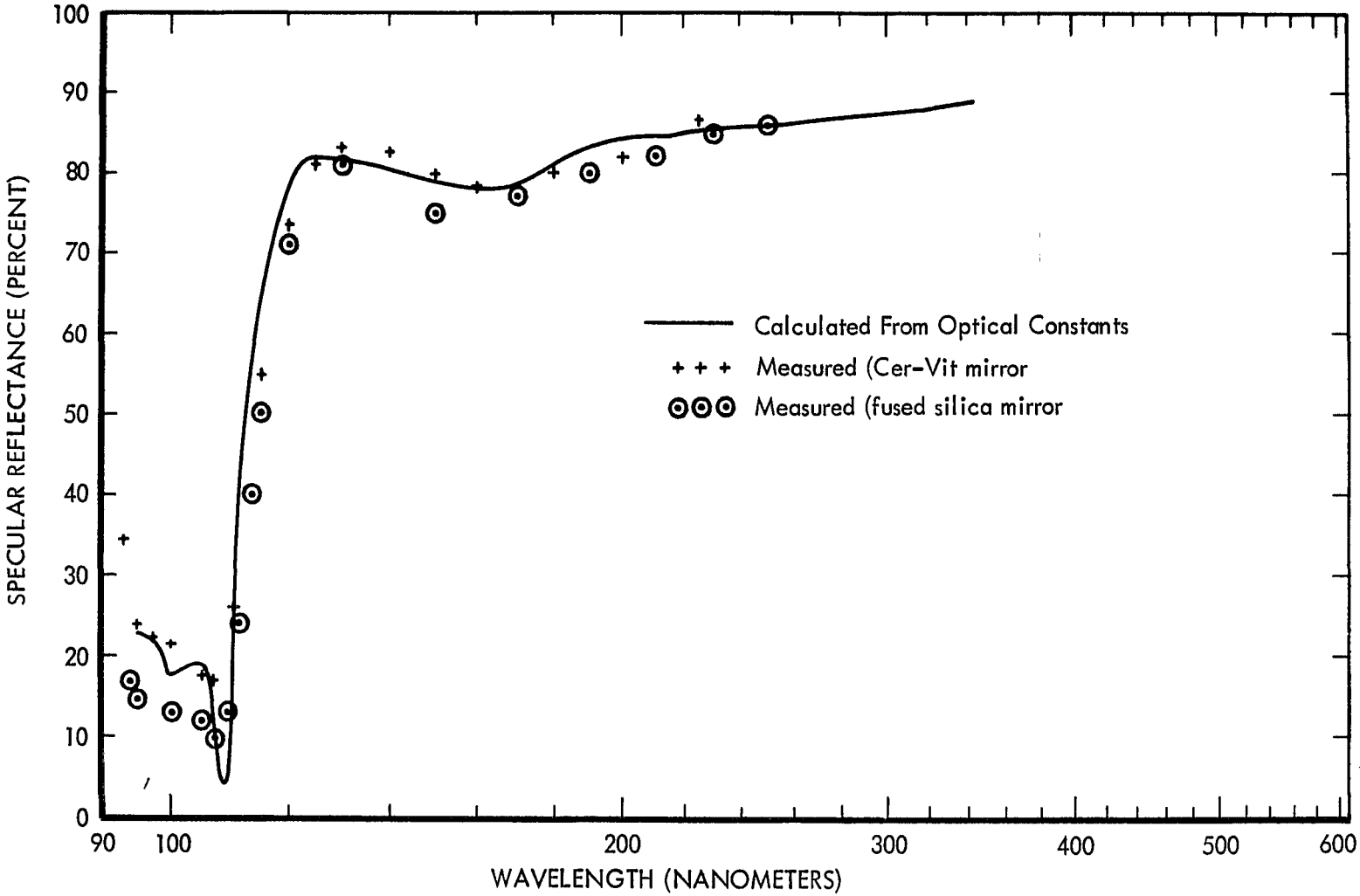

Figure 41: CALCULATED AND MEASURED REFLECTANCE OF MgF_2/Al- COATED MIRRORS(25 NM OF MgF_2)

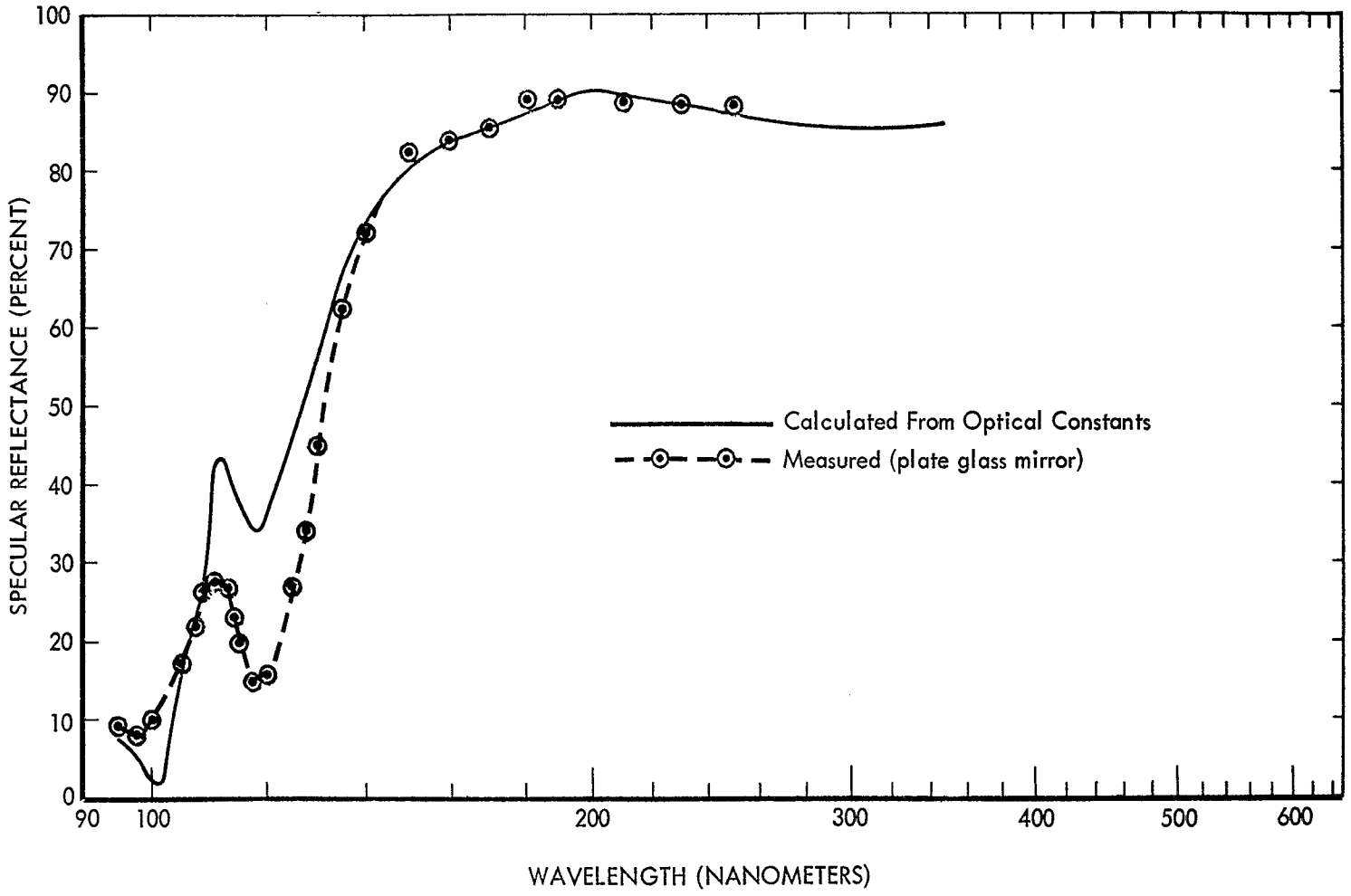

Figure 42: CALCULATED AND MEASURED REFLECTANCE OF MgF_2/Al-COATED MIRRORS (43 NM OF MgF_2)

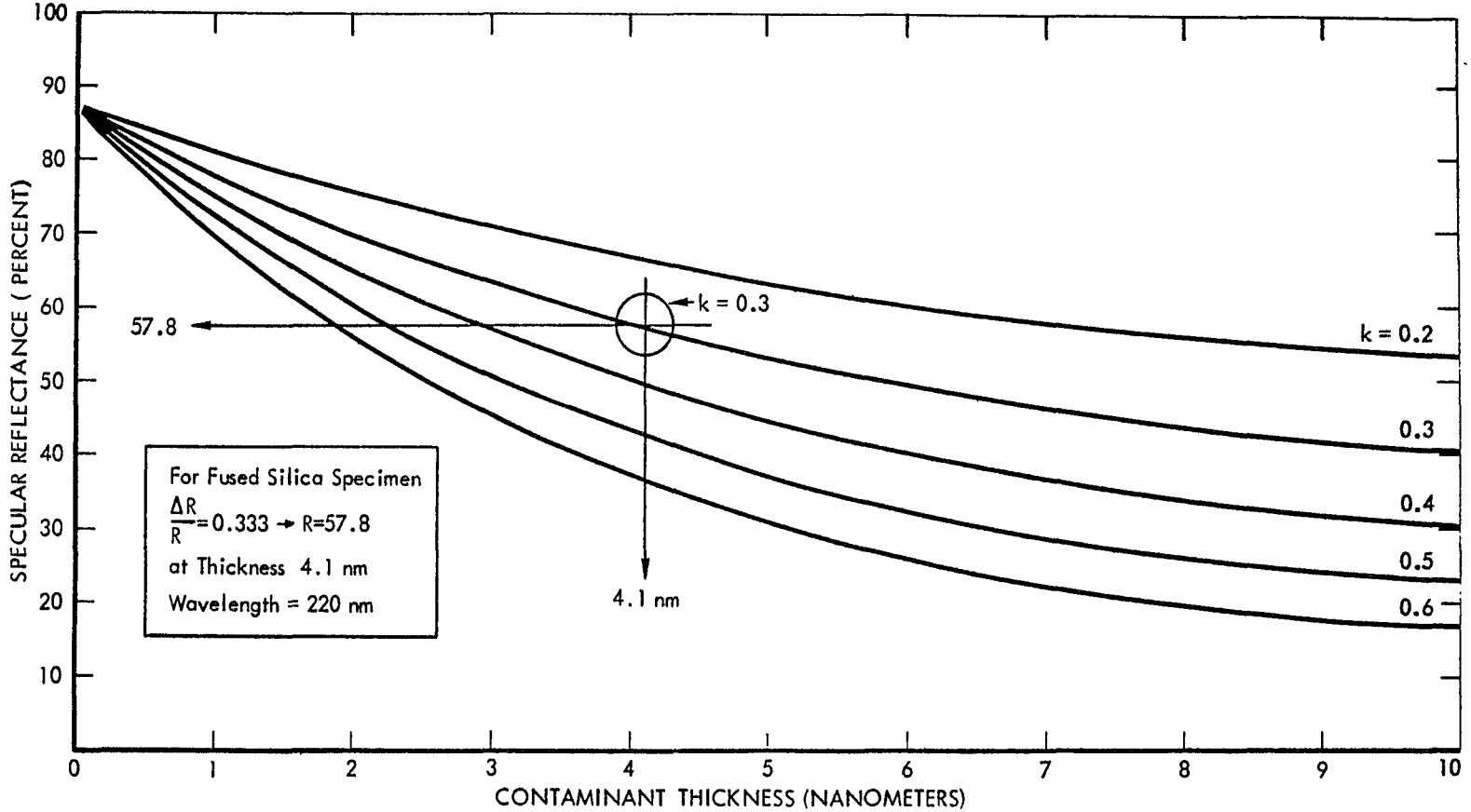

Figure 43: REFLECTANCE OF MIRROR COATED WITH Al + 25 NM MgF_2 + CONTAMINANT FILM WITH COMPLEX REFRACTIVE INDEX (1.40 - ik)

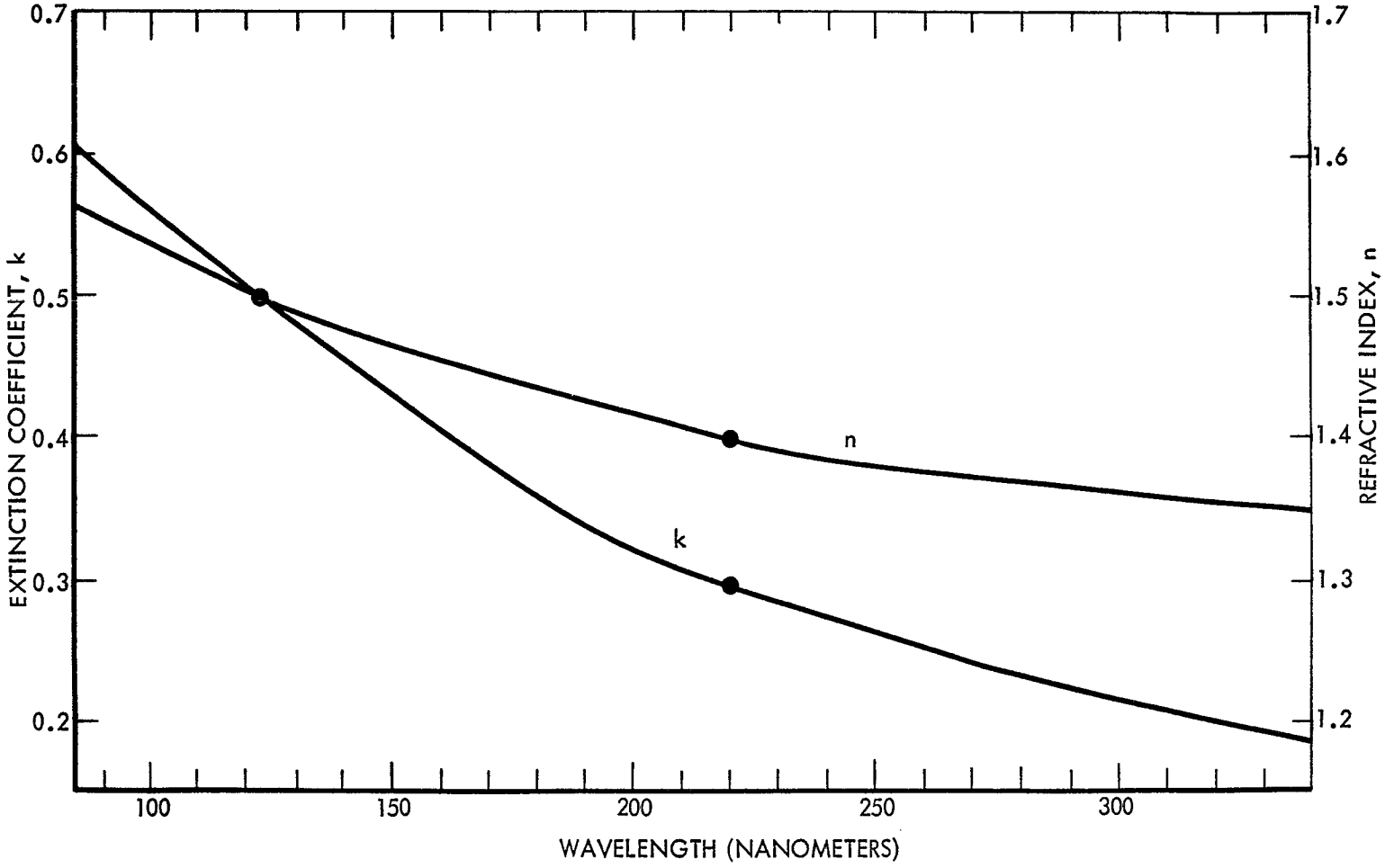

Figure 44: ASSUMED OPTICAL CONSTANTS FOR CONTAMINANT FILM